

AD-A166 838

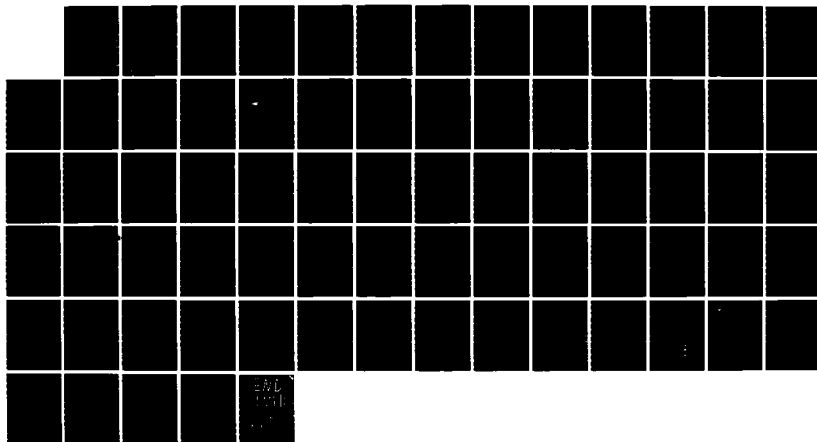
STUDIES OF HIGHLY EXCITED ATOMS(U) SRI INTERNATIONAL  
MENLO PARK CA PHYSICAL SCIENCES DIV R KACHRU 02 APR 86  
N00014-79-C-0202

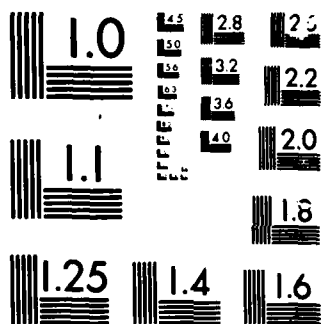
1/1

UNCLASSIFIED

F/G 17/5

NL





MICROCOPY

CHART

②

April 2, 1986

SRI International  
Final Report

STUDIES OF HIGHLY EXCITED ATOMS

By: Ravinder Kachru

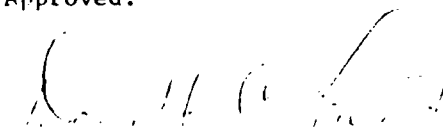
Prepared for:

OFFICE OF NAVAL RESEARCH  
800 North Quincy Street  
Arlington, VA 22217

Attention: Dr. E. R. Junker

Re: Contract N00014-79-C-0202  
SRI Project No. 8461  
MP 86-049

Approved:

  
Donald C. Lorents, Laboratory Director  
Chemical Physics Laboratory

G. R. Abrahamson  
Vice President  
Physical Sciences Division

DTIC FILE COPY

DTIC  
ELECTE

APR 23 1986

D

2

11

AD-A166 838

SRI International



333 Ravenswood Ave. • Menlo Park, CA 94025  
415 326-6200 • TWX 910-373-2046 • Telex 334 486

26 4 10 035

# ABSTRACT

Rydberg states of atoms have intrinsic properties that should allow their use as highly sensitive and tunable detectors at far infrared wavelengths. The intrinsic limit of such atomic detectors are collisional processes. This report describes the results of a research program to better understand an important class of collisions--namely, the resonant collision of two Rydberg atoms. We have extensively measured the linewidths and the collision cross sections and have determined their dependence on parameters such as the principal quantum number and the Rydberg state angular momentum. The resonant collisions are shown to occur for a wide variety of initial states with cross sections of the order of  $10^9 \text{ \AA}^2$  and scaling as  $(n^*)^4$ .

*square - Angstroms*

Accession For	
FILE	DATE
1	1
2	2
3	3
4	4
5	5
6	6
7	7
8	8
9	9
10	10
11	11
12	12
13	13
14	14
15	15
16	16
17	17
18	18
19	19
20	20
21	21
22	22
23	23
24	24
25	25
26	26
27	27
28	28
29	29
30	30
31	31
32	32
33	33
34	34
35	35
36	36
37	37
38	38
39	39
40	40
41	41
42	42
43	43
44	44
45	45
46	46
47	47
48	48
49	49
50	50
51	51
52	52
53	53
54	54
55	55
56	56
57	57
58	58
59	59
60	60
61	61
62	62
63	63
64	64
65	65
66	66
67	67
68	68
69	69
70	70
71	71
72	72
73	73
74	74
75	75
76	76
77	77
78	78
79	79
80	80
81	81
82	82
83	83
84	84
85	85
86	86
87	87
88	88
89	89
90	90
91	91
92	92
93	93
94	94
95	95
96	96
97	97
98	98
99	99
100	100

*A-1*



This document has been approved for publication and sale; its contents are confidential.

## CONTENTS

ABSTRACT.....	1
I INTRODUCTION.....	1
II RESONANT COLLISIONS.....	2
A. Resonant Collision of Rydberg Atoms.....	2
B. Theory of Resonant Collisions.....	5
C. Resonant Collisions of ns, nD, and nf States.....	9
III EXPERIMENTAL APPROACH.....	13
IV RESEARCH ACCOMPLISHMENTS.....	15
A. Resonant Collisions of Two np Rydberg Atoms.....	15
B. Measurements of the (ns) + (ns) → (np) + (n-1)p Cross Sections.....	15
C. Generalized Resonant Collision of Rydberg Atoms.....	28
D. Observations of Na(nd) + Na(nd) → Na[(n + 1)f] + Na(np) Resonant Collisions.....	35
V SUMMARY.....	41
REFERENCES.....	42
APPENDICES	
A RESONANT RYDBERG-ATOM-RYDBERG-ATOM COLLISIONS.....	A-1
B RESONANT RYDBERG-ATOM-RYDBERG-ATOM COLLISIONS.....	B-1
C RESONANT COLLISIONS OF Na nS AND nD RYDBERG ATOMS.....	C-1

## ILLUSTRATIONS

1. Energy-level diagram for the 16p-17s-17p states in a static electric field.....	4
2. Geometry of the collision of two atoms.....	6
3. Simplified energy-level diagram considered for the resonant-collision process.....	11
4. $ m_1 =0$ states of Na near the 20s state.....	12
5. Schematic of the experimental setup.....	14
6. The observed 17p ion signal after population of the 17s state versus dc electric field, showing the sharp collisional resonances.....	16
7. The blue-laser-intensity dependence of the 17p resonant collision signal and 17s signal after population of the 17s state, showing the quadratic dependence of the resonant signal.....	17
8. The population of the 23p state 2rs after the population of the 23s state, showing the collisional resonances.....	19
9. The positions of the 0,0 and 1,1 resonances.....	20
10. The fine-structure levels in zero field and at the field of the collisional resonances.....	25
11. The difference in widths of the 1,1 and 0,0 resonances and a plot of the calculated value of $\Delta f_s$ .....	26
12. The widths of the 0,0 resonances, the fit curve, and the a plot of the calculated dependence.....	27
13. The observed cross sections with their relative error bars, the fit curve, and the calculated dependence.....	30
14. Plot of ion current as a function of the applied static field for the na atoms initially excited to the 20s state.....	31
15. Collisional resonances similar to figure 14 observed with 20s atoms at higher field.....	33
16. Plot of ion current similar to that shown in figure 14 except that the SFI is set to detect only the $ m_1 =0$ component of the 20p and the nearly $n=19$ , high-I states.....	36
17. Plot of the ion current representing the population in the 16f state (or a nearby stark state) as a function of the static electric field...	37

## TABLES

I	Positions of the Resonances.....	21
II	Field Widths of the Resonances.....	23
III	Frequency Widths of the Resonances.....	24
IV	Radiative Lifetimes, Relative and Absolute Cross Sections.....	29
V	Calculated and Observed Positions of the Resonances in Terms of the Applied dc Field.....	34
VI	Calculated and Observed Cross Sections for Resonances with Both Final States with $ m_1 =0$ and Their Ratio $k$ with the Lowest-Field (20,1,0; 19, 1,0) Resonance Cross Section.....	39

## I INTRODUCTION

This report summarizes the results of a research program to study collision processes of Rydberg atoms relevant to their use as an infrared detector. The work was performed under Contract N00014-79-C-0202 over the last three years. The objective has been to systematically investigate the resonant collisions between highly excited states of sodium. The motivation for undertaking these studies has been to study collisional processes that would limit or interfere with the use of Rydberg states as sensitive and selective detectors of far infrared (FIR) and millimeter wave radiation.

The basic idea of using the Rydberg atoms as a highly sensitive, narrow bandwidth, large acceptance angle tunable detector at FIR wavelengths is as follows. Using a resonant laser excitation scheme, it is possible to excite enough atoms to a Rydberg state A so that it is optically thick to the far infrared (FIR) or millimeter radiation connecting state A to a higher state B. Thus an incoming FIR photon at frequency  $\nu_{AB}$  will be absorbed by one of the atoms in the sample and concomitantly make a transition to state B. The atomic transition can be easily detected by selective field ionization (SFI) of the atom in the B state. The intrinsic limit of such an atomic detector is due to collisional processes that lead to the same result--that is, excitation of the atom to state B or its ionization.

The results of this research program to provide understanding of the collisional effects of the Rydberg atoms with each other. In particular, we have extensively studied the resonant collisions between two excited atoms, under a variety of different initial states and conditions. Although the resonant collisions are by no means the only collisional mechanism that limits the performance of atomic FIR detectors, they constitute an important collisional channel.

In this report we review the physics of resonant collisions, then outline the laser excitation scheme and the SFI detection method on which this work is based, and finally, describe the research accomplishments. The papers resulting from this contract are listed in the Appendix.



## II RESONANT COLLISIONS

### A. Resonant Collision of Rydberg Atoms

Resonant collisional energy transfer is a process that has been of interest for some time. In this process, atom (or molecule) A loses as much internal energy as its collision partner atom (or molecule) B gains. Although this subject has been studied theoretically in some detail, both for atomic and molecular collisions,<sup>1-3</sup> the experimental exploration of resonant collisions has been hindered by the necessity of finding chance coincidences in the separations of the energy levels of the collision partners. In spite of this obstacle, considerable insight has been gained into the nature of resonant collisions using the available coincidences.<sup>4,5</sup>

Atomic Rydberg states are well suited for such studies for two reasons. First, for many collision processes they have large cross sections, which should allow the long interaction time necessary to produce sharp collisional resonances. Second, the energy spacings of Rydberg states may be varied in a systematic fashion. The most apparent approach is to vary the energy spacings by studying a progression of  $n$  or  $l$  states, where  $n$  and  $l$  are the principal and orbital angular momentum quantum numbers. Variation of  $n$  has already been used to study resonant electronic-to-vibrational energy transfer from Rydberg states of Na to  $\text{CH}_4$  and  $\text{CD}_4$ ,<sup>6</sup> and electronic-to-rotational energy transfer from Rydberg states of Xe to  $\text{NH}_3$ .<sup>7</sup> The widths of the resonances in these collision cross sections are 50 and 6  $\text{cm}^{-1}$ , respectively, although the exact widths are somewhat uncertain due to the comb-like nature of the energy spacing. In both these cases, at resonance the cross sections are smaller than the geometric size of the excited atom, and the dominant interactions in these collisions is thought to be the quasi-free electron scattering.

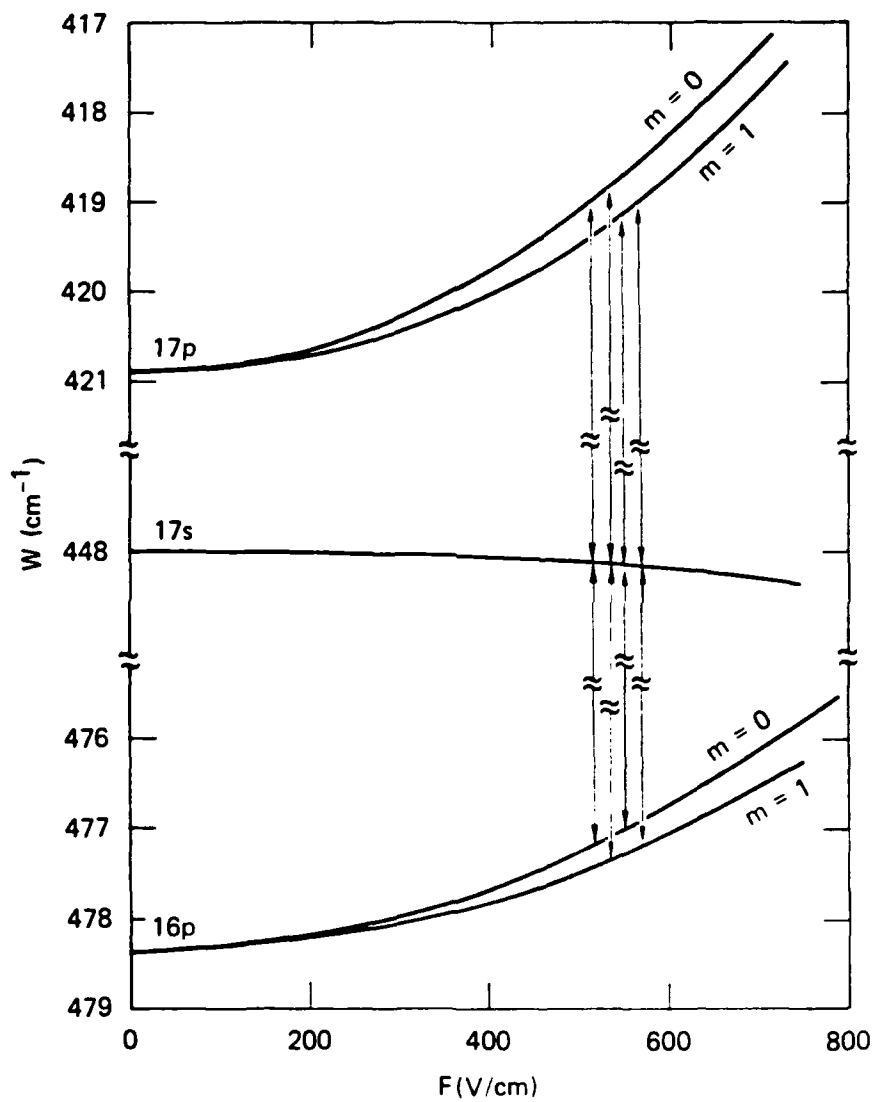
Because Rydberg atoms have large dipole moments, their energies are easily shifted by the application of very modest electric fields, thus allowing the study of resonant collisions with continuous tuning. This report describes experiments in which the electric field tuning of the Na Rydberg process:

$$(ns) + (ns) \rightarrow (np) + [(n-1)p]$$

Sharp resonances representing large transfers of population to the  $np$  and  $(n-1)p$  states from the initially excited  $ns$  states are observed at certain values of the static electric field. These sharp resonances occur when the laser-excited  $ns$  state lies midway between an upper  $np$  and lower  $(n-1)p$  state,<sup>8,9</sup> causing the process  $(ns) + (ns) \rightarrow [(n-1)p] + (np)$  to proceed resonantly because the energy lost by one  $Na(ns)$  atoms exactly equals the energy gained by the other colliding  $Na(ns)$  atom. The energy level diagram for the  $16p-17s-17p$  states in a static electric field is shown in Figure 1. The vertical lines in Figure 1 indicate the four-field values where collisional transfer occurs.

This report also describes the result of our effort to generalize and extend the capability of the electric-field-tuned resonant collisional energy transfer to include Rydberg states other than the  $s$  and  $p$  states of  $Na$ . The relative size of the resonant-collision cross sections for the different initial and final states is also an important check on the dipole-dipole interaction model for these collisions. Specifically, we observe electric-field-tuned resonant collisions of the type  $(ns) + (ns) \rightarrow (np) + (nl)$  or  $(ns) + (np) \rightarrow (nl) + [(n-1)p]$ , where one of the final states is a  $nl$  state ( $l > 2$ ). Although  $l$  is not a good quantum number in an electric field, it still serves as a convenient and unique way to label states (see below). We have also observed a large enhancement in the cross section at relatively low field (approximately  $17 \text{ V/cm}$ ) for the process  $(15d) + (15d) \rightarrow (16f) + (15p)$ , in which a collision between two  $Na(15d)$  atoms results in one atom being excited to a  $16f$  state and the other deexcited to a  $15p$  state. We find that both the cross sections and the linewidths of these resonant processes are comparable in magnitude to the process  $(ns) + (ns) \rightarrow [(n-1)p] + (np)$ .

Cross sections  $\sim 10^3$  times greater than the geometric cross sections of the atoms with resonance widths of  $\sim 0.03 \text{ cm}^{-1}$  are observed. Both of these striking features are consequences of the large dipole moments of the Rydberg atoms, which allow an efficient long range resonant dipole-dipole interaction. Such an interaction, termed a "rotational resonance" by Anderson,<sup>2</sup> has been observed, although not systematically, in molecular resonant rotational energy transfer.<sup>4</sup>



SA-8461-13

FIGURE 1 ENERGY-LEVEL DIAGRAM FOR THE 16p-17s-17p STATES IN A STATIC ELECTRIC FIELD

The vertical lines are drawn at the four fields where the s state is midway between the two p states and the resonance collisional transfer occurs.

## B. Theory of Resonant Collisions

The theory of resonant collisions, as it applies to the experiments described in this report, is best understood by referring to a concrete example. We consider the collisional process for Na,  $ns + ns \rightarrow np + (n-1)p$ , and generalize the results to other cases when appropriate. Consider two two-level atoms, 1 and 2, one in its upper and one in its lower state, as shown in Figure 2. The transition matrix elements for the two atoms at an identical transition frequency  $\omega$  are  $\mu_1$  and  $\mu_2$ , respectively. One of the atoms is assumed to be stationary at the origin and the other, passing the first atom with an impact parameter  $b$  at  $x = 0$ , is moving in the  $x$  direction, perpendicular to the page, with velocity  $v$ . We assume that the second atom travels in a straight line and is not deflected by the collision. In addition, we assume that there is a static electric field in the  $z$  direction. This choice of axes matches our experimental configuration. We construct the product states

$$\psi_A = \psi_1 ns \psi_2 ns \quad (1a)$$

$$\psi_B = \psi_1 np \psi_2 (n-1)p \quad (1b)$$

where  $\psi ns$  describes a Stark state wavefunction that is adiabatically connected to the corresponding zero field  $n, l$  coulomb wavefunction. The total wavefunction for the system may be written as

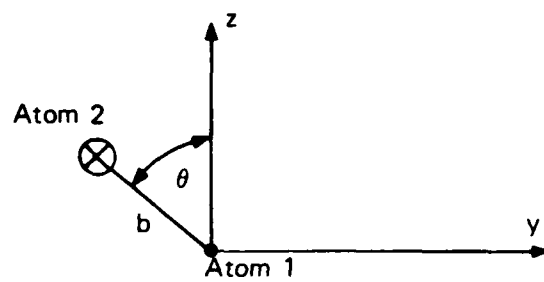
$$\psi(t) = \psi_A C_A(t) + \psi_B C_B(t) \quad (2)$$

where all the time dependence is in the coefficients  $C_A(t)$  and  $C_B(t)$ . The energies of the two states A and B at  $r = \infty$ , where  $r$  is the internuclear separation, are given by

$$W_A = W_{ns} + W_{ns} \equiv 0 \quad (3a)$$

and

$$W_B = W_{np} + W_{(n-1)p} \quad (3b)$$



SA-8461-30A

FIGURE 2 GEOMETRY OF THE COLLISION OF TWO ATOMS  
Atom 1 is at rest at the origin. Atom 2 is moving in the  $x$ -direction, perpendicular to the paper, with velocity  $v$  and impact parameter  $b$ .

which we take to be the eigenvalues of the unperturbed Hamiltonian  $H_0$  of two noninteracting (infinitely separated) atoms in the static electric field. For finite internuclear separations, the states A and B are coupled by the dipole-dipole interaction

$$\langle \psi_A | V | \psi_B \rangle = \langle \psi_A | \frac{\vec{\mu}_1 \cdot \vec{\mu}_2}{r^3} - \frac{3(\vec{\mu}_1 \cdot \vec{r})(\vec{\mu}_2 \cdot \vec{r})}{r^5} | \psi_B \rangle \quad (4)$$

Here  $\vec{r}$  is the vector between the two atoms.

The interaction matrix elements may be simplified by taking the PMS value of Equation (4) over the angle  $\theta$  in Figure 2. The resonances are labeled by the  $|M_e|$  values of final lower and upper p states.<sup>8</sup> Thus, for the (0,0) transition

$$\langle \psi_A | V | \psi_B \rangle = \frac{\langle ns | \mu_1 | np \rangle \langle ns | \mu_2 | n-1p \rangle}{r^3}, \quad (5)$$

which is the product of the two dipole matrix elements divided by  $r^3$ . Similar expressions are obtained for the other resonances.

Inserting the wavefunction of Equation (2) and the Hamiltonian  $H_0 + V$  yields the pair of equations, which for  $V$  real and  $W_A = 0$  may be written as a single equation

$$i\ddot{C}_A + \dot{C}_A \frac{V}{V} = V^2 C_A + iW_B \dot{C}_A \quad (6)$$

$V$  is nearly zero everywhere except where  $r = b$ , where it reaches a maximum. Inspection of a graph of  $V$  versus  $x$  suggests the approximation

$$V = \frac{\chi}{b^3} \text{ for } -\frac{b}{2} < x < \frac{b}{2} \quad (7)$$

$$V = 0 \text{ elsewhere.}$$

Here  $\chi = \langle ns | \mu_1 | np \rangle \langle ns | \mu_2 | (n-1)p \rangle$ . This makes the  $\dot{V}/V$  term  $\equiv 0$  and suggests choosing the time origin so that the interaction time is  $0 < t < b/v$ . Thus the problem is reduced to precisely the magnetic resonance problem described by Ramsey.<sup>10</sup>

Initially both atoms are in the  $s$  state; thus,  $C_A(0) = 1$  and  $C_B(0) = 0$ . With these initial conditions, for  $0 < t < b/v$ ,  $C_A$  and  $C_B$  are given by

$$C_A(t) = \left( \cos\left(\frac{\alpha t}{2}\right) \frac{-iW_B}{\alpha} \sin\left(\frac{\alpha t}{2}\right) \right) e^{\frac{iW_B t}{2}} \quad (8)$$

and

$$C_B(t) = \frac{-i2\chi}{b^3 \alpha} \sin\left(\frac{\alpha t}{2}\right) e^{\frac{iW_B t}{2}} \quad (9)$$

where  $\alpha = (W_B^2 + r\chi^2/b^6)^{1/2}$ . The probability  $P$  of finding the atoms in the two  $p$  states is given by  $C_B^2(b/v)$ . Thus we may write the probability as

$$P = \frac{4\chi^2/b^6}{W_B^2 + 4\chi^2/b^6} \sin^2 \frac{1}{2} [W_B^2 + \frac{4\chi^2}{b^6}]^{1/2} \frac{b}{v} \quad (10)$$

For  $P = 1$  at resonance ( $W_B = 0$ ), this defines an impact parameter  $b_0$

$$b_0^2 = 2\chi/\pi v \quad (11)$$

The cross section is given by

$$\sigma = \int_0^\infty 2\pi b P(b) db \quad (12)$$

Taking  $P = 1/2$  for  $b < b_0$  to approximate the rapid oscillations and numerically integrating Equation (12) for  $b > b_0$ , we find

$$\sigma = 2.3\pi b_0^2 \quad (13)$$

From Equations (10) and (11) it is apparent that the width of the resonances is given by

$$\Delta(\text{FWHM}) = \frac{4\chi}{b_0^3} = \frac{2\pi v}{b_0} = \left( \frac{2\pi^3 v^3}{\chi} \right)^{1/2} \quad (14)$$

To evaluate the cross sections and collision widths, we must use the actual values of the average collision velocity  $\bar{v} = 1.6 \times 10^{-4}$  and dipole moments  $\mu_1 = \mu_2 = 0.60 \text{ n}^*2$ . Here  $\text{n}^*2$  is the effective quantum number of the  $ns$  state of binding energy  $W = -1/2\text{n}^*2$ . Using our results, Equations (13) and (14), these values lead to cross sections and widths (FWHM) given by

$$\sigma = 1.03 \times 10^4 n^{*4} \quad (15)$$

and

$$\Delta = 2.64 \times 10^{-5} n^{*-2} \quad (16)$$

In laboratory units

$$\sigma = 2.90 \times 10^3 n^{*4} \text{ \AA}^2 \quad (17)$$

and

$$\Delta = 1.74 \times 10^2 n^{*-2} \text{ GHz} \quad (18)$$

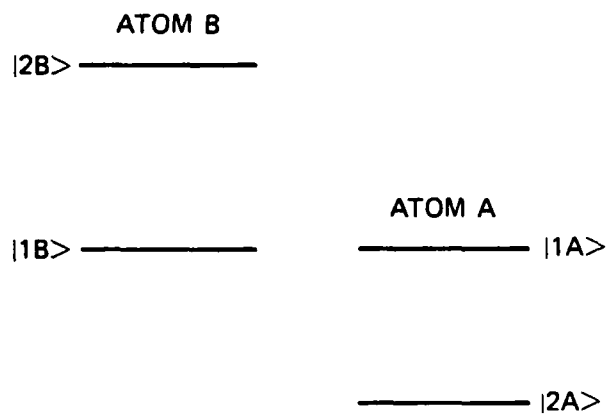
### C. Resonant Collisions of ns, nD, and nf States

The energy level diagram of two colliding atoms (which need not even be of similar species) is shown in Figure 3. The relevant energy levels are  $|1A\rangle$  and  $|2A\rangle$  for atom A and  $|1B\rangle$  and  $|2B\rangle$  for atom B. The pair of states  $|1A\rangle$  and  $|2A\rangle$  are, in principle, any pair for which  $\langle 2A | \mu | 1A \rangle \neq 0$ , where  $\mu$  is the electric-dipole-moment operator; this applies similarly to  $|1B\rangle$  and  $|2B\rangle$ .

An additional requirement for the resonant-collision process, in fact the most basic requirement, is that the condition  $W_{1A} - W_{2A} = W_{2B} - W_{1B}$  be satisfied at some value of the electric field. Figure 4 shows one of the several pairs of states for which these two basic requirements for resonant collisions is satisfied. For instance, as shown in Figure 4, we consider the pair of states  $|1A\rangle = |1B\rangle = 20s$ ,  $|2A\rangle = 19p$  ( $|m|=0$ ), and  $|2B\rangle = (n=19, \ell=18)$ . To simplify the notation the manifold of Stark states shown in Figure 4 (solid lines) near  $19d$  (long-dashed line above the  $20s$  state) is labeled by the  $n, \ell$  quantum numbers. Although  $\ell$  is no longer a good quantum number in the presence of a static electric field, the linear Stark states are adiabatically connected to the zero-field  $n\ell|m|$  states in a unique way. For instance, the Stark state with the lowest (highest) energy in the manifold is adiabatically connected to the zero-field state with the lowest (highest)  $\ell$ . Similarly, states that fall between the two extreme members of the manifold are adiabatically connected to the zero-field states with intermediate values of  $\ell$ . The



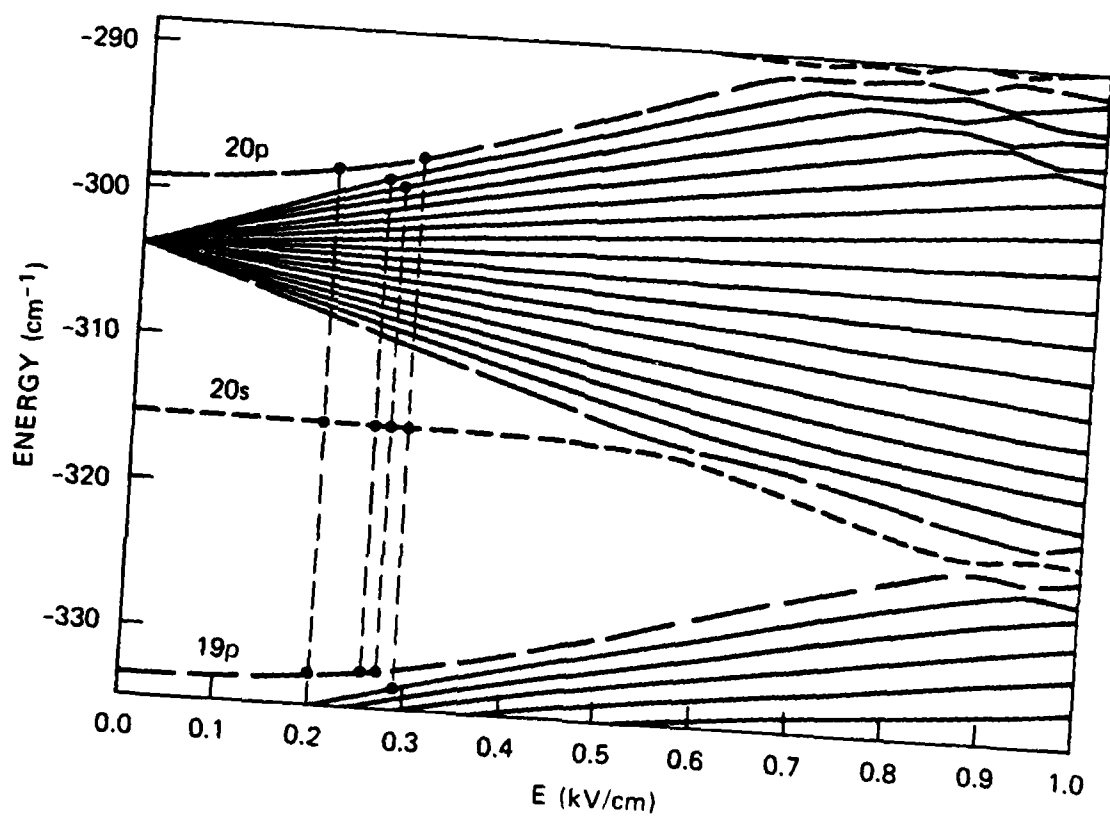
state with the highest energy in the  $n=19$  manifold is therefore labelled  $n = 19, l = 18$ . In the above example  $\mu_1 = \langle 19p | u | 20s \rangle \approx 200$  a.u. is quite large. Although the dipole matrix element  $\mu_2$  connecting  $20s$  to the  $n = 19, l = 18, |m| = 0$  state of the Stark manifold is zero in zero field (dipole selection rule), it can be quite large when a relatively low electric field is applied. For instance, calculations show that  $\mu_2 \approx 80$  a.u. at  $E = 300$  V/cm due to the Stark mixing. Calculations of the Stark shift show that the resonance condition for the process  $(20s) + (20s) \rightarrow (19p) + (n=19, l=18)$  is satisfied at  $E = 268$  V/cm. Here  $|m| = 0$  for both the final states. Using the calculated value of  $\mu_2 \approx 80$  a.u. (at 268 V/cm) and  $\mu_1 = 200$  a.u., we obtain  $\sigma \approx 10^9 \text{ \AA}^2$ . This cross section is comparable to the cross section for the process  $(20s) + (20s) \rightarrow (19p) + 20p$  and is easily observed. Similar calculations for the general process  $(20s) + (20s) \rightarrow (19p) + n=19, l$  or  $(20s) + (20s) \rightarrow (20p) + (n=18, l)$  show that the cross section is quite large.



SA-8461-57

FIGURE 3 SIMPLIFIED ENERGY-LEVEL DIAGRAM CONSIDERED FOR THE  
RESONANT-COLLISION PROCESS

Atoms A and B (which could even be of different species) have energy levels  $|1A\rangle$ ,  $|2A\rangle$  and  $|1B\rangle$ ,  $|2B\rangle$ , respectively. These energy levels are tuned (Stark-shifted) by the static electric field.



SA-8461-59A

FIGURE 4  $|m_l| = 0$  STATES OF Na NEAR THE 20s STATE

First vertical dashed lines on the left shows the  $|2A\rangle$  and  $|2B\rangle$  states for the resonant process  $(20s) + (20s) \rightarrow (19p) + (20p)$ . Second vertical line corresponds to the  $|2A\rangle$  and  $|2B\rangle$  states for the observed collision process  $(20s) + (20s) \rightarrow (19p) + (n = 19, l = 18)$ . Solid line just below the 20p (19p) state corresponds to  $n = 19, l = 18$  ( $n = 18, l = 17$ ) Stark state.

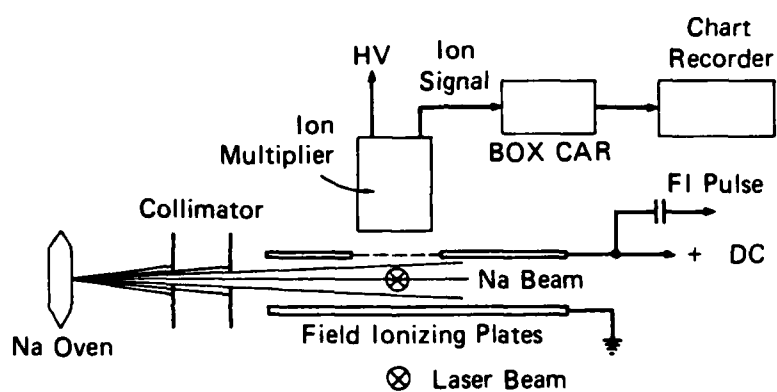
### III EXPERIMENTAL APPROACH

In the experiments described in this report, an effusive beam of Na passes between a plate and a grid as shown in Figure 5. The atoms are excited in a two-step process by two pulsed dye lasers; the first, yellow, laser is tuned to the 3s-3p transition at  $5890 \text{ \AA}$ , and the second, blue, laser is tuned to the 3p-ne transition at  $\sim 4140 \text{ \AA}$ . The laser excitation and subsequent collisions occur in a dc electric field that ranges from 10-800 V/cm in these experiments. At a variable time after the laser excitation, a positive high voltage pulse is applied to the field plate ionizing the Rydberg atoms and accelerating the resulting ions into the electron multiplier. The electron multiplier signal is averaged using a boxcar averager and recorded with a chart recorder.

The selectivity of electric field ionization<sup>11</sup> enables us to identify states present at the time the field ionizing pulse is applied. Thus we are able to monitor the populations in the ns, np, (n-1)p, nd, (n-1)d, or the (n-1)f states as functions of time after the laser pulse and dc electric field.

The atomic beam is collimated to a 0.4-cm diameter in the interaction region, has a density of  $\sim 10^8 \text{ cm}^{-3}$ , and is assumed to have the modified Maxwellian velocity distribution characteristic of a  $500^\circ\text{C}$  beam. The laser beams are focussed to 0.5 mm diameter in the interaction region, are usually approximately collinear, and cross the atomic beam at right angles as shown in Figure 5. With both laser beams crossing the atomic beam at  $90^\circ$ , the excitation volume is a cylinder of volume  $10^{-3} \text{ cm}^3$ . Typical densities of excited atoms are  $\sim 10^6 \text{ cm}^3$ .

The electron multiplier gain is measured to be  $5 \times 10^3$  and has a specified quantum efficiency of 30%. Including the 20-db (power) gain of the amplifier after the multiplier, we find that overall, one Rydberg atom leads to  $\sim 1.9 \times 10^{-15}$  coulomb of signal.



SA-8461-60

FIGURE 5 SCHEMATIC OF THE EXPERIMENTAL SETUP

Two dye-laser pulses which prepare either the ns or the nd state cross the effusive Na beam at right angles. A 0.3- $\mu$ s-risetime-pulsed field ionizes the atoms selectively and pushes the ions through a mesh into an ion multiplier.

#### IV RESEARCH ACCOMPLISHMENTS

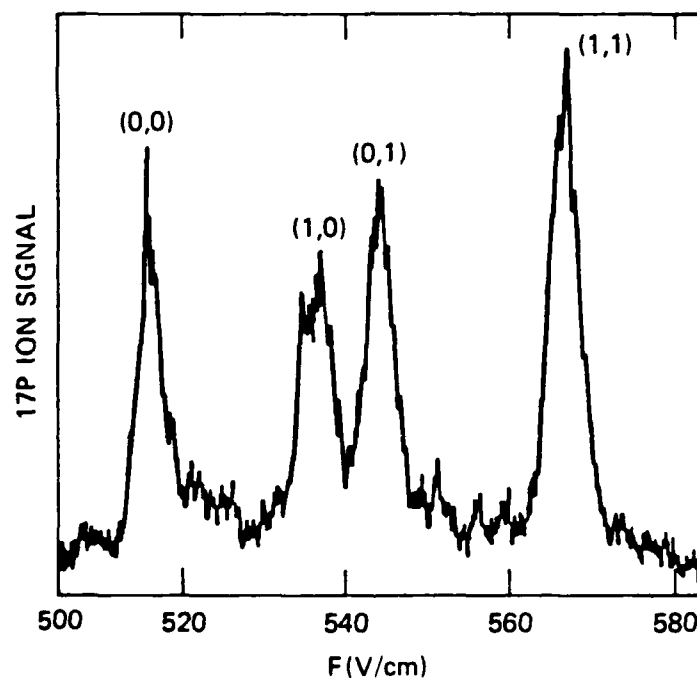
##### A. Resonant Collisions of Two np Rydberg Atoms

Before describing in detail the cross section measurements, it is useful to present qualitative observations that both identify the collision process and suggest the method used to measure the cross sections. The most striking feature of our observations is the sharply resonant increase in the populations when the levels are tuned into resonance with the field. An example is shown in Figure 6, which is a recording of the population in the 17p state as a function of dc field 2  $\mu$ s after the 17s state is populated by the lasers. The sharp increases in signal at 516 V/cm, 537 V/cm, 544 V/cm, and 566 V/cm are due to the resonant  $17s + 17s \rightarrow 16p + 17p$  collisions that occur as shown in Figure 1. As mentioned earlier, the resonances are labeled by the  $|m_l|$  values of the final lower and upper p states, which are determined from the field ionization behavior of the signal in the lowest n states studied. The resonant signal is approximately quadratic in the power of the blue laser, whereas the total population is linear, as shown by Figure 7. This suggests that the resonant signal is either due to an effect that depends on collisions with photoions produced by the absorption of two blue laser photons or to an effect varying as the square of the number of excited atoms. Since there are no photoions observed, we can immediately rule out the first possibility. Considering the small size of photoionization cross sections for Rydberg atoms by visible photons<sup>12</sup> and the likelihood of a resonant process, this seems unlikely in any case.

##### B. Measurement of the (ns) + (ns) $\rightarrow$ (np) + (n-1)p Cross Sections

If we allow collisions to occur for a time T during which time a small fraction of the initial population in the ns state is collisionally transferred to the np and (n-1)p states, then the population  $N_p$  in the np (and n-1)p state will be given by

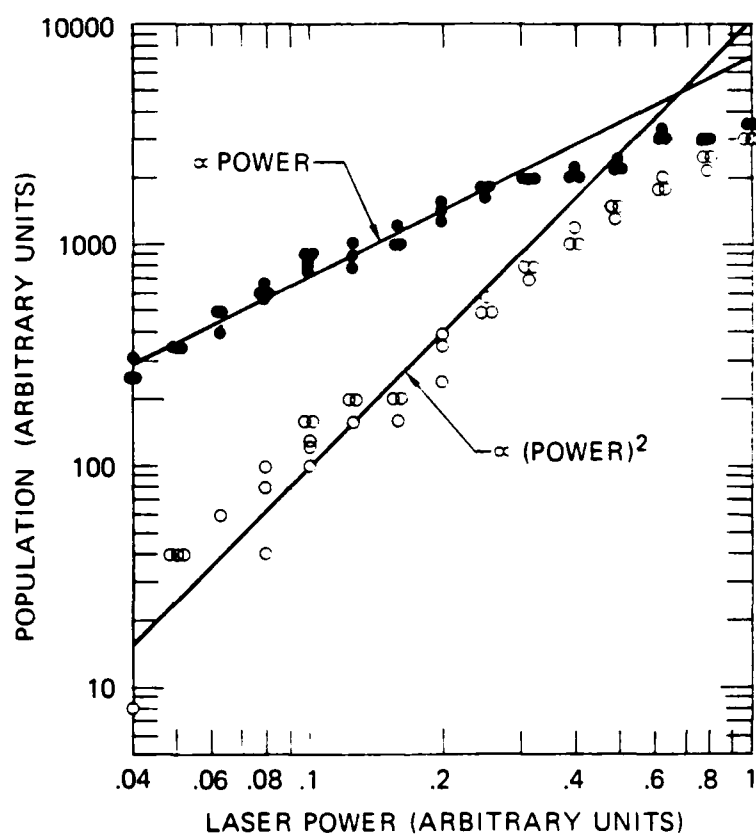
$$N_p = \frac{N_s^2 \sigma \bar{v} T}{V} \quad (19)$$



SA-8461-14

FIGURE 6 THE OBSERVED 17p ION SIGNAL AFTER POPULATION OF THE 17s STATE VERSUS dc ELECTRIC FIELD, SHOWING THE SHARP COLLISIONAL RESONANCES

The resonances are labeled by the  $|m_l|$  values of the lower and upper p states.



SA-8461-18

FIGURE 7 THE BLUE-LASER-INTENSITY DEPENDENCE OF THE 17p RESONANT COLLISION SIGNAL (○) AND 17s SIGNAL (●) AFTER POPULATION OF THE 17s STATE SHOWING THE QUADRATIC DEPENDENCE OF THE RESONANT SIGNAL



where  $N_s$  is the initial ns state population,  $\sigma$  is the cross section for the process,  $\bar{v}$  is the average collision velocity, and  $V$  is the sample volume.

Eq. (19) may be easily inverted to give the cross section. In doing so, it is convenient to replace  $N_s$  and  $N_p$  by the observed signals  $N'_s$  and  $N'_p$ , which are related to  $N_s$  and  $N_p$  by  $\Gamma$ , the overall sensitivity. Thus we may write

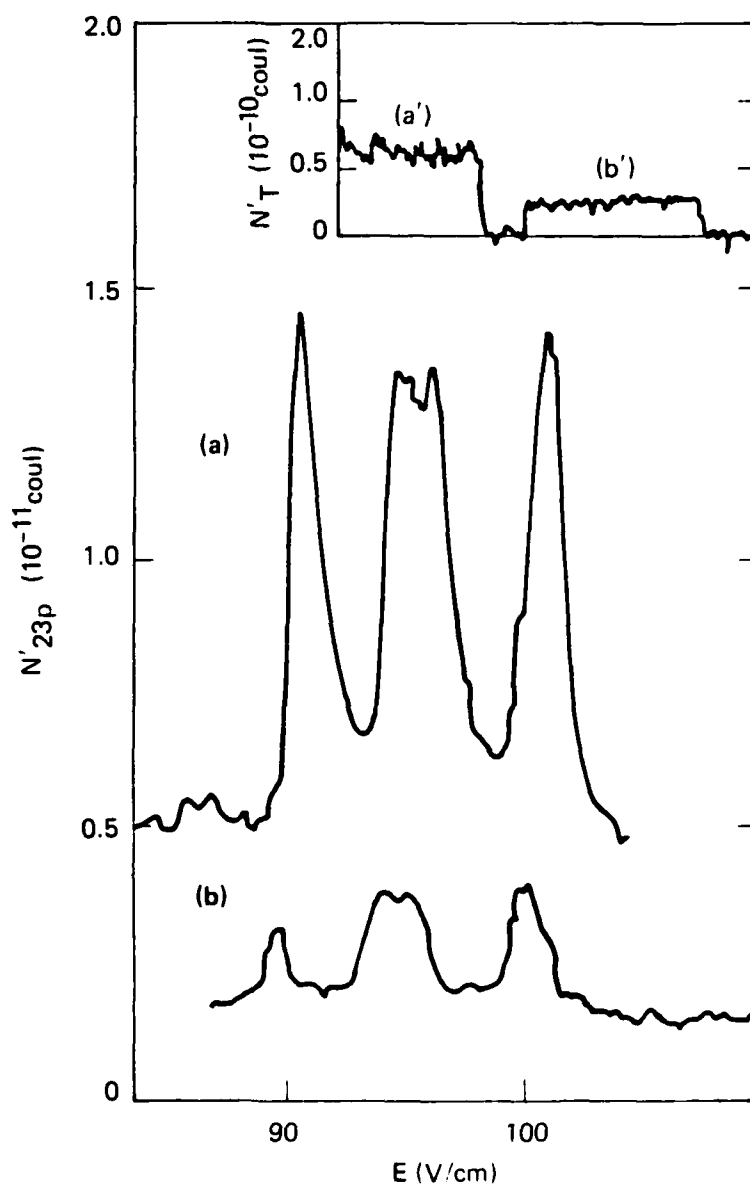
$$\sigma = \frac{N'_p}{N'^2_s} \frac{V}{\Gamma \bar{v} T} \quad (20)$$

By measuring the ratio  $N'_p/N'^2_s$  as a function of  $n$ , we may determine with good accuracy the  $n$  dependence of the cross section. Measurements of the quantities in brackets give the absolute cross sections. Because of the large difference in the fields at which the Na ns and np states ionize, these two are in all cases easily time resolved. Because of the small difference in the fields at which the ns and  $(n-1)p$  states ionize, these are not always clearly resolved under these conditions; however, this has no effect on the determination of the cross sections. With a 50-ns-wide gate we observe only the np state signal, which comes first, yielding  $N'_p$ , and with a 500-ns-wide gate we observe at the same time the entire ion signal,  $N'_T$ , from the np, ns, and  $(n-1)p$  states.

A typical example of a sweep through the collisional resonances is shown in Figure 8 for the excitation of the 23s state for two laser powers. Figures 8a and 8b are recordings of  $N'_{23p}$ , the number of atoms in the 23p state at two laser powers. Figures 8a' and 8b', in the inset, show the corresponding simultaneous measurements of  $N'_T$ , the number of atoms in the 22p, 23s, and 23p states, and these values are clearly unaffected by the collisional resonances. In Figures 8a and 8b, the quadratic dependence of the resonant signal on blue laser power is quite apparent, whereas the background (nonresonant) signal in Figures 8a and 8b as well as the signal in Figures 8a' and 8b' are clearly linear.

Table I gives the values of the electric field positions at which the resonances occur. Figure 9 shows the  $n$  dependence of the positions of the  $(0,0)$  and  $(1,1)$  resonances, whose locations are given by

$$1.21(2)n^{*-5.34(5)} \text{ V/cm} \quad (21a)$$



SA-8461-28A

FIGURE 8 (a) THE POPULATION OF THE 23p STATE  $2 \mu s$  AFTER THE POPULATION OF THE 23s STATE SHOWING THE COLLISIONAL RESONANCES

Notice that the (0, 1) and (1, 0) resonances are not resolved in this trace.

(b) The same as (a) except with 40% of the blue-laser power. (a') A recording of the total populations in the 23s, 22p, and 23p states taken simultaneously with (a). (b') A recording of the total populations in the 23s, 22p, and 23p states taken simultaneously with (b).

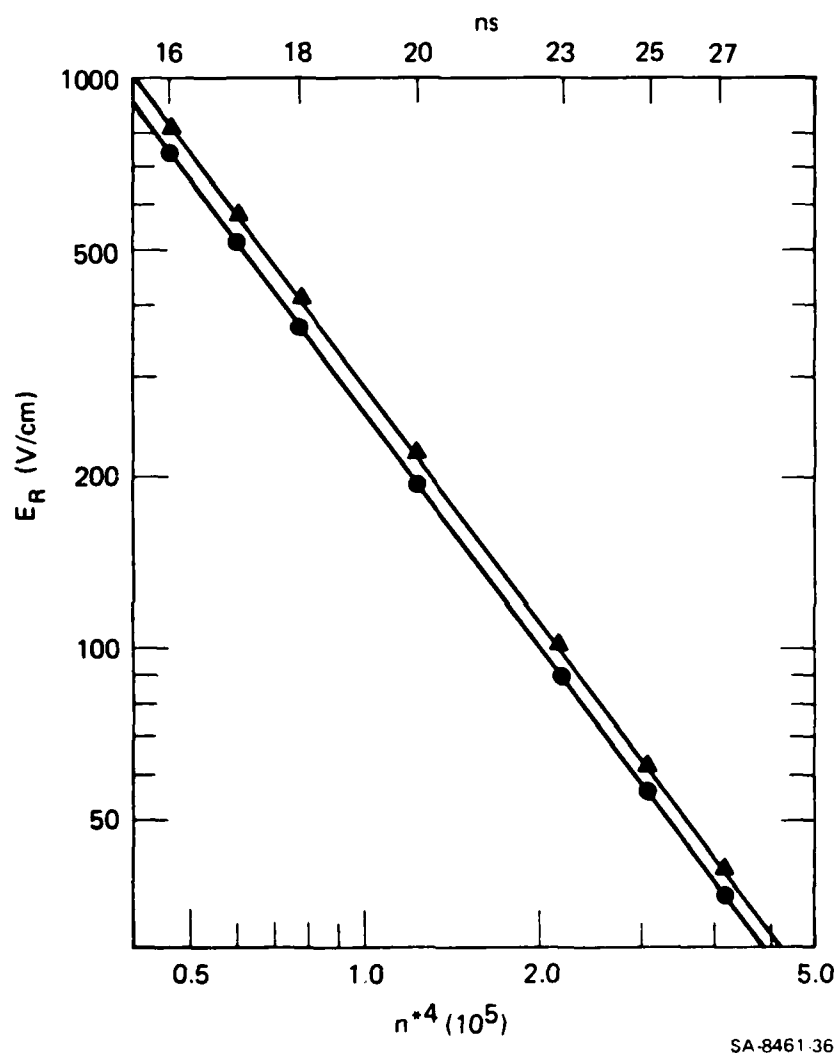


FIGURE 9 THE POSITIONS OF THE 0,0 (●) AND 1,1 (▲) RESONANCES

Table I  
POSITIONS OF THE RESONANCES

ns State/Resonance	(V/cm)			
	0,0	0,1	1,0	1,1
16s	741(15)	770(15)	781(15)	813(16)
17s	516(10)	537(10)	544(10)	566(10)
18s	364(8)	387(8)	393(8)	405(8)
20s	201(4)	210(4)	214(4)	222(4)
23s	91(2)	94.5(20)	95.9(20)	100(2)
25s	56.5(13)	--59.0(13) <sup>a</sup> --		63.1(14)
27s	36.6(8)	--38.7(8) <sup>a</sup> --		41.1(8)

<sup>a</sup>The average location of the unresolved 0,1 and 1,0 resonances.

and

$$E_R(1,1) = 1.42(2)n^{*-5.35(5)} \text{ V/cm} \quad (21b)$$

The field width (FWHM) of the resonances are given in Table II. Note that these widths are not appreciably broadened by spatial inhomogeneities in the applied dc field.

Physically, it is the frequency width of the resonances in which we are really interested, and we have used an approximate method, based on a suggestion of Cooke.<sup>13</sup> The frequency widths of the resonances are given in Table III. The widths of the resonances are the sum of the collisional width and unresolved fine structure as shown in Figure 10. Note that the  $|m_l| = 1$  states are split by  $\Delta_{fs}$ , which is given by

$$\Delta_{fs} = \frac{\Delta_{fso}}{3} \cdot k \quad (22)$$

where  $\Delta_{fso}$  is the fine structure interval of the zero field p state and k is the amount of p character remaining in the nominal p state in the electric field. At these fields  $k \sim 0.85$  and  $0.73$  for the lower and upper p states, respectively. From Figure 10 it is clear that the (0,0) resonance reflects only the collisional width; the other resonances have additional width from the unresolved fine structure. Figure 11 plots the difference in the observed widths,  $\Delta(1,1) - \Delta(0,0)$ ,  $n^{*4}$  and shows the calculated value of  $\Delta_{fs \text{ upper}} + \Delta_{fs \text{ lower}}$ , which is in good agreement with the data. In calculating  $\Delta_{fs \text{ upper}}$  and  $\Delta_{fs \text{ lower}}$ , we have used the previously determined np fine structure intervals.<sup>14</sup>

From the previous discussion it is clear that the (0,0) resonance is the only good probe of the collision width. The  $n^*$  variation of the width of the (0,0) resonance (FWHM) is given by

$$W(0,0) = 235(40)n^{*-1.95(20)} \text{ (GHz)} \quad (23)$$

Figure 12 plots the observed widths of the (0,0) resonance and calculated dependence from Eq. (26). Note that  $\Delta(0,0)$  scales as  $n^{*(1.9)}$ , in agreement with the predicted  $n^{*2}$  scaling, and is in reasonable agreement with the calculated magnitude. To simplify the presentation, we have corrected the observed

Table II

## FIELD WIDTHS OF THE RESONANCES

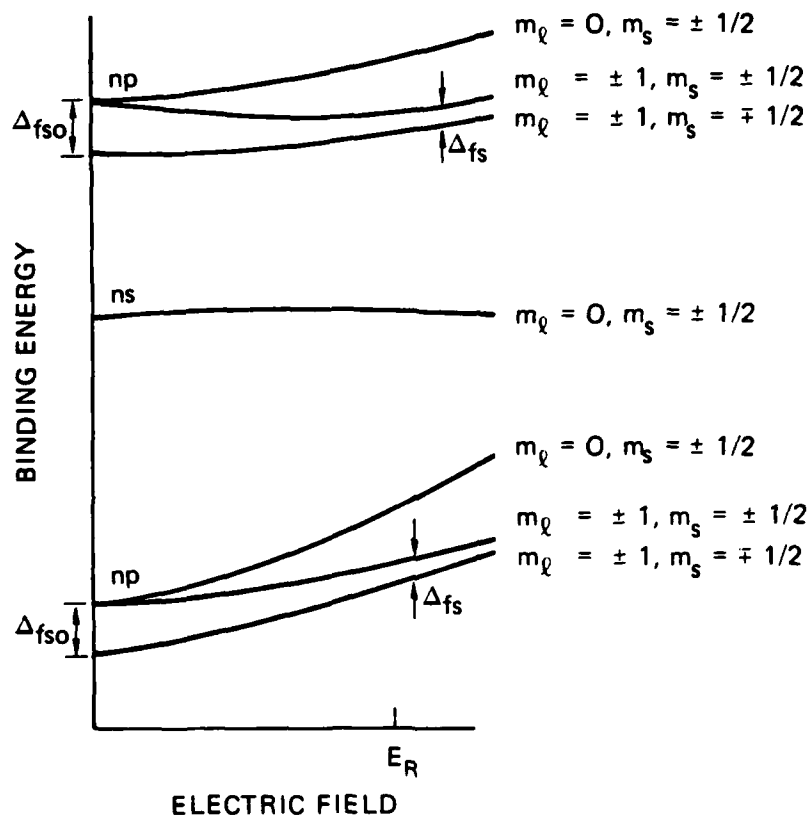
(V/cm)

ns State/Resonance	0,0	0,1	1,0	1,1
16s	4.0(8)	6.7(14)	4.6(9)	7.2(14)
17s	3.4(7)	4.8(10)	4.2(8)	5.3(11)
18s	2.7(6)	4.0(8)	3.6(8)	3.9(8)
20s	1.8(4)	2.7(4)	2.7(5)	2.4(5)
23s	1.35(50)	---	---	1.45(30)
25s	0.8(2)	---	---	1.15(22)
27s	0.55(20)	---	---	0.67(140)

Table III

## FREQUENCY WIDTHS OF THE RESONANCES

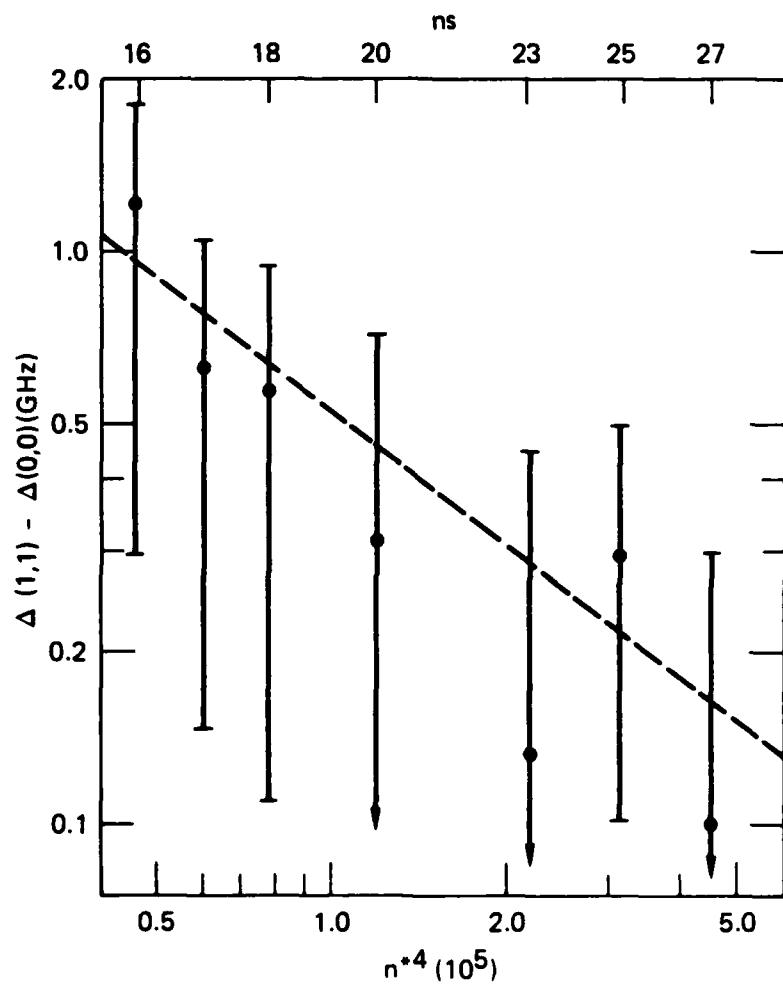
<u>ns State/Resonance</u>	(GHz)			
	<u>0,0</u>	<u>0,1</u>	<u>1,0</u>	<u>1,1</u>
16s	1.11(25)	1.95(50)	1.32(34)	2.31(6)
17s	1.08(23)	1.53(40)	1.34(40)	1.70(42)
18s	0.94(20)	1.45(35)	1.31(40)	1.52(38)
20s	0.77(16)	1.19(30)	1.19(30)	1.08(27)
23s	0.74(16)			0.88(22)
25s	0.50(12)			0.81(20)
27s	0.40(10)			0.51(13)



SA-8461-31

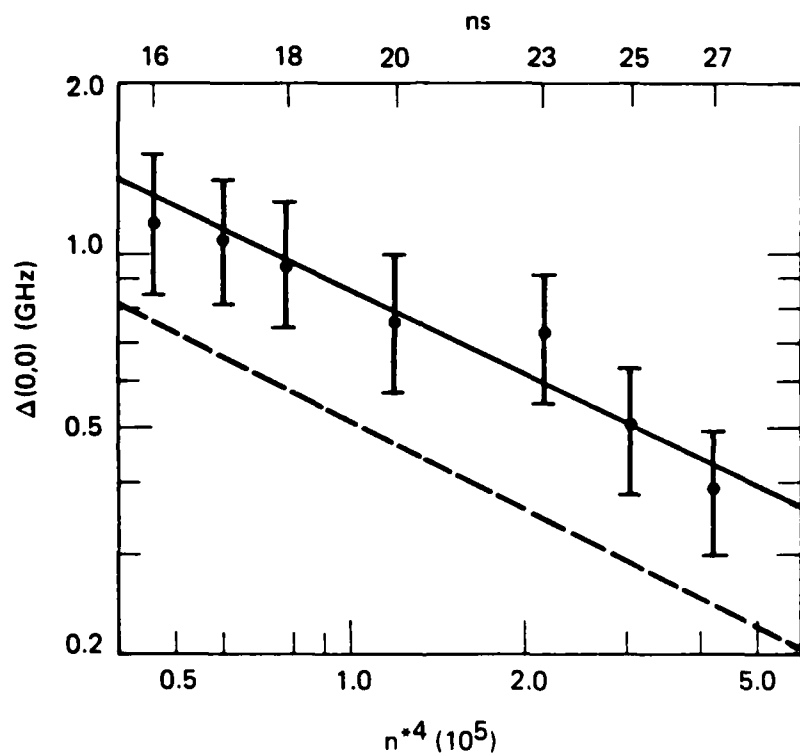
FIGURE 10 THE FINE-STRUCTURE LEVELS IN ZERO FIELD AND AT THE FIELD OF THE COLLISIONAL RESONANCES





SA-8461-35

FIGURE 11 THE DIFFERENCE IN WIDTHS OF THE 1,1 AND 0,0 RESONANCES (●) AND A PLOT OF THE CALCULATED VALUE OF  $\Delta_{fs}$  (---)



SA-8461-34

FIGURE 12 THE WIDTHS OF THE 0,0 RESONANCES (●), THE FIT CURVE (—), AND A PLOT OF THE CALCULATED DEPENDENCE (---)

$N'_p/N'_s$  ratios to account for s state depletion; these are presented in Table IV, along with the radiative lifetimes of the ns states. The  $N'_p/N'_s$  ratios are proportional to the cross sections and give the variation of the cross sections with n.

By evaluating the quantity in the braces of Eq. (30), we obtain absolute values for cross sections. The values used are  $\Gamma = 5.2 \times 10^{14}$  atoms/coulomb,  $T = 1 \mu s$ ,  $\bar{v} = 3.5 \times 10^4$  cm/s, and  $V = 10^{-3}$  cm<sup>3</sup>. We estimate the errors in this normalization to be at most of a factor of five. With the error bars of the relative cross sections from Table IV, the observed cross sections can be expressed as

$$\sigma = 3.3(6) \times 10^4 n^{3.7(5)} \text{ \AA}^2 \quad (24)$$

which is in good agreement with the calculated values of Section II.

Figure 13 plots the observed cross sections and the theoretical result, Equation (17), logarithmically  $n^{*4}$ .

#### C. Generalized Resonant Collision of Rydberg Atoms

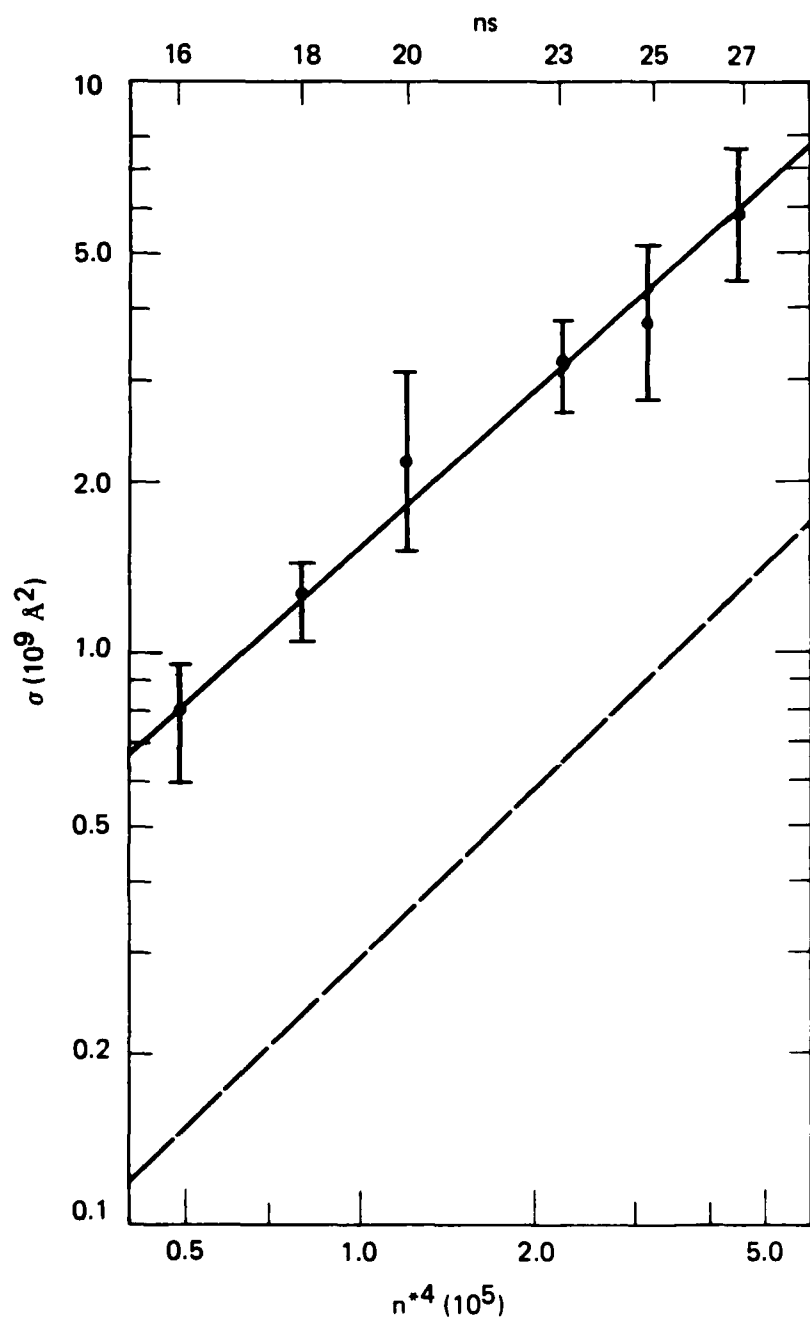
We first describe the resonant collision process  $(20s) + (20s) \rightarrow (19p) + (191)$  or  $(20s) + (20s) \rightarrow (20p) + (181)$ . Note that 1 is used as a label for the energy eigenstates to simplify the notation. Although we have observed the resonant collision process from other ns states ( $n = 18-24$ ), we describe here the observations made with the 20s state. Resonant collisions between Na atoms in other ns states ( $n = 18-24$ ) give qualitatively similar results.<sup>15</sup> Figure 14 shows the trace of the ion signal that represents the population in the 20p state or the 191 state as the static electric field is increased. The three resonances on the left-hand side are the collisional resonances described in the previous section and correspond to the ns state lying midway between the np and the  $(n-1)p$  state. In Figure 14 the second feature on the left-hand side consists of two unresolved resonances (see below). The sharp increases in the ion current represent large collisional transfers to the 20p state. Since the 20p state and 191 states with high-l field ionize at a lower field than does the initially excited 20s state, we set the amplitude of the field-ionization pulse so that only the 20p and the high-l states of the  $n=19$  manifold are field-ionized. In this way we obtain a signal only if the atoms

Table IV  
RADIATIVE LIFETIMES, RELATIVE AND ABSOLUTE CROSS SECTIONS

<u>State</u>	<u>Lifetime<sup>a</sup> (<math>\mu</math>s)</u>	<u><math>N'_p/N'^2_s</math> (Relative Cross Section (<math>10^9 \text{ coul}^{-1}</math>))</u>	<u><math>\sigma</math> (<math>10^9 \text{ \AA}^2</math>)</u>
16s	4.34	1.45(35)	0.78(18)
18s	6.37	2.31(23)	1.25(13)
20s	8.96	4.0(12)	2.16(66)
23s	14.0	6.0(9)	3.2(5)
25s	18.3	7.1(19)	3.8(10)
27s	23.3	10.7(33)	5.8(18)

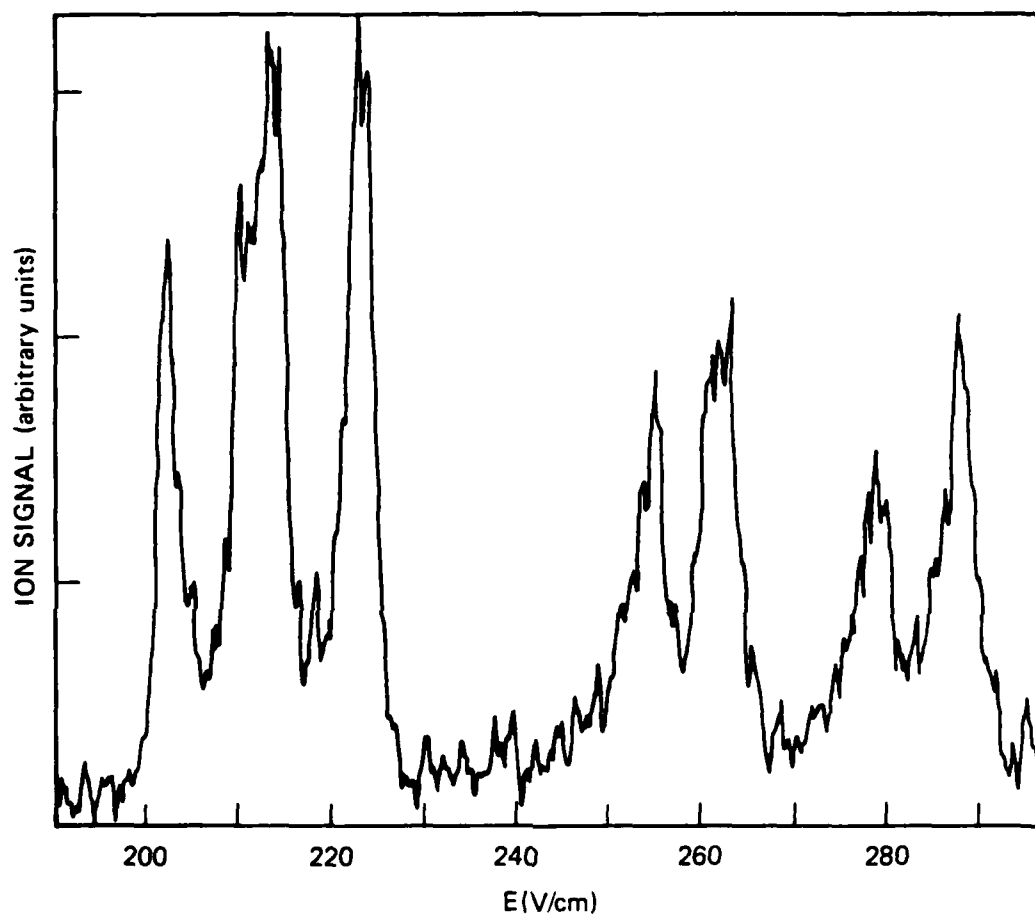
---

<sup>a</sup>See Reference 22.



SA-8461-33

FIGURE 13 THE OBSERVED CROSS SECTIONS WITH THEIR RELATIVE ERROR BARS (●), THE FIT CURVE (—), AND THE CALCULATED DEPENDENCE (---)



SA-8461-55

FIGURE 14 PLOT OF ION CURRENT AS A FUNCTION OF THE APPLIED STATIC FIELD FOR THE Na ATOMS INITIALLY EXCITED TO THE  $20s$  STATE

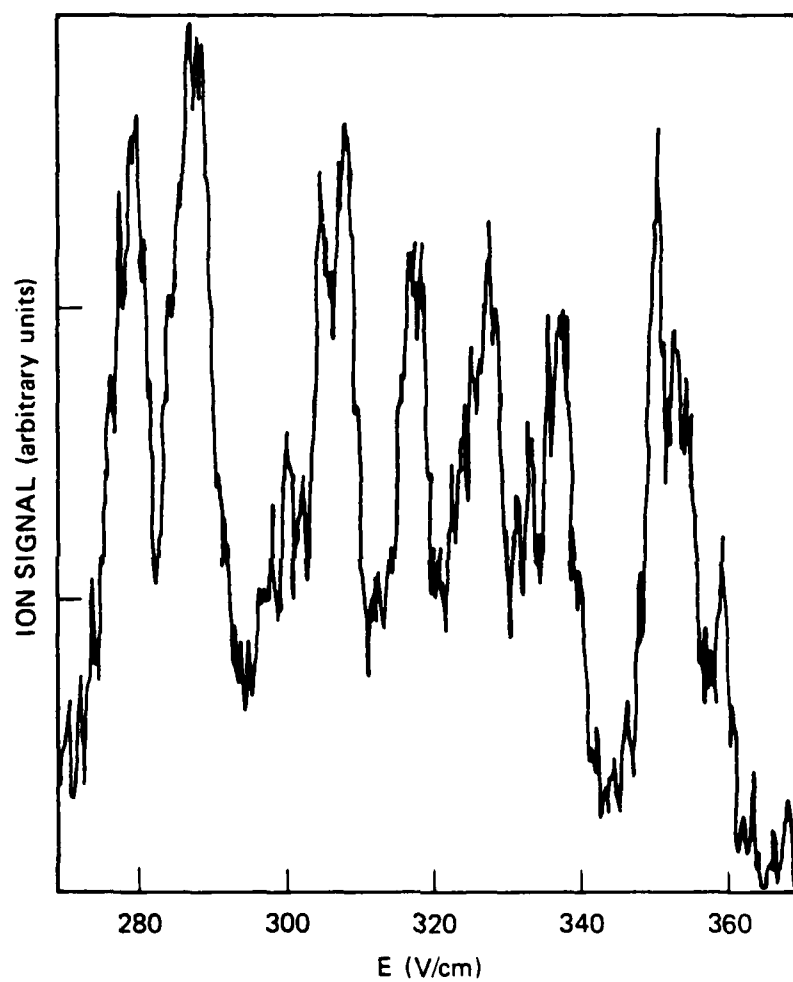
Sharp resonances show the large transfer of population into the  $20p$  state or the high- $\ell$  states ( $\ell = 18$  or  $17$ ) or the  $n = 19$  manifold.

end up in the 20p or the nearby high- $l$  states of  $n=19$  manifold. Note that the  $|m_1| = 0$  and 1 splitting of the p states leads to four resonances. We label these resonances by the pair of  $n, l, |m_1|$  values for the lower and upper states. At this point we note that experimentally we only observe the transfer of population to the upper state (state with the higher energy). We assign the other final state involved in the collision process by calculating the Stark shift<sup>16</sup> of the relevant states.

The resonances recorded in Figure 14 are labeled, in the order of increasing field, as follows: (19,1,0;20,1,0), observed at 202 V/cm; [(19,1,1;20,1,0) and (19,1,0;20,1,1)] observed at 212 V/cm; and (19,1,1;20,1,1) observed at 223 V/cm. The square brackets indicate that the two calculated resonances contained inside are experimentally unresolved. The pair of three numbers in the brackets corresponds to the  $n, l, |m_1|$  quantum numbers of the two final states involved in a given resonance. For instance, the first resonance in Figure 14 is labeled as (19,1,0;20,1,0) where  $|1A\rangle = |1B\rangle = 20s = (20,0,0)$ ,  $|2A\rangle = (19,1,0)$ , and  $|2B\rangle = (20,1,0)$ . In Figure 14, when the electric field is increased beyond 250 V/cm, additional sharp resonances appear. These resonances indicate a large transfer of population into either the 20p state or the high members of the  $n=19, l \geq 2$  manifold. The blue-laser-intensity dependence of these resonances (at lower laser power) shows that the observed signal is quadratic (to within  $\pm 10\%$ ) in laser intensity, implying that the observed resonances are collisional signals involving two Na(ns) atoms.

Collisional resonances observed at even higher fields are shown in Figure 15. Since the field-ionization thresholds for the 20p and the higher energy state of the  $n=19$  manifold are almost identical, it is frequently difficult to distinguish between these states using our experimental detection scheme. However, we can accurately calculate the Stark shift<sup>16</sup> of these states and assign two unique initial and final  $n, l, |m_1|$  labels to each of the sharp resonances seen in Figure 14. For instance, the first resonance (at  $E = 255$  V/cm) on the high-field side of the previously observed resonant-collision resonances is labeled [(19,18,0;19,1,0),(19,18,1;19,1,0)]. Again, the pair of resonances in the square brackets indicates that these resonances are experimentally unresolved.

Table V shows the calculated positions of the four high-field resonances seen in Figure 14 in terms of the static electric field. Similarly, the



SA-8461-56

FIGURE 15 COLLISIONAL RESONANCES SIMILAR TO FIGURE 14  
OBSERVED WITH 20s ATOMS AT HIGHER FIELDS



Table V

CALCULATED AND OBSERVED POSITIONS OF THE RESONANCES  
IN TERMS OF THE APPLIED DC FIELD (V/cm).

Resonance	Electric Field (V/cm)	
	Observed Position	Calculated Position
(20,1,0;19,1,0)	202(3)	202
(20,1,0;19,1,1)	212 <sup>a</sup>	210
(20,1,1;19,1,0)		213.7
(20,1,1;19,1,1)	223(3)	222.8
(19,18,0;19,1,0)	255 <sup>a</sup>	253
(19,18,1;19,1,0)		255
(19,18,0;19,1,1)	260 <sup>a</sup>	260
(19,18,1;19,1,1)		262
(20,1,0;18,17,0)	278 <sup>a</sup>	277
(19,17,0;19,1,0)		278
(20,1,0;18,17,1)		279
(19,17,1;19,1,0)		280
(20,1,1;18,17,0)	289 <sup>a</sup>	286
(20,1,1;18,17,1)		288
(19,17,0;19,1,1)		287
(19,17,1;19,1,1)		289

Note: Errors shown are typical and represent the statistical uncertainty in the data.

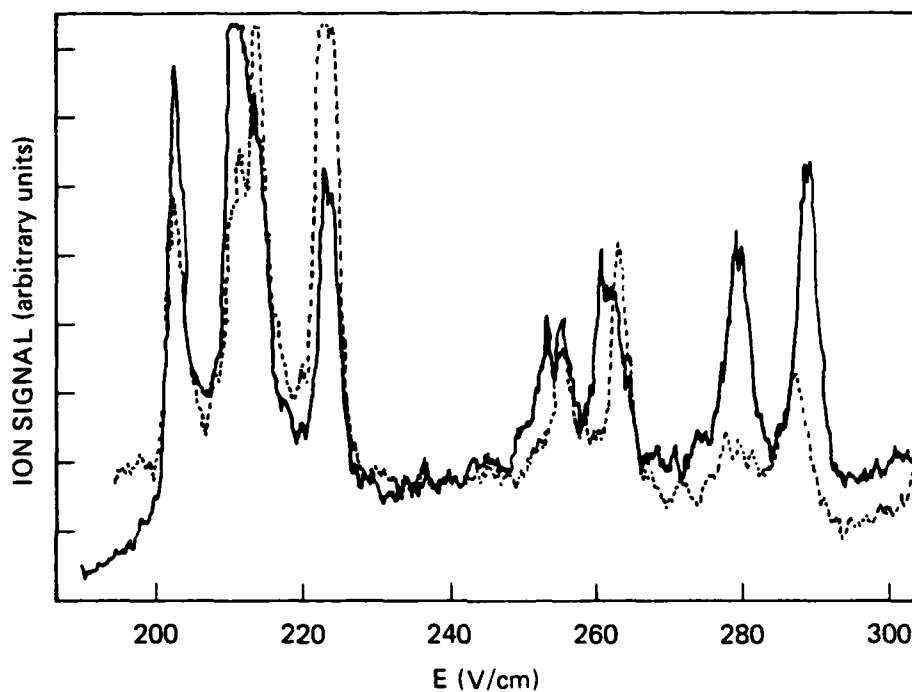
<sup>a</sup>Average location of the unresolved resonances.

resonances observed at even higher fields (see Figure 15) can be assigned a pair of final  $n, l, |m_l|$  states. It is clear that at higher fields some of the resonances overlap. For instance, the resonance seen in Figure 14 at approximately 278 V/cm is in fact composed of four unresolved resonances. In some cases we can verify the calculated  $|m_l|$  assignment of the resonances by using the fact that states with different  $|m_l|$  have slightly different SFI thresholds.<sup>11</sup> For instance  $|m_l| = 1$  states in the vicinity of 20p have a field-ionization threshold that is approximately 4.5% higher than that for  $|m_l| = 0$  states.<sup>11</sup>

The  $|m_l|$  labeling of the first few collisional resonances is experimentally confirmed in Figure 16, where the solid trace was obtained at a peak SFI field sufficient to field-ionize only the  $|m_l|=0$  component of the 20p and the in Figure 16 was similarly obtained with the SFI amplitude set to detect  $|m_l|=1$  component of the upper state ( $E \geq 2.3$  kV/cm). Comparison of Figures 14 and 16 indicate a resolution of the resonances in terms of the final  $|m_l|$  quantum number. For instance, the solid and broken traces in Figure 16, which indicate the  $|m_l|=0$  and 1 resonances, respectively, show that the resonance observed at  $E=255$  V/cm in Figure 14 is in fact composed of two partially overlapping resonances. This experimental observation is in agreement with the calculated positions, as indicated in Table V. Resonances with overlapping final states with the same  $|m_l|$  cannot be resolved in any straightforward manner.

#### D. Observations of $\text{Na}(nd) + \text{Na}(nd) \rightarrow \text{Na}[(n+1)f] + \text{Na}(np)$ Resonant Collisions

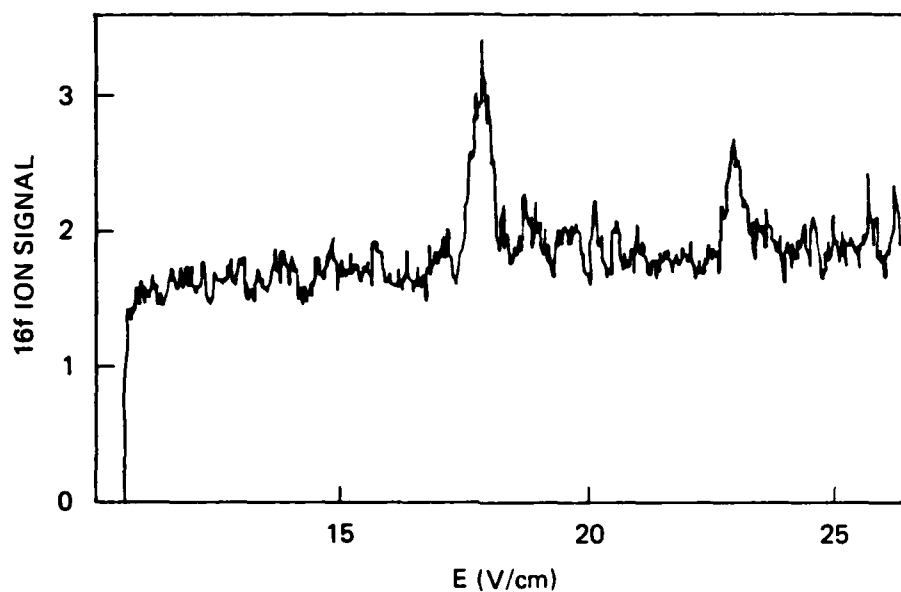
Although we have so far described observations of the resonant collisions with Na atoms initially in ns states, there are no fundamental limitations to the use of other Rydberg states. For instance, at relatively low fields (17 V/cm), the process  $(15d) + (15d) \rightarrow (15p) + (16f)$  becomes resonant. This process is confirmed by our observation of a sharp transfer of population into the 16f state, as shown in Figure 17. The SFI pulse amplitude in Figure 17 is set to detect states with  $n^* \sim 16$  (for instance, 16d or 16f) are detected via the ion multiplier. At zero electric field (see Figure 17) a very small non-resonant black-body-radiation-induced signal is observed. Large ion signals are observed when the electric field is set around 17 and 23 V/cm. From the Stark-shift calculations, it is clear that at low fields the only resonance



SA-8461-54

FIGURE 16 PLOT OF ION CURRENT (SOLID TRACE) SIMILAR TO THAT SHOWN IN FIGURE 14 EXCEPT THAT THE SFI IS SET TO DETECT ONLY THE  $|m_l| = 0$  COMPONENT OF THE  $20p$  AND THE NEARBY  $n \approx 19$ , HIGH- $\ell$  STATES

Broken trace is a recording of the  $|m_l| = 1$  final states; discrimination is based on the temporal resolution of ion signals from the  $|m_l| = 0$  and 1 states.



SA-8461-53

FIGURE 17 PLOT OF THE ION CURRENT REPRESENTING THE POPULATION IN THE 16f STATE (OR A NEARBY STARK STATE) AS A FUNCTION OF THE STATIC ELECTRIC FIELD

Atoms are initially excited to the 15d state. Amplitude of the SFI pulse is set to ionize states with  $n^* = 16$ .

condition occurs for the process  $(15d) + (15d) \rightarrow (16f) + (15p)$ ; that is, the  $15d$  state lies midway between  $16f$  and  $15p$ . The fine-structure splitting of the  $15p$  state results in the two resonances observed at 17 and 23 V/cm, respectively. From our calculations of Stark wave functions<sup>16</sup> for the Na Rydberg states, we obtain  $\mu_1 = \langle 19p | \mu | 20s \rangle = 200$  a.u. and  $\mu_2 = \langle n=19, l=18 | \mu | 20s \rangle = 80$  a.u. for the  $(19,18,0;19,1,0)$  collision resonance observed at 255 V/cm in Figure 14. For the  $(20,1,0;19,1,0)$  resonance,  $\mu_1 = \mu_2 = 200$  a.u. The calculated ratio between the cross sections for the  $(19,18,0;19,1,0)$  and  $(20,1,0;19,1,0)$  resonances is therefore approximately 0.4. From Figure 14 (and other similar data not shown here) we see the observed ratio is approximately 0.4 (see also Table VI). Calculated cross sections of some of the high-field ( $|m_1|=0$ ) resonances and their ratio compared to the lowest-field resonance, the  $(20,1,0;19,1,0)$  cross section, are listed in Table VI. As shown by Table VI, the magnitude of the cross section depends directly on the product of the dipole matrix elements, not on the geometric size of the atoms, which is roughly constant for all the cases listed in Table VI. Conversion of the electric field scale to the frequency scale indicates that the widths of the observed resonances are approximately 2 GHz (see Figure 14).

Finally, we have also observed resonant collisions between two Na atoms with  $l > 2$ . The Na atoms are initially excited to an  $nd$  state and subsequently excited to an  $nl$  state by applying a microwave field in the presence of a small static field (approximately 20 V/cm). Resonant collisions between a pair of laser-microwave-excited atoms then result in one of the atoms being excited to a state with  $n^* \sim n + 1$ . Since the FI threshold of the final state following the microwave transition and the subsequent resonant collision is much lower than that for the initial laser-excited state, using the SFI technique, we can detect the final state with a high signal-to-background ratio. We have, in fact, observed microwave transition from the  $18d$  (and  $16d$ ) state using the resonant collisions. The  $18d-18l$  ( $l > 2$ ) transitions occur as the microwave frequency is swept from 12.4 to 18.0 GHz in the presence of a 20-V/cm electric field. These microwave transitions are easily detected with the SFI amplitude set to detect states with  $n^* \approx 19$ .

From the above discussion and from Figure 14, it is clear that the newly observed resonant-collision process  $(ns) + (ns) \rightarrow (np) + [(n-1)l]$  (or  $(ns) + (ns) \rightarrow [(n-1)p] + nl$ ) occurs quite generally has a large cross

Table VI

CALCULATED AND OBSERVED CROSS SECTION FOR RESONANCES  
 WITH BOTH FINAL STATES WITH  $|m_1|=0$  AND THEIR RATIO R  
 WITH THE LOWEST-FIELD (20,1,0;19,1,0) RESONANCE CROSS SECTION.

Resonance	Calculated Cross Section ( $10^8 \text{ Å}^2$ )	Ratio Relative to Calculated Cross Section for (20,1,0;19,1,0)	Ratio Relative to to Observed Cross Section for (20,1,0;19,1,0)
(20,1,0;19,1,0)	3.5	1.0	1.0
(19,18,0;19,1,0)	1.36	0.4	0.4(0.08)
(20,1,0;18,17,0)	0.77	0.2	0.15(0.03)
(19,17,0;19,1,0)	1.1	0.3	0.2(0.04)

Note: Numbers in parentheses represent the statistical uncertainty in our data.

section, approximately  $10^9 \text{ \AA}^2$ , at resonance, and is easily observed. The large cross sections and narrow linewidths observed are largely due to the long-range dipole-dipole interaction between highly polarizable Rydberg atoms. Because of the large collision cross section and the long interaction time (approximately 1 ns), it appears possible to observe microwave-assisted collisions similar to the one observed recently for the process  $(ns) + (ns) + h\nu \rightarrow (np) + [(n-1)p]$ . Thus, it is quite feasible to observe resonant collisions between atoms of two different species. Resonant collisions involving higher multipole interactions between two atoms are also feasible.

## V SUMMARY

Under this contract, we have performed systematic experiments involving resonant collisions of sodium Rydberg atoms. Specifically, we have measured the resonant collision cross section and the linewidth as a function of the principal quantum number  $n$ .

We have also investigated the generalized resonant collisions involving collisions of  $n\ell$  states with  $\ell$  up to 3. Finally, we have developed the general theory for these collisions and have obtained good agreement with our observations.



## REFERENCES

1. N. F. Mott and H.S.W. Massey, The Theory of Atomic Collisions (Clarendon, Oxford, 1950).
2. P. W. Anderson, Phys. Rev. 76, 647 (1949).
3. J. van Kranendonk, Can. J. Phys. 41, 433 (1963).
4. T. Oka, in Advances in Atomic and Molecular Physics, edited by D. R. Bates and I. Esterman (Academic Press, New York, 1973) Vol. 9.
5. P. L. Houston, in Photo Selective Chemistry, Part 2, edited by J. Jortner (John Wiley and Sons, New York, 1981).
6. T. F. Gallagher, G. A. Ruff, and K. A. Safinya, Phys. Rev. A 22, 843 (1980).
7. K. A. Smith, F. G. Kellert, R. D. Rundel, F. B. Dunning, and R. F. Stebbings, Phys. Rev. Lett. 40, 1362 (1978).
8. K. A. Safinya, J. F. Delpech, F. Gounand, W. Sandner, and T. F. Gallagher, Phys. Rev. Lett. 47, 405 (1981).
9. T. F. Gallagher, K. A. Safinya, F. Gounand, J. F. Delpech, W. Sandner, and R. Kachru, Phys. Rev. A 25, 1905 (1982).
10. N. F. Ramsey, Molecular Beams (Oxford University Press, London, 1956).
11. T. F. Gallagher, L. M. Humphrey, W. E. Cooke, R. M. Hill, and S. A. Edelstein, Phys. Rev. A 16, 1098 (1977).
12. D. C. Lorents, D. J. Eckstrom, and D. L. Huestis, SRI Report MP 73-2 (unpublished).
13. W. E. Cooke, private communication.
14. T. F. Gallagher, L. M. Humphrey, R. M. Hill, W. E. Cooke, and S. A. Edelstein, Phys. Rev. A 15, 1937 (1977).
15. R. Kachru, T. F. Gallagher, F. Gounand, P. L. Pillet, and N. H. Tran, Phys. Rev. A 28, 2676 (1983).
16. M. L. Zimmerman, M. G. Littman, M. M. Kash, and D. Kleppner, Phys. Rev. A 20, 2251 (1979).
17. R. Kachru, N. H. Tran, and T. F. Gallagher, Phys. Rev. Lett. 49, 191 (1982).

## Resonant Rydberg-Atom-Rydberg-Atom Collisions

K. A. Safinya,<sup>(a)</sup> J. F. Delpech,<sup>(b)</sup> F. Gounand,<sup>(c)</sup> W. Sandner,<sup>(d)</sup> and T. F. Gallagher  
*Molecular Physics Laboratory, SRI International, Menlo Park, California 94025*

(Received 22 June 1981)

We have observed the sharply resonant enhancement of the cross section of the collision process  $ns + ns \rightarrow np + (n-1)p$  between two Na  $ns$  ( $16 \leq n \leq 27$ ) atoms which occurs when the levels are shifted by an electric field so that the  $ns$  level lies midway between the two  $p$  states. The widths of the collisional resonances scale as  $n^{-2}$  and the magnitudes of the cross sections as  $n^4$ , with values of 0.5 GHz and  $8 \cdot 10^8 \text{ \AA}^2$  for the 20s state. These results are in good agreement with calculations based on the long-range dipole-dipole interaction between the two atoms.

PACS numbers: 32.80.-t, 32.60.+i, 42.65.Gv

In collisional transfer of internal energy from atom  $A$  to atom (or molecule)  $B$  it is expected that if the collision is resonant, i.e., atom  $A$  loses as much internal energy as atom  $B$  gains, the cross section will be enhanced.<sup>1</sup> In low-lying states it is difficult to study the effect in a systematic fashion since one must rely upon chance coincidences in the energy levels. On the other hand, atomic Rydberg states are well suited for such studies for two reasons. First, for many collision processes they have large cross sections, which should allow the long interaction time necessary to produce sharp collisional resonances. Second, the energy spacings of Rydberg states may be varied in a systematic fashion. The most apparent approach is to vary the energy spacings by studying a progression of  $n$  or  $l$  states, where  $n$  and  $l$  are the principal and orbital angular momentum quantum numbers. Variation of  $n$  has already been used to study resonant electronic-to-vibrational energy transfer from Rydberg states of Na to  $\text{CH}_4$  and  $\text{CD}_4$ ,<sup>2</sup> and electronic-to-rotational energy transfer from Rydberg states of Xe to  $\text{NH}_3$ .<sup>3</sup> The widths of the resonances in these collision cross sections are 50 and 6  $\text{cm}^{-1}$ , respectively, far narrower than any previously observed. Changing  $n$  or  $l$  limits the tuning to discrete steps; however, it is possible to continuously tune the atomic levels with use of electric or magnetic fields, which is of course essential to observe very sharp resonances.

Here we report the use of electric field tuning to observe resonant collisions of two Rydberg atoms. Specifically, we observe that when the electric field is tuned so that an initially populated  $ns$  state lies midway between the two  $p$  states above and below it, two atoms in the  $ns$  state collide to yield one atom in each of the two  $p$  states. At resonance the process has a large cross section,  $\sim 10^3$  times the geometric cross

section which is the expected cross section for nonresonant collision processes.<sup>4</sup> Such large cross sections lead to long interaction times of  $\sim 1$  ns or resonant widths of  $\sim 0.03 \text{ cm}^{-1}$ , a width more characteristic of spectroscopy than collisions.

In these experiments Na atoms in an effusive thermal beam are crossed at  $90^\circ$  by two collinear pulsed-dye-laser beams which excite them via the route  $3s \rightarrow 3p \rightarrow ns$  to  $ns$  states where  $16 \leq n \leq 27$ . Typically the yellow  $3s \rightarrow 3p$  transition was saturated, but the blue  $3p \rightarrow ns$  transition was not. After the laser pulse the atoms collide with each other, and the final-state distribution is analyzed as a function of time after the laser excitation by using selective field ionization which enables us to discriminate between the states of interest, including the  $|m|$  values of the  $p$  states.<sup>5</sup> Here  $m$  is the component of orbital angular momentum along the field direction. As noted above, the experiment is carried out in the presence of a dc electric field which serves to tune the levels as shown in Fig. 1 for the  $19p$ ,  $20s$ , and  $20p$  states. Note that, because of the splitting of the  $|m| = 0$  and 1 levels of the  $p$  states, there are in fact four values of the electric field (resonances) at which the  $s$  state lies midway between the two  $p$  states.

The cross sections are determined by measuring the number of atoms  $N_p$  collisionally transferred to the  $np$  state and the number of atoms  $N_s$  excited to the  $ns$  state. In the limit where only a small fraction of the initial  $ns$  population is collisionally transferred to the  $p$  states we may express the population  $N_p$  at a time  $t$  after the laser excitation as

$$N_p = N_s^2 \sigma \bar{v} t / V, \quad (1)$$

where  $\sigma$  is the cross section for the process  $ns + ns \rightarrow np + (n-1)p$ ,  $\bar{v}$  is the average collision velocity, and  $V$  is the sample volume. To ac-

count for the depletion of the  $ns$  state by collisions and radiative decay we use the average value of  $N_s$  while the collisions are occurring. From Eq. (1) it is immediately apparent that if the second laser excitation step is not saturated,  $N_s$  will be linear in blue-laser power while  $N_p$  is quadratic. We actually observe signals  $N_s'$  and  $N_p'$  which are related to  $N_s$  and  $N_p$  by a factor  $\Gamma$ , the inverse of the detector sensitivity. It is useful to rewrite Eq. (1) as

$$\sigma = (N_p' / N_s'^2) [V / \Gamma \bar{v} t]. \quad (2)$$

From Eq. (2) it is apparent that we can measure the relative cross sections by obtaining the ratio  $N_p' / N_s'^2$ , leaving all other parameters fixed. Absolute normalization of the cross sections requires the values of the quantities in the square brackets.

To obtain the cross sections we field ionize the atoms 2  $\mu$ s after the laser excitation and set the amplitude of the ionizing pulse so that the signals from the  $np$ ,  $ns$ , and  $(n-1)p$  states are temporally well resolved.<sup>5</sup> With a narrow 50-ns gate we record only the  $np$  signal and with a wide 500-ns gate we record the entire signal as we sweep the dc field in the vicinity of the four resonances. The entire signal is easily related to the average value of  $N_s'$  by its observed time dependence. These two measurements give  $N_p'$  and  $N_s'$ . In

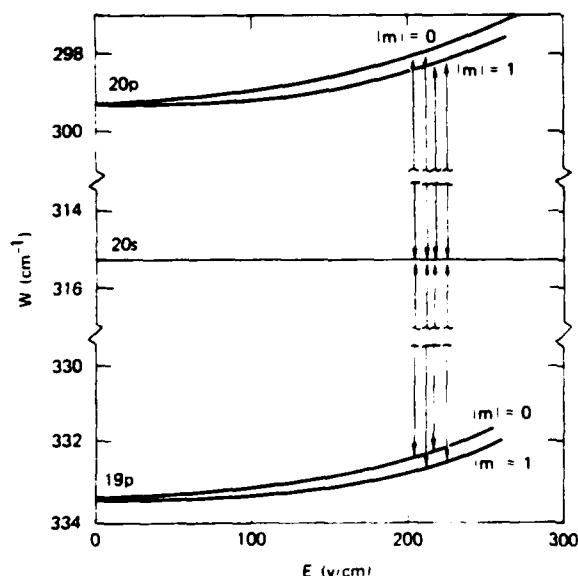


FIG. 1. Energy levels for the  $19p$ ,  $20s$ , and  $20p$  states in an electric field. The collisional resonances are shown by the arrows.

Fig. 2 we show  $N_p'$ , the  $20p$  signal observed after excitation of the  $20s$  state, as a function of dc field for two blue-laser powers. The background signal, such as is observed at  $E \sim 250$  V/cm, is due to blackbody-radiation-induced transitions<sup>6</sup> and depends linearly on  $N_s'$  and the blue-laser power. The four sharp peaks above the blackbody signal are due to resonant collisions and are obviously quadratic in the blue-laser power. The resonances are labeled by the  $|m|$  values of the lower and upper  $p$  states (see Fig. 1).

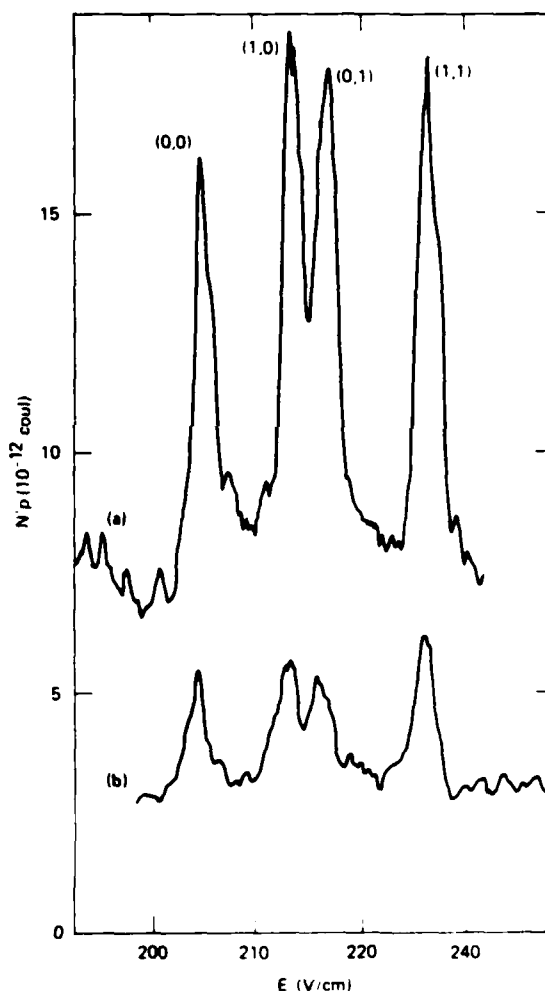


FIG. 2. Signal from the  $20p$  state, after population of the  $20s$  state, vs dc electric field at two exciting laser powers: (a) 1.0 and (b) 0.4. The background signal (at 190 or 250 V/cm) is due to blackbody radiation and is linear in laser power. The collisional resonance signals are clearly quadratic in power. The collisional resonances are labeled by the  $|m|$  values of the lower and upper  $p$  states (see Fig. 1).

From the values of  $N_s$  and  $N_p$  we obtain the  $n$  variation of the cross section which scales as  $n^{*(4.2 \pm 0.3)}$  and is shown with its errors in Fig. 3. Here  $n^*$  is the effective quantum number of the  $ns$  state whose binding energy  $W$  is given by  $W = -1/2n^{*2}$ . To provide a feeling for the magnitude of the cross sections we have put Fig. 3 on an absolute basis by evaluating the parameters in the square brackets of Eq. (2). The sample volume  $V$  is defined by the diameter of the laser beams (0.05 cm) and the width of the atomic beam (0.4 cm) to be  $10^{-3}$  cm<sup>3</sup>. From the velocity distribution of the beam we estimate  $\bar{v}$  to be  $5 \times 10^4$  cm/s. Time-resolved measurements indicate that collisions occur for 1  $\mu$ s, a time which is determined by the geometry of the excitation volume and the velocity distribution; thus we take  $t = 1$   $\mu$ s. The detector sensitivity,  $1/\Gamma = 1.9 \times 10^{-15}$  C/atom, indicates that we excited from  $10^3$  to  $10^4$  atoms per pulse in these experiments. We estimate the uncertainty in the absolute magnitude of the cross sections to be a factor of 5. Note that the observed cross sections are  $\sim 10^3$  times larger than the geometric cross sections.

Of as much interest as the magnitudes of the cross sections are the positions and particularly the widths of the resonances. Let us focus our

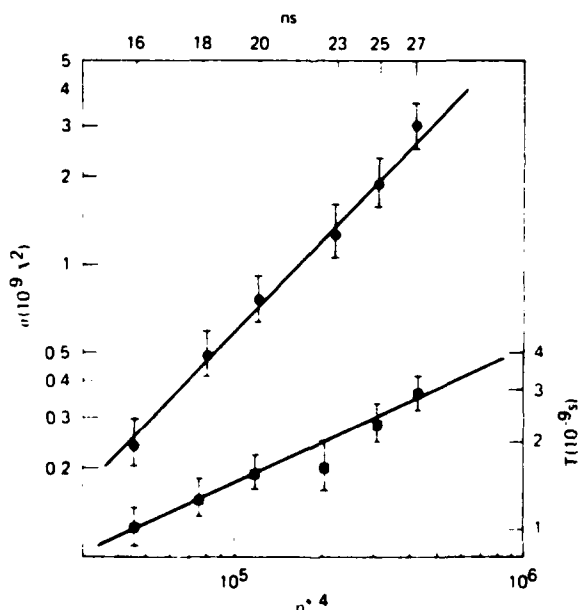


FIG. 3. Observed resonant cross sections (circles) and collision times (squares) (inverse widths) plotted vs  $n^{*4}$  on logarithmic scales. The values of the  $ns$  states are given at the top for reference.

attention on the (0,0) resonance, which has no spin-orbit splitting to broaden it. The position of the (0,0) resonance,  $E_R$ , is given to a good approximation by  $E_R(V/\text{cm}) = 1.21 \times 10^9 n^{*-5.34}$ , and the widths are given by  $\Delta E(V/\text{cm}) = 6.63 \times 10^4 n^{*-3.59}$ . If the Stark effect were hydrogenic and linear the frequency width  $\Delta W$  would be given by  $\Delta W(\text{GHz}) = 2.54 \times 10^{-3} n^{*2} \Delta E(V/\text{cm})$ .<sup>7</sup> However, as shown by Fig. 1 the Stark shift is not quite linear, and we find that at the (0,0) resonance  $\Delta W(\text{GHz}) = 2.42 \times 10^{-3} n^{*1.7} \Delta E(V/\text{cm})$ . Thus  $\Delta W$  scales as  $n^{*-1.9 \pm 2}$ , with a value of 1 GHz at  $n^* = 20$ . Equivalently we could say the collision time  $T = 1/\Delta W$  scales as  $n^{*1.9 \pm 0.2}$  with a value of  $\sim 1$  ns for 16s.

Since superradiance is known to be important for Rydberg states<sup>8</sup> it is worth mentioning why it or related phenomena are not expected to play a role here. First, by crossing the laser beams to reduce the sample volume we observed quantitatively similar, but smaller signals, indicating that the effect depended upon number density  $N_s/V$  rather than number  $N_s$  as would be expected for a cooperative effect in a small sample.<sup>9</sup> Second, superradiance from  $ns$  to  $(n-1)p$  was observed to disappear, presumably because of inhomogeneous broadening, in the 16s state with the application of 50 V/cm and in the 20s state by the application of 3 V/cm. (These fields are an order of magnitude lower than those at which the resonances occur.) At  $n = 27$  superradiance was never observed. Finally the time scale of a cooperative effect must be fast compared with the relaxation times.<sup>10</sup> In zero electric field Earth's magnetic field gives a time of  $\sim 0.3$   $\mu$ s, and at the electric fields we used we estimate that inhomogeneous electric fields lead to relaxation times of  $\sim 0.1$   $\mu$ s. For these reasons it seems most unlikely that a cooperative effect is responsible for these observations.

Finally it is interesting to compare our observed cross sections and resonance widths with calculations based on the interaction of the dipole moments of the two atoms. Using several approaches<sup>1,11,12</sup> we find that, at resonance, the cross section  $\sigma$  is given (in atomic units) to about an order of magnitude by

$$\sigma \sim \mu_1 \mu_2 / \bar{v} \sim n^{*4} / \bar{v}, \quad (3)$$

where  $\mu_1$  and  $\mu_2$  are the  $ns-np$  and  $ns-(n-1)p$  dipole moments, which are in our case both  $\sim n^{*2}$ , and  $\bar{v}$  is the collision velocity. Note that the cross section is larger than the geometric cross section by a factor  $\sim 1/\bar{v}$ . The collision time  $T$ ,

the inverse of the resonance width, is given by

$$T \sim \sqrt{\sigma}/\bar{v} \sim n^{*2}/\bar{v}^{3/2}. \quad (4)$$

Clearly the observed values of both  $\sigma$  and  $T$  exhibit the same  $n^*$  dependences as Eqs. (3) and (4). Our calculations indicate values of  $\sigma = 3 \times 10^8 \text{ \AA}^2$  and  $T = 10^{-9} \text{ s}$  for the  $18s$  state in good, somewhat fortuitous, agreement with the observed values shown in Fig. 3. It is interesting to note that according to our calculations the (0, 1) and (1, 0) resonances should not occur for a spinless system but occur here because of the spin-orbit coupling.

In conclusion we have observed that the long-range dipole-dipole interaction leads to enormous cross sections and the long interaction times requisite for sharp resonances in the collision cross section. The long duration (1 ns) of the collisions may open the way to such interesting investigations as the introduction of perturbations in mid collision.

It is a pleasure to acknowledge helpful and stimulating discussions with D. L. Huestis, W. E. Cooke, R. E. Olson, and R. M. Hill, as well as the financial support of the U. S. Office of Naval Research Physics Division under Contract No. N00014-79-C-0202. One of us (W.S.) is a Deutsche Forschungsgemeinschaft Fellow.

<sup>(a)</sup>Present address: Schlumberger-Doll Research,

Ridgefield, Conn. 06877.

<sup>(b)</sup>Permanent address: Institut d'Electronique Fondamentale, F-91405 Orsay, France.

<sup>(c)</sup>Permanent address: Centre d'Etudes Nucléaires de Saclay, Service de Physique Atomique, F-91191, Gif-sur-Yvette, France.

<sup>(d)</sup>Permanent address: Fakultät für Physik, Universität Freiburg, Hermann-Herder Strasse 3, D-7800 Freiburg, West Germany.

<sup>1</sup>N. F. Mott and H. S. W. Massey, *The Theory of Atomic Collisions* (Clarendon, Oxford, 1950).

<sup>2</sup>T. F. Gallagher, G. A. Ruff, and K. A. Safinya, *Phys. Rev. A* **22**, 843 (1980).

<sup>3</sup>K. A. Smith, F. G. Kellert, R. D. Rundel, F. B. Dunning, and R. F. Stebbings, *Phys. Rev. Lett.* **40**, 1362 (1978).

<sup>4</sup>R. E. Olson, *Phys. Rev. Lett.* **43**, 126 (1979).

<sup>5</sup>T. F. Gallagher, L. M. Humphrey, W. E. Cooke, R. M. Hill, and S. A. Edelstein, *Phys. Rev. A* **16**, 1098 (1977).

<sup>6</sup>T. F. Gallagher and W. E. Cooke, *Phys. Rev. Lett.* **42**, 835 (1979).

<sup>7</sup>H. A. Bethe and E. A. Salpeter, *Quantum Mechanics of One and Two Electron Atoms* (Academic, New York, 1957).

<sup>8</sup>M. Gross, C. Fabre, P. Goy, S. Haroche, and J. M. Raimond, *Phys. Rev. Lett.* **43**, 343 (1979).

<sup>9</sup>N. E. Rehler and J. H. Eberly, *Phys. Rev. A* **3**, 1735 (1971).

<sup>10</sup>J. C. MacGillivray and M. S. Feld, *Phys. Rev. A* **14**, 1169 (1976).

<sup>11</sup>E. M. Purcell, *Astrophys. J.* **116**, 457 (1952).

<sup>12</sup>T. F. Gallagher *et al.*, unpublished.

## Resonant Rydberg-atom — Rydberg-atom collisions

T. F. Gallagher, K. A. Safinya,\* F. Gounand,<sup>†</sup> J. F. Delpech,<sup>‡</sup> W. Sandner,<sup>§</sup> and R. Kachru*Molecular Physics Laboratory, SRI International, Menlo Park, California 94025*

(Received 16 November 1981)

The experimental investigation of the resonant collision process

 $Nans + Nans \rightarrow Nanp + Na(n-1)p$  which occurs when the levels are tuned with an electric field so that the  $ns$  level lies midway between the two  $p$  levels is described in detail.

The observations are shown to be in good agreement with a long-range resonant dipole-dipole interaction.

## I. INTRODUCTION

Resonant collisional energy transfer, the process in which atom (or molecule)  $A$  loses as much internal energy as its collision partner atom (or molecule)  $B$  gains, is a process which has been of interest for some time. While it has been studied theoretically in some detail, both for atomic and molecular collisions,<sup>1-3</sup> the experimental exploration of this subject has been hindered by the necessity of finding chance coincidences in the separations of the energy levels of the collision partners. In spite of this obstacle considerable insight has been gained into the nature of resonant collisions using the available coincidences.<sup>4,5</sup>

The study of resonance effects in collisions is greatly facilitated by the use of Rydberg atoms. First there is a high probability of finding chance coincidences because of the systematic variation of the energy separations with principal quantum number  $n$  and orbital angular-momentum quantum number  $l$ . This allows much more systematic studies than were previously possible. For example, the variation of energy separation with  $n$  produces a comb of allowed transition frequencies which is nearly continuous in some spectral regions, and this has been used to probe resonance effects in electronic to rotational and vibrational energy transfer.<sup>6-8</sup> Using the resulting discrete step tuning it has been possible to determine the widths of these collisional resonances to be  $6\text{ cm}^{-1}$  and  $50\text{ cm}^{-1}$ , respectively, although the exact widths are somewhat uncertain due to the comb-like nature of the energy spacing. It is interesting to note that in both these cases, at resonance the cross sections are slightly smaller in size than the geometric size of the Rydberg atom, and the dominant interaction in these collisions is thought to be the quasifree electron scattering of the Rydberg electron from the

perturbing atom or molecule.

Since Rydberg atoms have large dipole moments their energies are easily shifted by the application of very modest electric fields thus allowing the study of resonant collisions with continuous tuning. Previously we described the first application, to our knowledge, of such an approach to study resonant collisions of two Rydberg atoms.<sup>9</sup> We notice that in nuclear magnetic resonance, magnetic field tuning has been used to observe roughly analogous resonant energy transfer between nuclear spins in solids.<sup>10</sup> Although several mechanisms are responsible for the observed effects, such processes are frequently termed cross relaxation.<sup>10</sup>

Specifically, we have studied the sharply resonant thermal-collision process  $Na\ ns + ns \rightarrow np + (n-1)p$  which occurs when the  $Na\ ns$  levels are tuned with an electric field so that the  $ns$  level lies midway between the two  $p$  states. As shown by Fig. 1 for the  $17s$ ,  $16p$ , and  $17p$  states, there are in fact four collisional resonances due to the splitting of  $|m_l| = 0$  and  $1$  levels in the electric field. We shall designate the four resonances by the  $|m_l|$  levels of the lower and upper  $p$  states, respectively. Thus in order of increasing field the four resonances are  $(0,0)$ ,  $(1,0)$ ,  $(0,1)$ , and  $(1,1)$ .

Cross sections  $\sim 10^3$  times greater than the geometric cross sections of the atoms with resonance widths of  $\sim 0.03\text{ cm}^{-1}$  were observed. Both of these striking features are consequences of the large dipole moments of the Rydberg atoms which allow an efficient long-range resonant dipole-dipole interaction. Such an interaction was termed a "rotational resonance" by Anderson,<sup>2</sup> and has been observed, although not systematically, in molecular resonant rotational energy transfer.<sup>4</sup>

It is our purpose here to give a more detailed description of the experimental approach and observations as well as a simple treatment of resonant collisions.

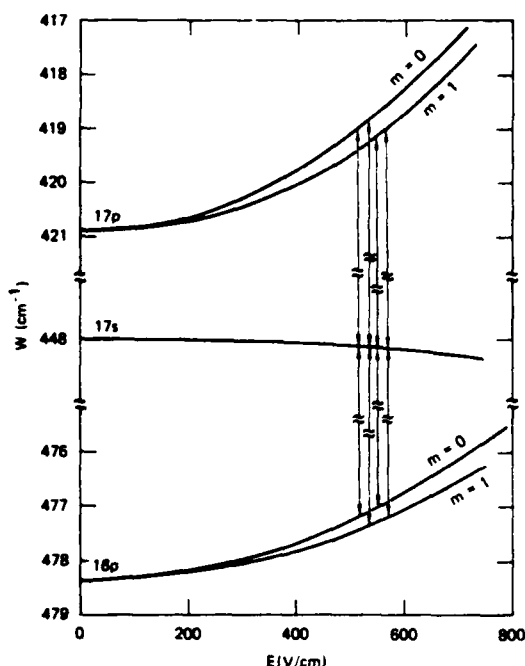


FIG. 1. Energy-level diagram for the 16p-17s-17p states in a static electric field. The vertical lines are drawn at the four fields where the s state is midway between the two p states and the resonance collisional transfer occurs.

## II. RESONANT COLLISIONS

Since the formal theory of long-range dipole-dipole collisions has been developed from the scattering point of view and can be found in several places,<sup>1</sup> there is little point in repeating such a treatment here. Rather we present two treatments derived from radio-frequency spectroscopy. The first is an order-of-magnitude argument derived from Purcell's<sup>11</sup> treatment of electron-collision-induced hydrogen 2s-2p transitions. The second more elaborate treatment serves mainly to produce an explicit analytic expression for the width of the collisional resonances. In both we use atomic units.

The treatment based upon Purcell's work gives quickly the approximate values of the cross sections and resonance widths. Imagine that we have two two-state atoms 1 and 2, one in its upper and one in its lower state, which have transition matrix elements  $\mu_1$  and  $\mu_2$  for transitions at the same frequency  $\omega$ . Further, these atoms pass each other with relative velocity  $v$  and impact parameter  $b$  as shown in Fig. 2. Atom 1 may be viewed as a clas-

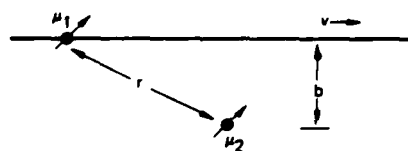


FIG. 2. Geometry of the collision of two dipoles.  $\mu_2$  is at rest and  $\mu_1$  passes with velocity  $v$  and impact parameter  $b$ . The dipoles are separated by  $r$ .

sical dipole of magnitude  $\mu_1$ , rotating at frequency  $\omega$ . This produces an oscillating field  $E$  at atom 2 the magnitude of which is given by

$$E \sim \frac{\mu_1}{r^3}, \quad (1)$$

where  $r$  is the distance between the atoms. For this field to induce a transition of atom 2

$$\mu_2 E t \sim 1, \quad (2)$$

where  $t$  is the interaction time. Since  $E$  is only appreciable when  $r \sim b$ , we may use  $E = \mu_1/b^3$  and  $t = b/v$  in Eq. (2) and rewrite Eq. (2)

$$\frac{\mu_1 \mu_2}{b^2 v} \sim 1. \quad (3)$$

This yields the value of the impact parameter for which the resonant-energy transfer will occur with unit probability. Thus

$$\sigma \sim b^2 = \frac{\mu_1 \mu_2}{v}. \quad (4)$$

Similarly the width of the resonance  $1/t$  is given by

$$1/t \approx \left( \frac{v^3}{\mu_1 \mu_2} \right)^{1/2}. \quad (5)$$

Since for these Rydberg transitions  $\mu_1 \approx \mu_2 \approx n^2$ , then Eqs. (4) and (5) can be written as

$$\sigma = \frac{n^4}{v} \quad (6)$$

and

$$1/t = \frac{v^{3/2}}{n^2}. \quad (7)$$

Thus the cross section scales as  $n^4$  and the interaction time as  $n^2$ .

In atomic units the thermal velocity  $v \sim 10^{-4}$ , thus the cross sections are  $\sim 10^4$  times larger than the geometric cross sections. In more familiar units, at  $n = 20$ ,  $\sigma \sim 10^9 \text{ \AA}^2$  and  $t \sim 1 \text{ nsec}$ .

The fact that we are able to sweep through the collisional resonance suggests that we treat the problem in such a way that the resonant behavior emerges in much the same way it does in treatments of radio-frequency resonance. Accordingly, the following discussion, which leads to a simple expression for the width of the resonances, draws heavily upon the two-state magnetic resonance treatment of Ramsey,<sup>12</sup> and is formally identical to the perturbation treatment of Kleppner.<sup>13</sup>

Consider two colliding atoms as shown in Fig. 3. One of the atoms is assumed to be stationary at the origin and the other, passing the first atom with an impact parameter  $b$  at  $x=0$ , is moving in the  $x$  direction, perpendicular to the page, with velocity  $v$ . We shall assume that the second atom travels in a straight line and is not deflected by the collision. In addition we shall assume that there is a static electric field in the  $z$  direction. This choice of axes matches our experimental configuration. We construct the product states

$$\psi_A = \psi_{1ns} \psi_{2ns}, \quad (8a)$$

$$\psi_B = \psi_{1np} \psi_{2(n-1)p}, \quad (8b)$$

where  $\psi_{nl}$  describes a Stark-state wave function that is adiabatically connected to the corresponding zero-field  $n, l$  Coulomb wave function. The total wave function for the system may be written as

$$\psi(t) = \psi_A C_A(t) + \psi_B C_B(t), \quad (9)$$

where all the time dependence is in the coefficients  $C_A(t)$  and  $C_B(t)$ . The energies of the two states  $A$  and  $B$  at  $r = \infty$ , where  $r$  is the internuclear separation, are given by

$$W_A = W_{ns} + W_{ns} \equiv 0 \quad (10a)$$

and

$$W_B = W_{np} + W_{(n-1)p}, \quad (10b)$$

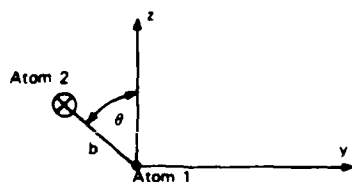


FIG. 3. Geometry of the collision of two atoms. Atom 1 is at rest at the origin. Atom 2 is moving in the  $x$  direction, perpendicular to the paper, with velocity  $v$  and impact parameter  $b$ . At  $x=0$ , the plane of the paper, the vector from atom 1 to atom 2 makes an angle  $\theta$  with the  $z$  axis, the axis of quantization.

which we take to be the eigenvalues of the unperturbed Hamiltonian  $H_0$  of two noninteracting (infinitely separated) atoms in the static electric field. For finite internuclear separations the states  $A$  and  $B$  are coupled by the dipole-dipole interaction

$$\langle \psi_A | V | \psi_B \rangle = \left\langle \psi_A \left| \frac{\vec{\mu}_1 \cdot \vec{\mu}_2}{r^3} - \frac{3(\vec{\mu}_1 \cdot \vec{r})(\vec{\mu}_2 \cdot \vec{r})}{r^5} \right| \psi_B \right\rangle. \quad (11)$$

Here  $\vec{r}$  is the vector between the two atoms.

Strictly speaking the assumption of an undeflected path for the moving atom does not allow the (0,1) or (1,0) resonances, as the change in the orbital angular momentum must come from the translational motion. However, because of the large impact parameter the amount of energy transferred is negligible,  $\sim 1.6 \times 10^{-3} \text{ cm}^{-1}$ . Thus the approximation of undeflected paths is quite good.

The interaction matrix elements may be simplified by taking the RMS value of Eq. (11) over the angle  $\theta$  in Fig. 3. This yields for the (0,0) transition

$$\langle \psi_A | V | \psi_B \rangle = \frac{\langle ns | \mu_1 | np \rangle \langle ns | \mu_2 | n-1p \rangle}{r^3}, \quad (12)$$

that is the product of the two dipole-matrix elements divided by  $r^3$ . Similar expressions are obtained from the other resonances.

Inserting the wave function of Eq. (9) and the Hamiltonian  $H_0 + V$  yields the pair of equations

$$i\dot{C}_A = W_A C_A(t) + V C_B(t), \quad (13a)$$

$$i\dot{C}_B = V^* C_A(t) + W_B C_B(t). \quad (13b)$$

For  $V$  real and  $W_A = 0$ , this may be recast in the form

$$i\ddot{C}_A + \dot{C}_A \frac{\dot{V}}{V} = V^2 C_A + iW_B \dot{C}_A. \quad (14)$$

Recall from Eq. (12) the form of the matrix element  $V$ . It is nearly zero everywhere except where  $r=b$ , where it reaches a maximum. Inspection of a graph of  $V$  vs  $x$  suggests the approximation

$$V = \begin{cases} \frac{\chi}{b^3} & \text{for } \frac{b}{2} < x < \frac{b}{2} \\ 0 & \text{elsewhere.} \end{cases} \quad (15)$$

Here  $\chi = \langle ns | \mu_1 | np \rangle \langle ns | \mu_2 | (n-1)p \rangle$ . This makes the  $\dot{V}/V$  term  $\equiv 0$  and suggests choosing the time origin so that the interaction time is  $0 < t < b/v$ . Thus the problem is reduced to pre-



cisely the magnetic resonance problem described by Ramsey.<sup>12</sup>

Initially both atoms are in the  $s$  state, thus  $C_A(0)=1$  and  $C_B(0)=0$ . With these initial conditions, for  $0 < t < b/v$ ,  $C_A$  and  $C_B$  are given by

$$C_A(t) = \left[ \cos \left[ \frac{\alpha t}{2} \right] \frac{-iW_B}{\alpha} \sin \left[ \frac{\alpha t}{2} \right] \right] \times \exp(iW_B t/2) \quad (16)$$

and

$$C_B(t) = \frac{-i2\chi}{b^3\alpha} \sin \left[ \frac{\alpha t}{2} \right] \exp(iW_B t/2), \quad (17)$$

where  $\alpha = (W_B^2 + 4\chi^2/b^6)^{1/2}$ . The probability  $P$  of finding the atoms in the two  $p$  states is given by  $C_B^2(b/v)$ . Thus we may write the probability as

$$P = \frac{4\chi^2/b^6}{W_B^2 + 4\chi^2/b^6} \sin^2 \frac{1}{2} \left[ W_B^2 + \frac{4\chi^2}{b^6} \right]^{1/2} \frac{b}{v}. \quad (18)$$

For  $P=1$  at resonance ( $W_B=0$ ) this defines an impact parameter  $b_0$ :

$$b_0^2 = 2\chi/\pi v. \quad (19)$$

The cross section is given by

$$\sigma = \int_0^\infty 2\pi b P(b) db. \quad (20)$$

Taking  $P = \frac{1}{2}$  for  $b < b_0$  to approximate the rapid oscillations and numerically integrating Eq. (20) for  $b > b_0$ , we find

$$\sigma = 2.3\pi b_0^2 \quad (21)$$

in good agreement with Anderson's result which is<sup>2</sup>

$$\sigma = \pi^2 \left( \frac{b}{v} \right) b_0^2. \quad (22)$$

From Eqs. (18) and (19) it is apparent that the width of the resonances is given by

$$\Delta(\text{FWHM}) = \frac{4\chi}{b_0^3} = \frac{2\pi v}{b_0} = \left[ \frac{2\pi^3 v^3}{\chi} \right]^{1/2}, \quad (23)$$

which is in good agreement with the result of van Kranendonk,<sup>3</sup>

$$\Delta(\text{FWHM}) = 5v/b_0, \quad (24)$$

for dipole-dipole collisions if we make the reasonable approximation that  $1/b_0$  is the average value of  $1/b$ . We notice that in our treatment the maximum probability occurs exactly on resonance, at

$W_B=0$ , whereas in the treatment of van Kranendonk it occurs for  $W_B \neq 0$ . This difference comes from the fact that we have discarded the term containing  $\dot{V}/V$  in Eq. (14).

To evaluate the cross sections and collision widths we must use the actual values of the average collision velocity  $\bar{v} = 1.6 \times 10^{-4}$  and dipole moments  $\mu_1 = \mu_2 = 0.60n^{*2}$ . Here  $n^{*2}$  is the effective quantum number of the  $ns$  state of binding energy  $W = -1/2n^{*2}$ . Using our results, Eqs. (21) and (22), these values lead to cross sections and widths (FWHM) given by

$$\sigma = 1.03 \times 10^4 n^{*4} \quad (25)$$

and

$$\Delta = 2.64 \times 10^{-5} n^{*-2}. \quad (26)$$

In laboratory units

$$\sigma = 2.90 \times 10^3 n^{*4} \text{ \AA}^2 \quad (27)$$

and

$$\Delta = 1.74 \times 10^2 n^{*-2} \text{ GHz}. \quad (28)$$

### III. EXPERIMENTAL APPROACH

In the experiment, an effusive beam of Na passes between a plate and a grid as shown in Fig. 4 where it is excited in two steps by two pulsed dye lasers, the first, yellow laser, tuned to the  $3s$ - $3p$  transition at 5890 \AA, and the second, blue laser, tuned to the  $3p$ - $ns$  transition at  $\sim 4140$  \AA. The laser excitation and subsequent collisions occur in a dc electric field which ranges from 80–800 V/cm in these experiments. At a variable time after the

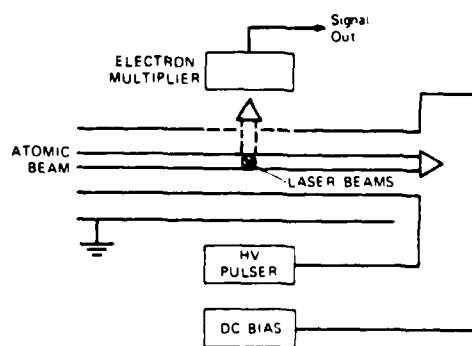


FIG. 4. The interaction region of the apparatus, showing both laser beams perpendicular to the atomic beam.

laser excitation a positive high-voltage pulse is applied to the plate field ionizing the Rydberg atoms and accelerating the resulting ions into the electron multiplier. The electron multiplier signal is averaged using a boxcar averager and recorded with a chart recorder.

The selectivity of electric field ionization enables us to identify states present at the time the field-ionizing pulse is applied. In this work we chiefly use the temporal resolution of ion signals from different states at a fixed ionizing-field amplitude. As noted previously, it is possible to discriminate between states of different  $n$ ,  $l$ , and  $|m_l|$  using this technique.<sup>14</sup> Thus we are able to monitor the populations in the  $ns$ ,  $np$ , and  $(n-1)p$  states as functions of time after the laser pulse and dc electric field.

Although most of the details of the experimental apparatus may be found elsewhere<sup>13</sup> we note here points of particular importance for this experiment. First, the atomic beam is collimated to a 0.4-cm diameter in the interaction region, has a density of  $\sim 10^8 \text{ cm}^{-3}$ , and is assumed to have the modified Maxwellian velocity distribution characteristic of a 500°C beam.

The laser beams are focused to 0.5-mm diameter in the interaction region, are usually approximately collinear, and cross the atomic beam at right angles as shown in Fig. 4. To vary the excitation volume the blue laser is sometimes introduced along the atomic-beam axis counterpropagating to the atomic beam. With both laser beams crossing the atomic beam at 90° the excitation volume is a cylinder of volume  $10^{-3} \text{ cm}^3$ . Typical densities of excited atoms are  $\sim 10^6 \text{ cm}^{-3}$ .

The electron multiplier gain is measured to be  $5 \times 10^{-3}$ , and has a specified quantum efficiency of 30%. Including the 20 db (power) gain of the amplifier after the multiplier, we find that overall, one Rydberg atom leads to  $\sim 1.9 \times 10^{-15} \text{ C}$  of signal.

#### IV. OBSERVATIONS

##### A. Qualitative observations

Before describing in detail the cross-section measurements it is useful to present qualitative observations which both identify the collision process and suggest the method used to measure the cross sections. The most striking feature of our observations is the sharply resonant increase in the populations when the levels are tuned into resonance with

the field. An example is shown in Fig. 5, a recording of the population in the  $17p$  state as a function of dc field 2  $\mu\text{sec}$  after the  $17s$  state is populated by the lasers. The sharp increases in signal at 516, 537, 544, and 566 V/cm are due to the resonant  $17s + 17s \rightarrow 16p + 17p$  collisions which occur as shown in Fig. 1. As mentioned earlier, the resonances are labeled by the  $|m_l|$  values of the final lower and upper  $p$  states, which are determined from the field-ionization behavior of the signal in the lowest  $n$  states studied. Since the field-ionization identification for the lowest  $n$  states is consistent with the energy levels of Fig. 1, we assumed this to be true for all  $n$  values we studied. In addition, the resonant signal is approximately quadratic in the power of the blue laser, whereas the total population is linear, as shown by Fig. 6. This suggests that the resonant signal is either due to an effect which depends upon collisions with photoions produced by the absorption of two blue-laser photons or to an effect varying as the square of the number of excited atoms. Since there are no photoions observed we can immediately rule out the first possibility. Considering the small size of photoionization cross sections for Rydberg atoms by visible photons<sup>15</sup> and the likelihood of a resonant process this seems unlikely in any case.

Thus the process must be either a collision between two excited atoms or some sort of cooperative effect involving the  $ns$ ,  $np$ , and  $(n-1)p$  states—such as superradiance. Since superradiance occurs quite easily in Rydberg-atom systems,<sup>16</sup> it is interesting to consider the possibility of a coopera-

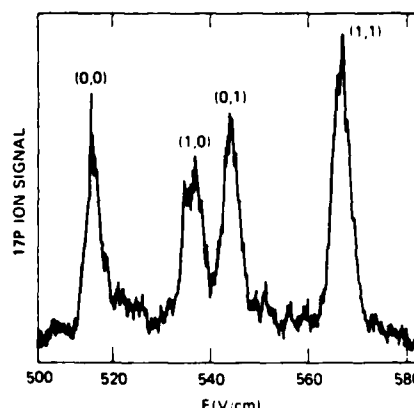


FIG. 5. The observed  $17p$  ion signal after population of the  $17s$  state vs dc electric field, showing the sharp collisional resonances. The resonances are labeled by the  $|m_l|$  values of the lower and upper  $p$  states.

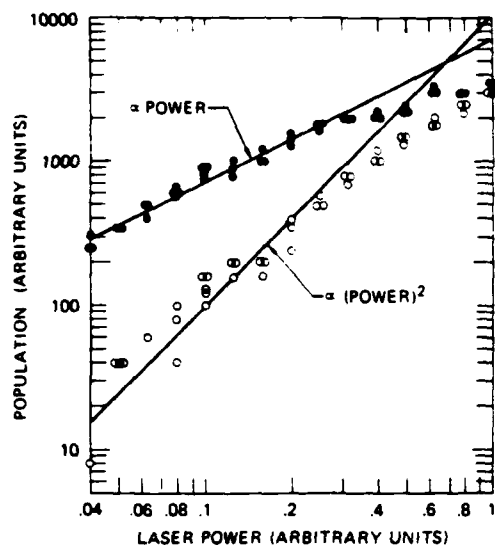


FIG. 6. The blue-laser-intensity dependence of the  $17p$  resonant collision signal (○) and  $17s$  signal (●) after population of the  $17s$  state showing the quadratic dependence of the resonant signal.

tive phenomenon to show why we have ruled it out in this case. For a cooperative effect to occur a macroscopic dipole must be set up in the medium and the effect must occur in a time short compared to the relaxation times.<sup>17</sup>

In a two-level Rydberg-atom system prepared entirely in the upper level the dipole is usually established by amplified blackbody radiation. Whether or not the dipole is actually established is determined by the amplification or gain of the sample for the transition under study.<sup>16</sup> Typically there must be a gain of  $\sim 1$  in the sample. Stated another way, in traversing the sample a photon at the correct frequency has a probability of one of inducing an atom to emit a second photon. This occurs when  $n_u \sigma_0 l \sim 1$ , where  $n_u$  is the number density of atoms in the upper state,  $\sigma_0$  is the optical cross section, and  $l$  is the sample length. This requirement is easily met by the zero electric field  $Nans$  states, for example, because of the large,  $\sim n^2$ , dipole moments connecting them to the  $(n-1)p$  states. Under this circumstance the thermal blackbody radiation is amplified and establishes the macroscopic polarization. In the electric field case we are considering here in which the transitions  $ns-np$  and  $ns-(n-1)p$ , absorption and stimulated emission, respectively, are at the same frequency, and whether there is gain or absorption depends upon the magnitude of the dipole-matrix

elements. Since they are the same to within a few percent in this case, there is apparently no net gain to establish the macroscopic dipole.

Even though, in principle, it appears impossible for a cooperative effect to occur we have a direct experimental check, the time scale of the observed effects. In zero field the  $Nans$  states exhibit superradiance in times  $< 300$  nsec after the laser pulse. We never observe a time delay greater than 300 nsec indicating that the relaxation times are  $< 300$  nsec. When we begin to apply a dc field we find that the superradiance disappears at 50 V/cm for  $16s$  and 3 V/cm for  $20s$ . We attribute the decrease in superradiance in these fields, which are ten times smaller than the fields in which the resonant collisions occur, to a diminishing of the  $ns-(n-1)p$  matrix element with the electric field and broadening by electric field inhomogeneities. For  $27s$  we never observe superradiance. In this connection it is interesting to note that as  $n$  goes from 16 to 27 the wavelength of the  $ns \rightarrow (n-1)p$  transition increases from 0.3 to 1.6 mm, i.e., from smaller than the sample size to larger than the sample size. It has been suggested that under such circumstances superradiance will not occur because of the direct dipole-dipole interaction between the atoms.<sup>18,19</sup>

From the considerations above it is clear that in the field the relaxation times are certainly less than 300 nsec, and if the effect is cooperative it must occur faster than 300 nsec. However, that is not the case as shown by Fig. 7 which shows the time evolution of the  $20p$  signal after the laser excitation of the  $20s$  state for the on- and off-resonant cases. As shown by Fig. 7 the resonant increase in the population of the  $20p$  state occurs over a  $1\text{-}\mu\text{sec}$  period (determined by the sample geometry), certainly not in a time fast compared to 300 nsec. (The fact that the nonresonant signal is not zero at  $t=0$  indicates that we are partially ionizing the parent  $20s$  state as well; however, this has no effect upon our conclusions.)

To investigate whether number or number density of excited atoms was important, we introduced the blue laser along the atomic beam, perpendicular to the yellow laser, so as to excite a smaller number of atoms but the same number density. We found the relative magnitudes of the resonant and nonresonant signals to be the same. Equivalently, if when the laser beams are parallel the blue laser is attenuated to produce the same initial number of  $20s$  atoms as are produced with the laser perpendicular, the resonant signal is proportionally much smaller. These observations indicate

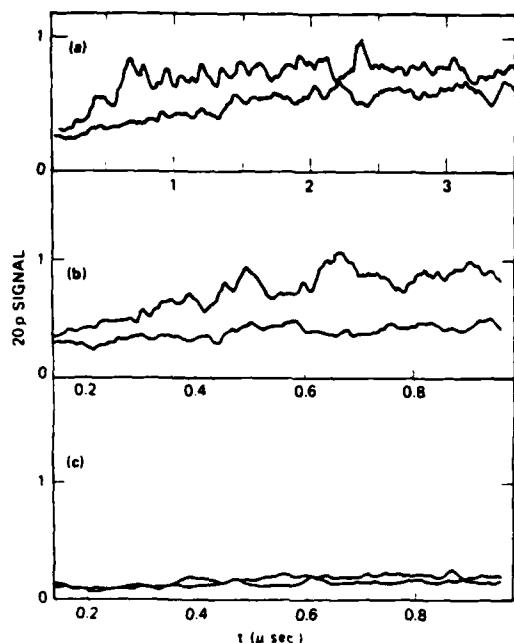


FIG. 7. Time dependence of the 20p signal after the population of the 20s state with the two laser beams parallel to each other. In each case the upper trace is on and the lower is off resonance. Thus, the difference is the buildup of the resonant collision signal. The off-resonance signal at  $t \sim 0$  is from partial ionization of the 20s state. (a) A scan of  $\sim 4 \mu\text{sec}$  showing the 1- $\mu\text{sec}$  time scale of the process. (b) A scan of  $\sim 1 \mu\text{sec}$  showing the early development of the signal. (c) A scan of  $\sim 1 \mu\text{sec}$  with the laser power reduced to 40% of that used in (b). Notice the drastic reduction of the resonant signal.

that the effect depends upon the number density of Rydberg atoms as expected for a collision process. When the above observations are considered together it is difficult to imagine that the process is cooperative, not collisional.

#### B. Measurement of the cross sections

If we allow collisions to occur for a time  $T$  (not to be confused with the collision time  $t$ ) during which time a small fraction of the initial population in the  $ns$  state is collisionally transferred to the  $np$  and  $(n-1)p$  states then the population  $N_p$  in the  $np$  (and  $n-1)p$  state will be given by

$$N_p = \frac{N_s^2 \sigma \bar{v} T}{V}, \quad (29)$$

where  $\bar{v}$  is the average collision velocity,  $\sigma$  is the

cross section for the process,  $V$  is the sample volume, and  $N_s$  is the initial  $ns$  state population.

Equation (29) may be easily inverted to give the cross section. In doing so it is convenient to replace  $N_s$  and  $N_p$  by the signals we observe  $N'_s$  and  $N'_p$  which are related to  $N_s$  and  $N_p$  by  $\Gamma$  the overall sensitivity, given in Sec. III. Thus we may write

$$\sigma = \frac{N'_p}{N'^2_s} \left[ \frac{V}{\Gamma \bar{v} T} \right]. \quad (30)$$

By measuring the ratio  $N'_p/N'^2_s$  as a function of  $n$  we may determine with good accuracy the  $n$  dependence of the cross section. Measurements of the quantities in curly brackets give the absolute cross sections.

Basically the cross-section measurement consists of measuring  $N_p$  the population in the  $np$  state, and  $N_T$ , the total population in  $np$ ,  $ns$ , and  $(n-1)p$  states, as the dc electric field is swept through the collisional resonances. Specifically, we field ionize the atoms 2  $\mu\text{sec}$  after the laser pulse and set the amplitude of the ionizing field so that all the  $ns$ ,  $np$ , and  $(n-1)p$  states are ionized, with the  $(n-1)p$  state being just barely ionized. Because of the large difference in the fields at which the Na  $ns$  and  $np$  states ionize these two are in all cases easily time resolved. Owing to the small difference in the fields at which the  $ns$  and  $(n-1)p$  state ionize these are not always clearly resolved under these conditions; however, this has no effect on the determination of the cross sections. With a 50-nsec wide gate we observe only the  $np$  state signal, which comes first, yielding  $N_p$ , and with a 500-nsec wide gate we observe at the same time the entire ion signal  $N_T$  from the  $np$ ,  $ns$ , and  $(n-1)p$  states. A typical example of a sweep through the collisional resonances is shown in Fig. 8 for the excitation of the 23s state for two laser powers. Figures 8(a) and 8(b) are recordings of  $N'_{23p}$ , the number of atoms in the 23p state at two laser powers. Figures 8(a') and 8(b'), in the inset, show the corresponding simultaneous measurements of  $N'_T$ , the number of atoms, in the 22p, 23s, and 23p states, which is clearly unaffected by the collisional resonances. In Figs. 8(a) and 8(b) the quadratic dependence of the resonant signal on blue-laser power is quite apparent, whereas the background (nonresonant) signal in Figs. 8(a) and 8(b) as well as the signal in Figs. 8(a') and 8(b') is clearly linear. Figures 8(a) and 8(b) were obtained on sweeps of increasing and decreasing field, respectively, which leads to apparent slight offsets

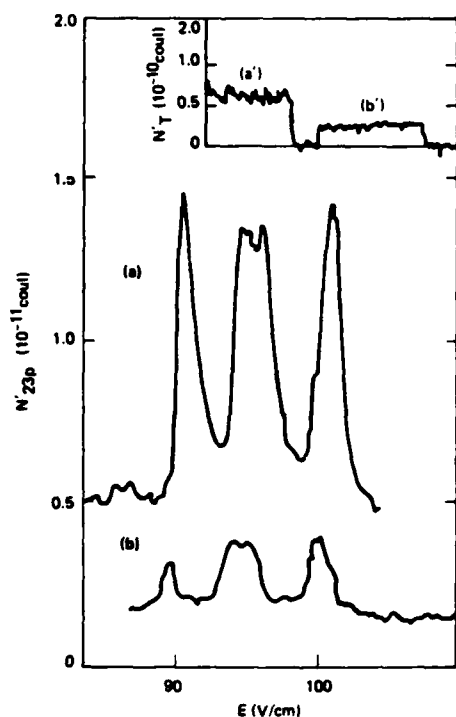


FIG. 8. (a) The population of the  $23p$  state  $2 \mu\text{sec}$  after the population of the  $23s$  state showing the collisional resonances. Notice that the  $(0,1)$  and  $(1,0)$  resonances are not resolved in this trace. (b) The same as (a) except with 40% of the blue-laser power. (a') A recording of the total populations in the  $23s$ ,  $22p$ , and  $23p$  states taken simultaneously with (a). (b') A recording of the total populations in the  $23s$ ,  $22p$ , and  $23p$  states taken simultaneously with (b).

in the positions of the resonances due to the time constant of the signal averager. Where necessary we averaged positions obtained with increasing and decreasing field sweeps to obtain the positions of the resonances. Data such as Fig. 8 were taken for

at least two laser powers for each state. Quantities of particular interest are the locations of the resonances, their widths, and the ratio of the signal  $N'_p$  to the signal  $N'_T$ .

In Table I we give the values of the electric field positions at which the resonances occur. In Fig. 9 we show the  $n$  dependence of the positions of the  $(0,0)$  and  $(1,1)$  resonances, whose locations are given by

$$E_R(0,0) = 1.21(2)n^{*-5.34(5)} \text{ V/cm} \quad (31a)$$

and

$$E_R(1,1) = 1.42(2)n^{*-5.35(5)} \text{ V/cm} \quad (31b)$$

The field widths (FWHM) of the resonances are given in Table II. We are reasonably confident that these widths, which are  $\sim 1\%$  of the applied fields, are not appreciably broadened by spatial inhomogeneities in the applied dc field because the widths appear the same whether the blue laser is brought into the interaction region parallel or perpendicular to the yellow laser, thus radically changing the volume occupied by the sample of excited atoms.

Physically it is the frequency width of the resonances in which we are really interested, and we have used an approximate method, based on a suggestion of Cooke,<sup>20</sup> outlined in the Appendix to make the conversion. The frequency widths of the resonances are given in Table III. The widths of the resonances are the sum of the collisional width and unresolved fine structure as shown in Fig. 10. Note that the  $|m_l| = 1$  states are split by  $\Delta_{fs}$ , which is given by

$$\Delta_{fs} = \frac{\Delta_{fs0}}{3} k, \quad (32)$$

where  $\Delta_{fs0}$  is the fine-structure interval of the

TABLE I. Positions of the resonances (V/cm).

State	Resonance			
	0,0	0,1	1,0	1,1
16s	741(15)	770(15)	781(15)	813(16)
17s	516(10)	537(10)	544(10)	566(10)
18s	364(8)	387(8)	393(8)	405(8)
20s	201(4)	210(4)	214(4)	222(4)
23s	91(2)	94.5(20)	95.9(20)	100(2)
25s	56.5(13)		59.0(13) <sup>a</sup>	63.1(14)
27s	36.6(8)		38.7(8) <sup>a</sup>	41.4(8)

<sup>a</sup>The average location of the unresolved 0,1 and 1,0 resonances.

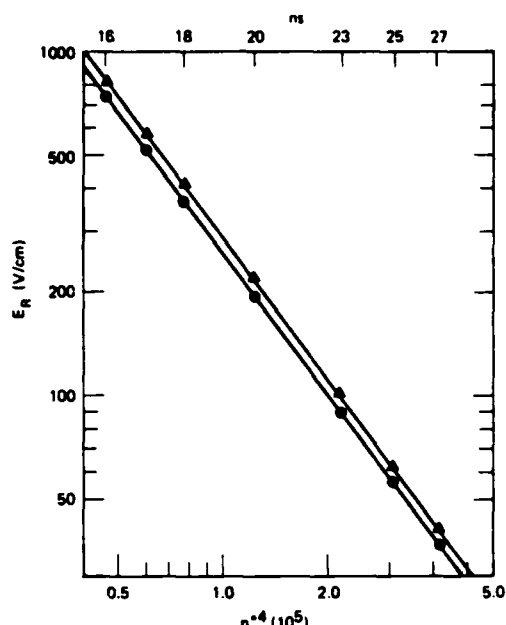


FIG. 9. The positions of the 0,0 (●) and 1,1 (▲) resonances.

zero-field  $p$  state and  $k$  is the amount of  $p$  character remaining in the nominal  $p$  state in the electric field. At these fields  $k \sim 0.85$  and  $0.73$  for the lower and upper  $p$  state, respectively. From Fig. 10 it is clear that only the (0,0) resonance reflects only the collisional width, the other resonances have additional width from the unresolved fine structure. The (0,1) and (1,0) resonances should each be broader by an amount  $\Delta_{fs, upper}$  and  $\Delta_{fs, lower}$ , respectively. Similarly, the additional width of the (1,1) resonance would be  $\Delta_{fs, upper} + \Delta_{fs, lower}$ , scaling as  $n^{-3}$ . Here we are implicitly assuming that there is no observable spin selection effect, which seems reasonable in view of the fact that we do not specify the spins of the  $s$  state atoms. In Fig. 11 we plot the difference in the observed widths,

$\Delta(1,1) - \Delta(0,0)$  vs  $n^{*4}$  and show the calculated value of  $\Delta_{fs, upper} + \Delta_{fs, lower}$  which is in good agreement with the data. In calculating  $\Delta_{fs, upper}$  and  $\Delta_{fs, lower}$  we have used the previously determined  $np$  fine-structure intervals.<sup>21</sup>

From the previous discussion it is clear that the (0,0) resonance is the only good probe of the collision width. The  $n^*$  variation of the width of the (0,0) resonance (FWHM) is given by

$$\Delta(0,0) = 235(40)n^{*-1.95(20)} \text{ GHz}. \quad (33)$$

In Fig. 12 we plot the observed widths of the (0,0) resonance and calculated dependence from Eq. (26). Note that  $\Delta(0,0)$  scales as  $n^{*1.9}$ , in agreement with the predicted  $n^{*2}$  scaling, and is in reasonable agreement with the calculated magnitude.

The cross sections themselves are taken from the ratios  $N'_p/N'_s$ .<sup>22</sup> For  $N'_p$  we use the height of the resonances above the flat background signal in recordings such as Figs. 8(a) and 8(b). The average value of  $N'_s$  while collisions are occurring is obtained by extrapolating the observed  $N'_T$  signal back to  $0.5 \mu\text{sec}$  after the laser pulse, the middle of the time interval during which collisions occur. For the extrapolation we use the 0 K radiative lifetime,<sup>22</sup> not the 300 K radiation decay rate of the  $ns$  states since in addition to the  $ns$  state we detect the  $np$  and  $(n-1)p$  states which account for  $> 80\%$  of the blackbody radiation induced decay of the  $ns$  state.<sup>23</sup> In some of the higher-lying states, at the highest laser powers used the resonant collisions were depleted the  $s$  state by 30% in which case Eq. (30) is not valid and we used an expansion of which Eq. (30) is the leading term. To simplify the presentation we have corrected the observed  $N'_p/N'_s$  ratios to account for depletion and present them in Table IV along with the radiative lifetimes of the  $ns$  states. The  $N'_p/N'_s$  ratios are proportional to the cross sections and give the variation of the cross sections with  $n$ .

TABLE II. Field widths of the resonances (V/cm).

State	Resonance			
	0,0	0,1	1,0	1,1
16s	4.0(8)	6.7(14)	4.6(9)	7.2(14)
17s	3.4(7)	4.8(10)	4.2(8)	5.3(11)
18s	2.7(6)	4.0(8)	3.6(8)	3.9(8)
20s	1.8(4)	2.7(4)	2.7(5)	2.4(5)
23s	1.35(50)			1.45(30)
25s	0.8(2)			1.15(22)
27s	0.55(20)			0.67(140)

TABLE III. Frequency widths of the resonances (GHz).

State	Resonance			
	0,0	0,1	1,0	1,1
16s	1.11(25)	1.95(50)	1.32(34)	2.31(6)
17s	1.08(23)	1.53(40)	1.34(40)	1.70(42)
18s	0.94(20)	1.45(35)	1.31(40)	1.52(38)
20s	0.77(16)	1.19(30)	1.19(30)	1.08(27)
23s	0.74(16)			0.88(22)
25s	0.50(12)			0.81(20)
27s	0.40(10)			0.51(13)

By evaluating the quantity in the braces of Eq. (30) we obtain absolute values for cross sections. The values used are  $\Gamma = 5.2 \times 10^{14}$  atoms/C,  $T = 1$   $\mu$ sec,  $\bar{v} = 3.5 \times 10^4$  cm/sec, and  $V = 10^{-3}$  cm<sup>3</sup>. We estimate the errors in this normalization to be at most of a factor of 5. With the error bars of the relative cross sections from table IV, the observed cross sections can be expressed as

$$\sigma = 3.3(6) \times 10^4 n^{0.37(5)} \text{ \AA}^2, \quad (34)$$

which is in good agreement with the calculated values of Sec. II. In Fig. 13 we plot the observed cross sections and the theoretical result, Eq. (27) logarithmically vs  $n^{*4}$ .

## VI. CONCLUSION

The observed resonant-collision process is perhaps one of the best examples of resonant

dipole-dipole collisions with little contribution from higher multipole or hard-sphere effects. As such it is of interest from a fundamental point of view because it is theoretically tractable and experimentally very accessible. For example, systematic studies of the collisional resonances involving the manifold of Stark states should allow one to probe the effect of varying dipole moments without changing the size of the atom. In addition the long time duration of the collision,  $\sim 1$  nsec, and the large dipole moments imply that it should be straightforward to study perturbations of the collisions. For example, using microwaves it should be possible to do experiments analogous to laser-induced collision experiments.<sup>24</sup> Finally we notice that the magnitude of the collision cross sections suggests that they must be considered in applica-

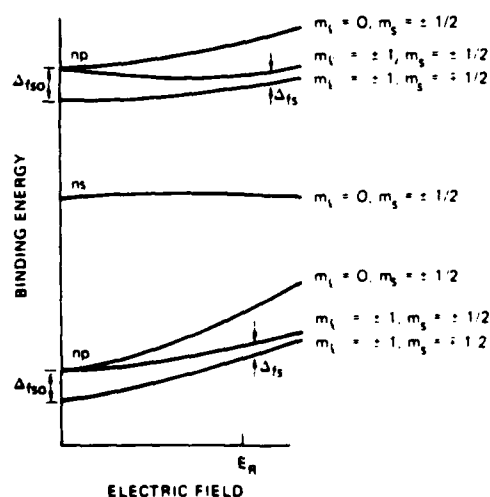


FIG. 10. The fine-structure levels in zero field and at the field of the collisional resonances.

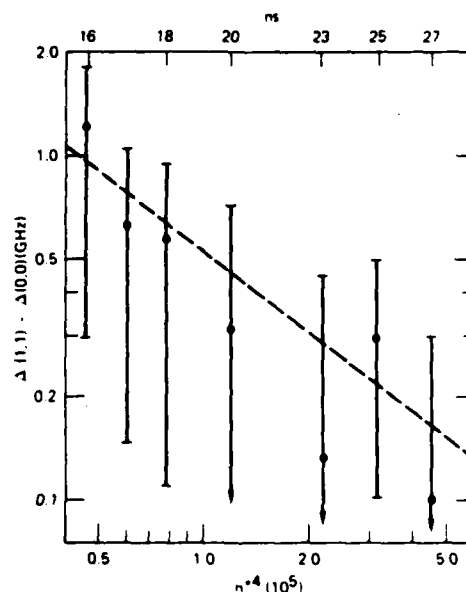


FIG. 11. The difference in widths of the 1,1 and 0,0 resonances ( $\bullet$ ) and a plot of the calculated value of  $\Delta(1,1)$  (---).

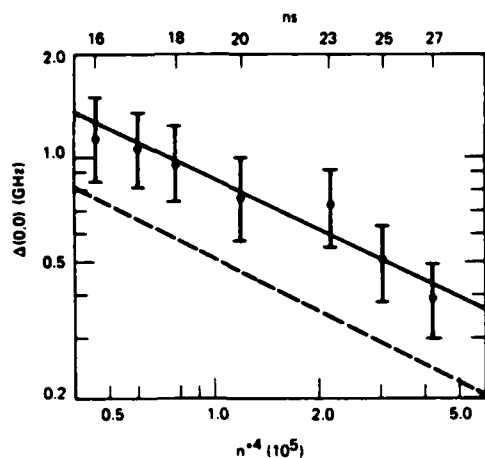


FIG. 12. The widths of the 0,0 resonances (●), the fit curve (—), and a plot of the calculated dependence (---).

tions such as far-infrared or microwave detection requiring samples of Rydberg atoms which are somewhat dense.<sup>25-28</sup> While at first such processes appear to be a nuisance, it may be possible to put the effect to good use.

#### ACKNOWLEDGMENTS

It is a pleasure to acknowledge stimulating and helpful conversations with W. E. Cooke, R. M. Hill, T. Oka, B. R. Junker, S. E. Harris, and J. Briggs in the course of this work, which was supported by the Office of Naval Research under Contract No. N00014-79-C-0212.

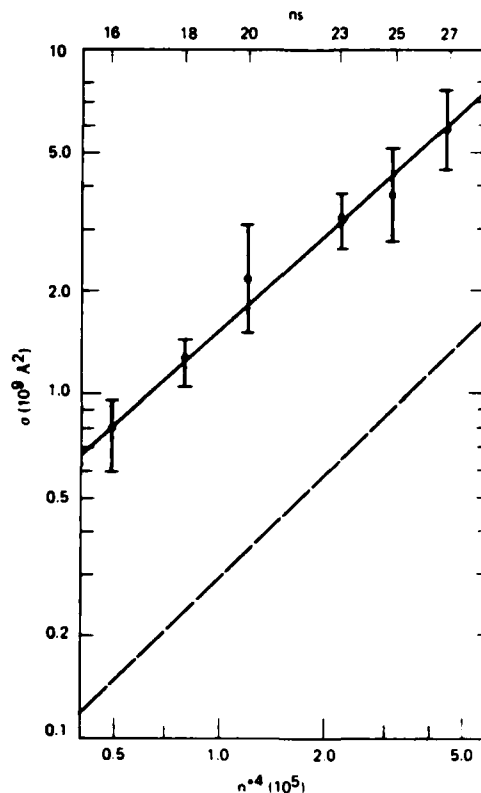


FIG. 13. The observed cross sections with their relative error bars (●), the fit curve (—), and the calculated dependence (---).

#### APPENDIX

To convert the widths from their field values to frequency we use the following approach.<sup>29</sup> In Fig. 14 we show the atomic levels in an electric field.

TABLE IV. Radiative lifetimes, relative and absolute cross sections.

State	Lifetime <sup>a</sup> (μsec)	$N_p'/N_i'^2$ (Relative cross section) ( $10^9 \text{ C}^{-1}$ )	$\sigma$ ( $10^9 \text{ Å}^2$ )
16s	4.34	1.45(35)	0.78(18)
18s	6.37	2.31(23)	1.25(13)
20s	8.96	4.0(12)	2.16(66)
23s	14.0	6.0(9)	3.2(5)
25s	18.3	7.1(19)	3.8(10)
27s	23.3	10.7(33)	5.8(18)

<sup>a</sup>See Ref. 22.



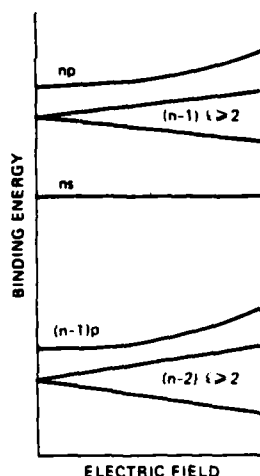


FIG. 14. Energy levels of the Rydberg states in an electric field, showing the Stark shifts of the  $s$ ,  $p$ , and hydrogenic  $l \geq 2$  states.

The position of the  $s$  state is essentially independent of field in the region shown so we shall assume it has zero Stark shift. Note that the  $p$  states are displaced from the hydrogenic position by an amount  $\Delta p = \delta p / n^3$  in zero field and exhibit a linear Stark shift  $\sim n^2 E$  at high field. This suggests that the Stark shift  $W_p$  of a  $P$  state be written as

$$W_p = (\Delta p^2 + n^{*4} E^2)^{1/2} - \Delta p. \quad (\text{A1})$$

The average stark shift of the two  $p$  states may be written as

$$\bar{W}_p = (\Delta p^2 + n^{*4} E^2)^{1/2} - \frac{\delta p}{n^{*3}}, \quad (\text{A2})$$

where for  $n^*$  we use the effective quantum number of the  $s$  state which lies halfway between the two  $p$  states. The slope of this curve yields the desired conversion of widths from fields to frequencies. Explicitly

$$\frac{d\bar{W}_p}{dE} = \frac{n^{*4} E}{(\delta p / n^{*3} + n^{*4} E^2)^{1/2}}. \quad (\text{A3})$$

We are, of course, interested in this value at the resonances for which the average value of the energies of the two  $p$  states above and below the  $s$

states equals the energy of the  $s$  state. If  $\Delta_0$  is the amount by which the average of the two  $p$  state energies lies below the  $s$  state energy, then at resonance  $\bar{W}_p = \Delta_0$ . From the spectroscopy of the Na  $s$  and  $p$  states  $\Delta_0 = M n^{*-3.73}$  where  $M = 0.236$ .<sup>30</sup> Thus at resonance the average field  $E_R$  must satisfy

$$\left[ \left( \frac{\delta p}{n^{*3}} \right)^2 + n^{*4} E_R^2 \right]^{1/2} - \frac{\delta p}{n^{*3}} = \frac{M}{n^{*3.73}}. \quad (\text{A4})$$

In fact the two sides of Eq. (A4) are equal to 10% justifying the approximation of Eq. (A1).

Equation (A3) can be rewritten for  $E = E_R$

$$\left. \frac{d\bar{W}_p}{dE} \right|_{E_R} = \frac{n^{*4} E_R}{\delta p / n^{*3} + M / n^{*3.73}}. \quad (\text{A5})$$

Since  $E_R$  for the (0,0) resonance is given by  $E_R = Q n^{*-5.35}$ , with  $Q = 0.236$ , we can write Eq. (A5) as

$$\left. \frac{d\bar{W}_p}{dE} \right|_{E_R} = \frac{Q n^{*-1.35}}{\delta p / n^{*3} + M / n^{*3.73}}. \quad (\text{A6})$$

We may rewrite Eq. (A6) as

$$\left. \frac{d\bar{W}_p}{dE} \right|_{E_R} = \frac{Q n^{*1.65}}{\delta p + M n^{*-0.73}}. \quad (\text{A7})$$

If we replace  $M n^{*-0.73}$  by its average value, 0.027, over the range of  $n$  studied we can rewrite Eq. (A7) with 3% accuracy as

$$\left. \frac{d\bar{W}_p}{dE} \right|_{E_R} = 1.33 n^{*1.65}. \quad (\text{A8})$$

We may express Eq. (A8) in more practical units as

$$\Delta \bar{W}_p (\text{GHz}) = 1.72 \times 10^{-3} n^{*1.65} \Delta E (\text{V/cm}). \quad (\text{A9})$$

Since the frequency of the  $ns$ - $np$  transition is shifted up at the rate given by Eq. (A9) while the frequency of the  $ns$ -( $n-1$ ) $p$  transition is shifted down by the same rate, the width  $\Delta$  of the collisional resonances is twice as large as shown by Eq. (A9).

$$\Delta (\text{GHz}) = 3.44 \times 10^{-3} n^{*1.65} \Delta E (\text{V/cm}). \quad (\text{A10})$$

- \*Permanent address: Schlumberger-Doll Research, Ridgefield, Conn. 06877.
- †Permanent address: CEN Saclay, Service de Physique des Atomes et des Surfaces, 91191 Gif-sur-Yvette, Cedex, France.
- ‡Permanent address: Institut d'Electronique Fondamental, 91405 Orsay, France.
- §Permanent address: Fakultät für Physik, 3 Herman Herder Strasse, D7800 Freiburg, West Germany.
- <sup>1</sup>N. F. Mott and H. S. W. Massey, *The Theory of Atomic Collisions* (Clarendon, Oxford, 1950).
- <sup>2</sup>P. W. Anderson, *Phys. Rev.* **76**, 647 (1949).
- <sup>3</sup>J. van Kranendonk, *Can. J. Phys.* **41**, 433 (1963).
- <sup>4</sup>T. Oka, in *Advances in Atomic and Molecular Physics*, edited by D. R. Bates and I. Esterman (Academic, New York, 1973), Vol. 9.
- <sup>5</sup>P. L. Houston, in *Photoselective Chemistry, Part 2*, edited by J. Jortner (Wiley, New York, 1981).
- <sup>6</sup>K. A. Smith, F. G. Kellert, R. D. Rundel, F. B. Dunning, and R. F. Stebbings, *Phys. Rev. Lett.* **40**, 1362 (1978).
- <sup>7</sup>T. H. Jeys, G. B. McMillan, K. A. Smith, F. B. Dunning, and R. F. Stebbings, *Proceedings of the Twelfth ICPEAC*, 1981, p. 1107 (unpublished).
- <sup>8</sup>T. F. Gallagher, G. A. Ruff, and K. A. Safinya, *Phys. Rev. A* **22**, 843 (1980).
- <sup>9</sup>K. A. Safinya, J. F. Delpech, F. Gounand, W. Sandner, and T. F. Gallagher, *Phys. Rev. Lett.* **47**, 405 (1981).
- <sup>10</sup>G. E. Pake, *Paramagnetic Resonance* (Benjamin, New York, 1962).
- <sup>11</sup>E. M. Purcell, *Astrophys. J.* **116**, 457 (1952).
- <sup>12</sup>N. F. Ramsey, *Molecular Beams* (Oxford University Press, London, 1956).
- <sup>13</sup>D. Kleppner, in *Atomic Physics and Astrophysics*, edited by M. Chrétien and E. Lipworth (Gordon and Breach, New York, 1971).
- <sup>14</sup>T. F. Gallagher, L. M. Humphrey, W. E. Cooke, R. M. Hill, and S. A. Edelstein, *Phys. Rev. A* **16**, 1098 (1977).
- <sup>15</sup>D. C. Lorents, D. J. Eckstrom, and D. L. Huestis, SRI Report No. MP 73-2 (unpublished).
- <sup>16</sup>M. Gross, C. Fabre, P. Goy, S. Haroche, and J. M. Raimond, *Phys. Rev. Lett.* **43**, 343 (1979).
- <sup>17</sup>J. C. MacGillivray and M. S. Feld, *Phys. Rev. A* **14**, 1169 (1976).
- <sup>18</sup>R. Freidberg, S. R. Hartmann, and J. T. Manassah, *Phys. Lett.* **40A**, 372 (1972).
- <sup>19</sup>N. E. Rehler and J. H. Eberly, *Phys. Rev. A* **3**, 1735 (1971).
- <sup>20</sup>W. E. Cooke (private communication).
- <sup>21</sup>T. F. Gallagher, L. M. Humphrey, R. M. Hill, W. E. Cooke, and S. A. Edelstein, *Phys. Rev. A* **15**, 1937 (1977).
- <sup>22</sup>F. Gounand, *J. Phys. (Paris)* **40**, 457 (1979).
- <sup>23</sup>W. E. Cooke and T. F. Gallagher, *Phys. Rev. A* **21**, 588 (1980).
- <sup>24</sup>R. W. Falcone, W. R. Green, J. C. White, J. F. Young, and S. E. Harris, *Phys. Rev. A* **15**, 1333 (1977).
- <sup>25</sup>D. Kleppner, and T. W. Ducas, *Bull. Am. Phys. Soc.* **21**, 600 (1976).
- <sup>26</sup>T. F. Gallagher and W. E. Cooke, *Appl. Phys. Lett.* **34**, 369 (1979).
- <sup>27</sup>T. Ducas, W. Spencer, A. Vaidyanathan, W. Hamilton, and D. Kleppner, *Appl. Phys. Lett.* **35**, 382 (1979).
- <sup>28</sup>H. Figger, G. Leuchs, R. Straubinger, and H. Walther, *Opt. Commun.* **33**, 37 (1980).
- <sup>29</sup>W. E. Cooke (private communication).
- <sup>30</sup>C. Fabre, These de Doctor d'Etat, Université Pierre et Marie Curie, Paris, France, 1980 (unpublished).

Resonant collisions of Na  $nS$  and  $nD$  Rydberg atoms

R. Kachru, T. F. Gallagher, F. Gounand,\* P. L. Pillet,<sup>†</sup> and N. H. Tran  
*Molecular Physics Laboratory, SRI International, Menlo Park, California 94025*  
 (Received 17 December 1982; revised manuscript received 25 April 1983)

A large enhancement in the resonant collisional energy-transfer process  $\text{Na}(ns) + \text{Na}(ns) \rightarrow \text{Na}[(n-1)p] + \text{Na}(nl)$  or  $\text{Na}(ns) + \text{Na}(ns) \rightarrow \text{Na}(np) + \text{Na}[(n-1)l]$  is observed when the initial  $ns$  state lies midway between  $(n-1)p$  and an  $nl$  state or between  $np$  and an  $(n-1)l$  state. This resonance condition, achieved by the electric field tuning of the levels, leads to large cross sections  $\sim 10^9 \text{ Å}^2$  and narrow linewidths  $\sim 1 \text{ GHz}$ . These cross sections and linewidths are comparable to the previously observed resonant process  $\text{Na}(ns) + \text{Na}(ns) \rightarrow \text{Na}[(n-1)p] + \text{Na}(np)$ . We have also observed a similar collisional energy transfer starting from a completely different initial state, i.e.,  $\text{Na}(15d) + \text{Na}(15d) \rightarrow \text{Na}(16f) + \text{Na}(15p)$ . In this case the enhancement in the cross section ( $\sim 10^9 \text{ Å}^2$ ) is observed at a relatively low electric field  $\sim 17 \text{ V/cm}$ .

## I. INTRODUCTION

Resonant collisional energy transfer, the process in which one atom (atom  $A$ ) loses as much internal energy as another atom (atom  $B$ ) gains, has long attracted considerable interest.<sup>1-3</sup> Recent revival of interest in this phenomenon stems from the availability of tunable dye lasers and the ability to selectively excite a large number of atoms or molecules. Recently the term progression in the atomic Rydberg series was used to match the transition energies of two species. By varying  $n$ , enhancement in the cross section for the transfer of energy from the  $\text{Na}(nl)$  Rydberg states to the vibrational transitions<sup>4</sup> of  $\text{CH}_4$  and  $\text{CD}_4$  and the rotational transitions<sup>5</sup> of  $\text{NH}_3$  have been reported. More recently, the electric field tuning of the Na Rydberg states has been used to resonantly enhance the collisional energy transfer process<sup>6,7</sup>

$$(ns) + (ns) \rightarrow (np) + [(n-1)p].$$

Sharp resonances representing large transfers of population to the  $np$  and  $(n-1)p$  states from the initially excited  $ns$  states were observed at certain values of the static electric field. These sharp resonances occur when the laser-excited  $ns$  state lies midway between an upper  $np$  and a lower  $(n-1)p$  state,<sup>6,7</sup> causing the process  $(ns) + (ns) \rightarrow [(n-1)p] + (np)$  to proceed resonantly because the energy lost by one  $\text{Na}(ns)$  atom exactly equals the energy gained by the other colliding  $\text{Na}(ns)$  atom.

The resonant-collision process represents a classic example of a long-range electric dipole-dipole interaction between two atoms. Since the electric dipole moment between the adjacent Rydberg states (the dipole moment between  $ns$  and  $np$  states, for instance) is large, approximately  $n^2$ , where  $n^*$  is the effective quantum number, this strong interaction at resonance leads to a very large collision cross section, approximately  $10^9 \text{ Å}^2$  (for  $n=20$ ). Furthermore, this collisional interaction is very long ranged and gives rise to resonances which have very narrow linewidths (approximately  $1 \text{ GHz}$ ), which implies approximately 1-ns-long interaction times. As a function of

$n^*$ , the effective quantum number of the  $ns$  state, the resonant collision cross section  $\sigma$  scales as  $n^{*4}$ , whereas the linewidths  $\Delta$  scale as  $(n^*)^{-2}$ . Recently, the use of a microwave field to resonantly enhance the collisional energy transfer between two Na atoms when the collisional defect  $\Delta W$  is nonzero has been reported.<sup>8</sup>

Here we report the result of our effort to generalize and extend the capability of the electric-field-tuned resonant collisional energy transfer to include Rydberg states other than the  $s$  and  $p$  states of Na. In the present work we look for resonant collisions between two Na atoms whose initial or final states differ from the  $ns$  and  $np$  or  $(n-1)p$  states, respectively. The relative size of the resonant-collision cross sections for the different initial and final states is also an important check on the dipole-dipole interaction model for these collisions. For instance, we observe electric-field-tuned resonant collisions of the type  $(ns) + (ns) \rightarrow (np) + (nl)$  or  $(ns) + (np) \rightarrow (nl) + [(n-1)p]$ , where one of the final states is a  $nl$  state ( $l \geq 2$ ). While  $l$  is not a good quantum number in an electric field it still serves as a convenient and unique way to label states (see below). We have also observed a large enhancement in the cross section at relatively low fields (approximately  $17 \text{ V/cm}$ ) for the process  $(15d) + (15d) \rightarrow (16f) + (15p)$ , in which a collision between two  $\text{Na}(15d)$  atoms results in one atom being excited to a  $16f$  state and the other deexcited to a  $15p$  state. We find that both the cross sections and the linewidths of these resonant processes are comparable in magnitude to those observed for the now familiar process  $(ns) + (ns) \rightarrow [(n-1)p] + (np)$ .

While a detailed account of the resonant-collision phenomena may be found in Ref. 7, it is worthwhile to consider a simple physical picture of the collision process here. The energy-level diagram of two colliding atoms (which need not be of similar species) is shown in Fig. 1. The relevant energy levels are  $|1A\rangle$  and  $|2A\rangle$  for atom  $A$  and  $|1B\rangle$  and  $|2B\rangle$  for atom  $B$ . The pair of states  $|1A\rangle$  and  $|2A\rangle$  are, in principle, any pair for which  $\langle 2A | \mu | 1A \rangle \neq 0$ , where  $\mu$  is the electric-dipole-moment operator; this applies similarly to  $|1B\rangle$  and  $|2B\rangle$ . Assume for simplicity that atom  $B$  is fixed. Atom  $A$  moving

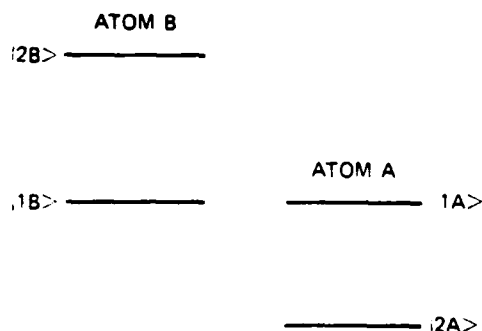


FIG. 1. Simplified energy-level diagram considered for the resonant-collision process. Atoms  $A$  and  $B$  (which could even be of different species) have energy levels  $|1A\rangle$ ,  $|2A\rangle$  and  $|1B\rangle$ ,  $|2B\rangle$ , respectively. These energy levels are tuned (Stark-shifted) by the static electric field. The resonant-collision cross section is greatly enhanced when the energy separation of the two levels for atom  $A$  equals that for atom  $B$ . Note that in the present experiment we always have  $W_{1A} = W_{1B}$ . The resonant-collision process, in principle, only requires  $W_{1A} - W_{2A} = W_{2B} - W_{1B}$  (see text).

with relative velocity  $v$  and viewed as a classical dipole with dipole moment  $\mu_1 = \langle 2A | \mu | 1A \rangle$  produces an oscillating field

$$E_1 \approx \frac{\mu_1}{R^3} \cos(W_{1A} - W_{2A})t / \hbar$$

at the site of atom  $B$ , where  $W_{1A}$  ( $W_{2A}$ ) is the energy of state  $1A$  ( $2A$ ) in the static electric field and  $R$  is the distance between the atoms. Here  $\hbar = 2\pi\hbar$  is Planck's constant and  $t$  is the time. At resonance, i.e., when

$$(W_{1A} - W_{2A}) - (W_{2B} - W_{1B}) = \Delta W = 0,$$

this dipolar electric field of atom  $A$  drives the  $|1B\rangle \rightarrow |2B\rangle$  transition in atom  $B$ . This transition probability is unity if  $E_1 \mu_2 \tau / \hbar \approx 1$ , where  $\mu_2 = \langle 2B | \mu | 1B \rangle$ , and  $\tau$  is the effective collisional interaction time. We may approximate  $\tau$  by  $b/v$ , where  $b$  is the impact parameter. At resonance the collision cross section is then given by

$$\sigma \approx \frac{\mu_1 \mu_2}{\hbar v} \quad (1)$$

while the collision interaction time is

$$\tau \approx (\mu_1 \mu_2)^{1/2} / v^{3/2}. \quad (2)$$

As a specific example consider the previously observed resonant-collision process  $(ns) + (ns) \rightarrow (np) + (n-1)p$ . We have  $|1A\rangle = ns$ ,  $|1B\rangle = ns$ ,  $|2A\rangle = np$  ( $m=0$ ), and  $|2B\rangle = (n-1)p$  ( $m=0$ ). To calculate the resonant cross section we use  $\mu_1 = \mu_2 \approx 0.6n^2$  (Ref. 9) in Eqs. (1) and (2). For  $n=20$ ,  $\sigma \approx 10^4 \text{ \AA}^2$  and the linewidth is approximately equal to 1 GHz. Such large cross sections result from the large dipole moments associated with the Rydberg transitions in this example between the  $ns$  and the  $n-1p$  and  $np$  states, respectively. As remarked earlier, the initial and final collision states need not just be

$s$  and  $p$  states but instead any pair of states connected by a reasonable dipole moment. An additional requirement for the resonant-collision process, in fact the most basic requirement, is that the condition  $W_{1A} - W_{2A} = W_{2B} - W_{1B}$  be satisfied at some value of the electric field. Figure 2 shows one of the several pairs of states for which these two basic requirements for resonant collisions is satisfied. For instance, as shown in Fig. 2, we consider the pair of states  $|1A\rangle = |1B\rangle = 20s$ ,  $|2A\rangle = 19p$  ( $m=0$ ), and  $|2B\rangle = (n=19, l=18)$ . To simplify the notation the manifold of Stark states shown in Fig. 2 (solid lines) near  $19d$  (long-dashed line above the  $20s$  state) is labeled by the  $n, l$  quantum numbers. Although  $l$  is no longer a good quantum number in presence of a static electric field, the linear Stark states are adiabatically connected to the zero-field  $nl |m\rangle$  states in a unique way. For instance, the Stark state with the lowest (highest) energy in the manifold is adiabatically connected to the zero-field state with the lowest (highest)  $l$ . Similarly states that fall between the two extreme members of the manifold are adiabatically connected to the zero-field states with intermediate values of  $l$ . The state with the highest energy in the  $n=19$  manifold (see Fig. 2) is therefore labeled  $n=19, l=18$ . In the above example  $\mu_1 = \langle 19p | \mu | 20s \rangle \approx 200$  a.u. is quite large. Although the dipole matrix element  $\mu_2$  connecting  $20s$  to the  $n=19, l=18, m=0$  state of the Stark manifold is zero in zero field (dipole selection rule), it can be quite large when a relatively low electric field is applied. For instance, calculations show that  $\mu_2 \approx 80$  a.u. at  $E=300$  V/cm due to the Stark mixing. Calculations of the Stark shift (see Fig. 3) show that the resonance condition for the process  $(20s) + (20s) \rightarrow (19p) + (n=19, l=18)$  is satisfied at  $E=268$  V/cm. Here  $m=0$  for both the final states. Using the calculated value of  $\mu_2 \approx 80$  a.u. (at 268 V/cm) and  $\mu_1=200$  a.u., we obtain  $\sigma \approx 10^4 \text{ \AA}^2$ . This cross section is comparable to the cross section for the process  $(20s) + (20s) \rightarrow (19p) + (20p)$  and is easily observed. Similar calculations for the general process  $(20s) + (20s) \rightarrow (19p) + (n=19, l)$  or  $(20s) + (20s) \rightarrow (20p) + (n=18, l)$  show that the cross section is quite large, ap-

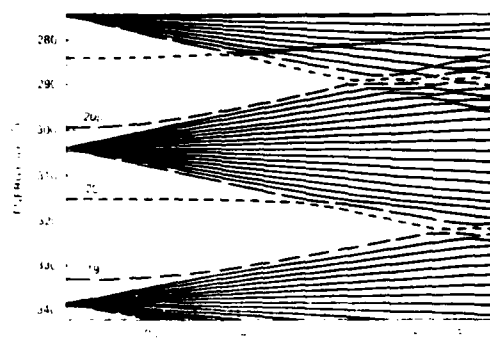


FIG. 2. Energy-level diagram of  $|m|=0$  states of Na in the vicinity of the  $20s$  state as a function of electric field.  $s$  states are shown by the short-dashed lines, the medium-dashed lines represent the  $p$  states, while the  $d$  states are represented by the very-long-dashed lines. Solid lines are Stark states with  $l=2$ . For instance, the manifold of solid lines between the  $20p$  and the  $20s$  states indicated above are states of  $n=19$  and  $3 \leq l \leq 18$ .

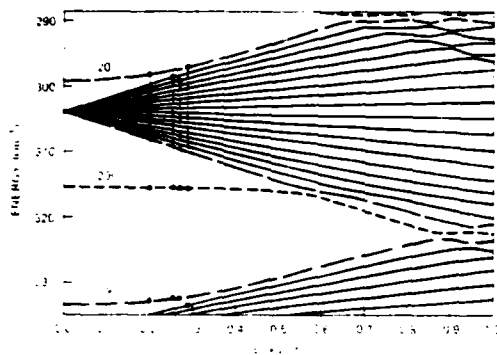


FIG. 3.  $m_l = 0$  states of Na near the 20s state, similar to Fig. 2, but shown in greater detail. First vertical dashed lines on the left shows the  $2A$  and  $2B$  states for the resonant process  $(20s) + (20s) \rightarrow (19p) \rightarrow (20p)$ . Second vertical line corresponds to the  $2A$  and  $2B$  states for the newly observed collision process  $(20s) + (20s) \rightarrow (19p) \rightarrow (n=19, l=18)$ . Solid line just below the  $20p$  ( $19p$ ) state corresponds to  $n=19, l=18$  ( $n=18, l=17$ ) Stark state (see text). Initial collision states  $1A$  and  $B$  in all the cases shown in this energy-level diagram are 20s. Third and fourth vertical lines (at higher fields) correspond to the resonant-collision processes  $(20s) + (20s) \rightarrow (19p) \rightarrow (n=19, l=17)$  and  $(20s) + (20s) \rightarrow (20p) \rightarrow (n=18, l=17)$ , respectively.

proximately  $10^7 - 10^8 \text{ Å}^2$ , and the resonances occur at successively higher electric fields.

Finally we consider the process  $(nd) + (nd) \rightarrow [(n+1)f] + (np)$  in which the initial state is not an  $s$  state. For  $n=15$  using  $\mu_1=21$  a.u. and  $\mu_2=70$  a.u., we get  $\sigma \sim 10^7 \text{ Å}^2$  from Eq. (1). For this example the resonance condition is obtained at a relatively low field of 17 V/cm.

## II. EXPERIMENT

While the details of the set up may be found elsewhere,<sup>7</sup> we describe the experimental arrangement briefly here. The experimental arrangement consists of an effusive Na beam which crosses the dye laser beams at right angles between a plate and a grid (see Fig. 4). A Quanta-Ray Neodymium:yttrium-aluminum-garnet (Nd:YAG) laser is used to simultaneously pump two dye lasers. The first dye laser (yellow laser) pumps the Na  $3s-3p_{3/2}$  transition ( $\lambda=5890 \text{ Å}$ ), while the second dye laser (blue laser) pumps the  $3p_{3/2}-ns(nd)$  transition. Both dye-laser beams are linearly polarized parallel to the applied electric field. Electric field tuning of the energy levels is achieved by applying a variable static voltage to the field plate. A field-ionizing pulse (risetime  $\approx 0.3 \mu\text{s}$ ) applied  $1 \mu\text{s}$  after the laser pulses selectively field-ionizes the Na atoms and accelerates the ions through the grid into an ion multiplier. The signal from the ion multiplier is amplified (typically by a factor of 10) and fed into a boxcar averager [Princeton Applied Research (PAR) Model 162]. The output of the averager is recorded on a chart recorder as the static electric field on the plates is slowly increased.

We use selective field ionization (SFI) to detect the initial and final collision states. With the use of SFI it is

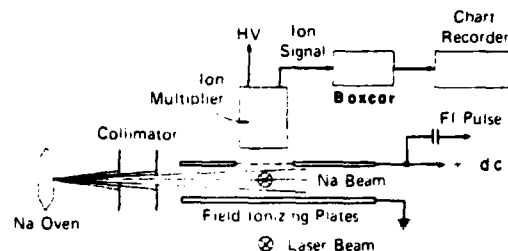


FIG. 4. Schematic of the experimental setup used in this experiment. Two dye-laser pulses which produce either the  $ns$  or the  $nd$  state cross the effusive Na beam at right angles. A  $0.3\text{-}\mu\text{s}$ -risetime-pulsed field ionizes the atoms selectively and pushes the ions through a mesh into an ion multiplier. Static voltage is applied to the upper plate while the lower plate is grounded. Signal from the ion multiplier is amplified and averaged by a PAR boxcar averager and finally displayed on a chart recorder.

straightforward to resolve not only the initially excited  $ns$  and the final  $nl$  states but also the different  $m_l$  components of the final  $nl$  state. The atomic beam is collimated to 0.4 cm diam. in the interaction region, while the laser beams are focused to approximately 1 mm diam. The effusive Na atomic beam is produced from a resistively heated oven. The oven temperature is  $\approx 500^\circ\text{C}$ . The atomic density in the interaction region is approximately  $10^8 \text{ cm}^{-3}$ .

## III. OBSERVATIONS

### A. Resonant collisions of Na(20s) atoms

We first describe the resonant collision process  $(20s) + (20s) \rightarrow (19p) + (19l)$  or  $(20s) + (20s) \rightarrow (20p) + (18l)$ . Here and throughout this paper  $l$  is used as a label for the energy eigenstates to simplify the notation (see above). Although we have observed the resonant collision process from other  $ns$  states ( $n=18-24$ ) we describe here the observations made with the 20s state. Resonant collisions between Na atoms in other  $ns$  states ( $n=18-24$ ) give qualitatively similar results. Figure 5 shows the trace of the ion signal which represents the population in the  $20p$  state or the  $19l$  state as the static electric field is increased. The three resonances on the left-hand side are the collisional resonances observed in the earlier work and correspond to the  $ns$  state lying midway between the  $np$  and the  $(n-1)p$  state. In Fig. 5 the second feature on the left-hand side consists of two unresolved resonances (see below). Thus the three features on the left-hand side in Fig. 5 correspond to the four resonances identified below and in Ref. 7. The sharp increases in the ion current represent large collisional transfers to the  $20p$  state. Since the  $20p$  state and  $19l$  states with high  $l$  field ionize at a lower field than does the initially excited 20s state, we set the amplitude of the field-ionization pulse so that only the  $20p$  and the high- $l$  states of the  $n=19$  manifold are field-ionized. In this way we obtain a signal only if the atoms end up in the  $20p$  or the nearby high- $l$  states of  $n=19$  manifold. Note that the  $m_l = 0$  and 1 splitting of the  $p$  states leads to four resonances. We label these resonances

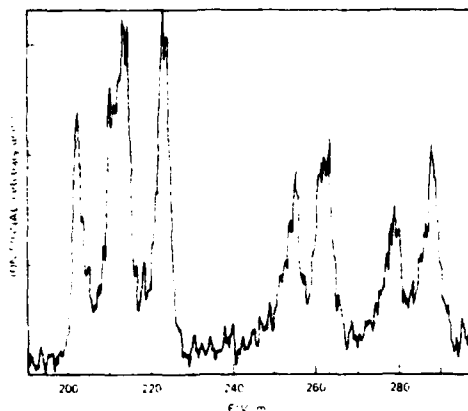


FIG. 5. Plot of ion current as a function of the applied static field for the Na atoms initially excited to the  $20s$  state. Sharp resonances show the large transfer of population into the  $20p$  state or the high- $l$  states ( $l=18$  or  $17$ ) or the  $n=19$  manifold. The atoms are detected by applying a FI pulse  $1\ \mu\text{s}$  after the laser pulses, and the amplitude of this pulse is set so that only states with  $n^*=19$  or higher are detected. First three resonances on the low-field end represent the resonant-collision process  $(20s)+(20s)\rightarrow(19p)+(20p)$ . Four peaks on the high-field end are the newly observed collisional resonances. Note that each of these resonances seen at high field are in fact composed of two or more overlapping resonances. For instance the resonance observed at  $255\ \text{V/cm}$  are labeled  $(19,18,0;19,1,0)$  and  $(19,18,0;19,1,1)$  (see text for the  $n,l,m_l$  labeling convention used here).

by the pair of  $n,l,m_l$  values for the lower and upper states. At this point we note that experimentally we only observe the transfer of population to the upper state (state with the higher energy). We assign the other final state involved in the collision process by calculating the Stark shift<sup>10</sup> of the relevant states. The resonances recorded in Fig. 5 are labeled, in the order of increasing field, as follows:  $(19,1,0;20,1,0)$  observed at  $202\ \text{V/cm}$ ;  $[(19,1,1;20,1,0)$  and  $(19,1,0;20,1,1)]$  observed at  $212\ \text{V/cm}$ ; and  $(19,1,1;20,1,1)$  observed at  $223\ \text{V/cm}$ . The square brackets indicate that the two calculated resonances contained inside are experimentally unresolved. The pair of three numbers in the brackets corresponds to the  $n,l,m_l$  quantum numbers of the two final states involved in a given resonance. For instance, the first resonance in Fig. 5 is labeled as  $(19,1,0;20,1,0)$  where  $|1A\rangle=|1B\rangle=20s=(20,0,0)$ ,  $|2A\rangle=(19,1,0)$ , and  $|2B\rangle=(20,1,0)$ .

As the static electric field is increased beyond  $250\ \text{V/cm}$  (see Fig. 5) additional sharp resonances appear. These resonances indicate a large transfer of population into either the  $20p$  state or the high members of the  $n=19, l\geq 2$  manifold. The blue-laser-intensity dependence of these resonances (at lower laser power) shows that the observed signal is quadratic (to within  $\pm 10\%$ ) in laser intensity implying that the observed resonances are collisional signals involving two Na atoms. At sufficiently high blue-laser power some of these resonances become saturated and the resonance signal no longer increases as the square of the laser intensity. Collisional resonances observed at even higher fields are shown in Fig. 6.

The sharp increase in the ion signal, as before, represents the large transfers of population into either the  $20p$  state or the high members of the  $n=19, l>2$  manifold. Since the field-ionization thresholds for the  $20p$  and the higher energy state of the  $n=19$  manifold are almost identical, it is frequently difficult to distinguish between these states using our experimental detection scheme. However, we can accurately calculate the Stark shift<sup>10</sup> of these states and assign two unique initial and final  $n,l,m_l$  labels to each of the sharp resonances seen in Fig. 5. For instance, the first resonance (at  $E=255\ \text{V/cm}$ ) on the high-field side of the previously observed resonant-collision resonances is labeled  $[(19,18,0;19,1,0),(19,18,1;19,1,0)]$ . Again, the pair of resonances in the square brackets indicates that these resonances are experimentally unresolved (see Fig. 5).

Table I shows the calculated positions of the four high-field resonances seen in Fig. 5 in terms of the static electric field. Similarly the resonances observed at even higher fields (see Fig. 6) can be assigned a pair of final  $n,l,m_l$  states. It is clear that at higher fields some of the resonances overlap. For instance the resonance seen in Fig. 5 at approximately  $278\ \text{V/cm}$  is in fact composed of four unresolved resonances. In some cases we can verify the calculated  $|m_l|$  assignment of the resonances by using the fact that states with different  $|m_l|$  have slightly different SFI thresholds.<sup>11</sup> For instance  $|m_l|=1$  states in the vicinity of  $20p$  have a field-ionization threshold which is approximately  $4.5\%$  higher than that for  $|m_l|=0$  states.<sup>11</sup> The  $|m_l|$  labeling of the first few collisional resonances is experimentally confirmed in Fig. 7 where the solid trace was obtained at a peak SFI field sufficient to field-ionize only the  $|m_l|=0$  component of the  $20p$  and the nearby high- $l$  states of the  $n=19$  manifold ( $E=2.2\ \text{kV/cm}$ ). The broken trace in Fig. 7 was similarly

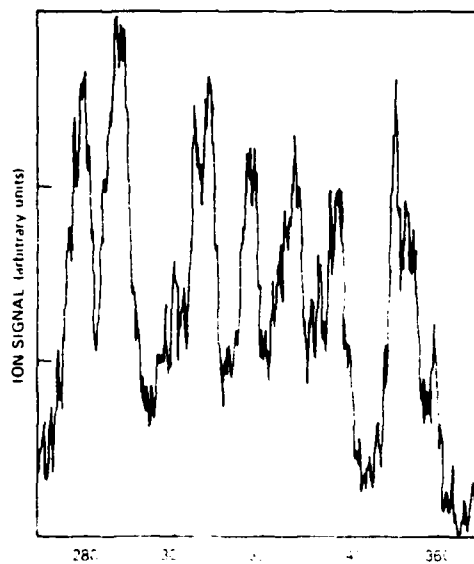


FIG. 6. Collisional resonances observed in Fig. 5 observed with  $20s$  atoms at higher field.

TABLE I. Calculated and observed positions of the resonances in terms of the applied dc field (V/cm). Errors shown are typical and represent the statistical uncertainty in the data.

Resonance	Electric field (V/cm)	
	Observed position	Calculated position
(20,1,0;19,1,0)	202(3)	202
(20,1,0;19,1,1)	212*	210
(20,1,1;19,1,0)		213.7
(20,1,1;19,1,1)	223(3)	222.8
(19,18,0;19,1,0)	255*	253
(19,18,1;19,1,0)		255
(19,18,0;19,1,1)	260*	260
(19,18,1;19,1,1)		262
(20,1,0;18,17,0)		277
(19,17,0;19,1,0)	278*	278
(20,1,0;18,17,1)		279
(19,17,1;19,1,0)		280
(20,1,1;18,17,0)		286
(20,1,1;18,17,1)	289*	288
(19,17,0;19,1,1)		287
(19,17,1;19,1,1)		289

\*Average location of the unresolved resonances.

obtained with the SFI amplitude set to detect  $|m_l| = 1$  component of the upper state ( $E \geq 2.3$  kV/cm). While setting the field-ionization (FI) pulse amplitude to detect the  $m_l = 1$  component of the upper state does not preclude detection of the  $m_l = 0$  components which have lower thresholds, we have recorded the  $|m_l| = 1$  component in the broken trace by using the temporal resolution of the

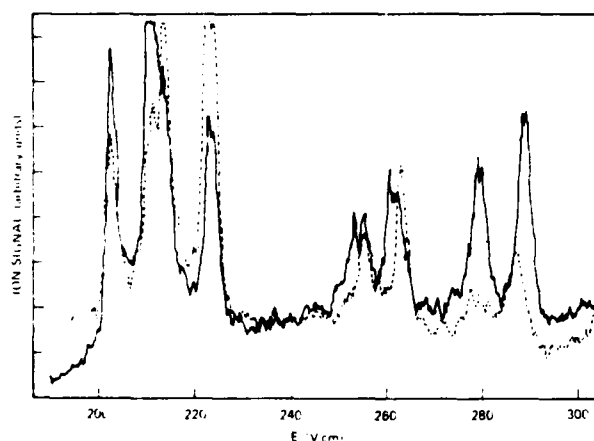


FIG. 7. Plot of ion current (solid trace) similar to that shown in Fig. 5 except that the SFI is set to detect only the  $m_l = 0$  component of the  $20p$  and the nearby  $n=19$ , high- $l$  state. Broken trace is a recording of the  $m_l = 1$  final states; discrimination is based on the temporal resolution of ion signals from the  $m_l = 0$  and 1 states (see text).

detected ion pulse. This temporal resolution of the  $|m_l| = 0$  and 1 components of the final states results from the finite risetime of the SFI pulse (risetime  $\sim 0.3$   $\mu$ s) whereby the states with lower SFI threshold ionize earlier. Comparison of Figs. 5 and 7 indicates a resolution of the resonances in terms of the final  $m_l$  quantum number. For instance the solid and broken traces in Fig. 7, which indicate the  $|m_l| = 0$  and 1 resonances, respectively, show that the resonance observed at  $E=255$  V/cm in Fig. 5 is in fact composed of two partially overlapping resonances. This experimental observation is in agreement with the calculated positions, as indicated in Table I. Resonances with overlapping final states with the same  $m_l$  cannot be resolved in any straightforward manner. In the above discussion we have implicitly assumed that the  $|m_l|$  quantum number of the final collision state can be 0 or 1. This assumption is reasonable since the dipole-dipole-interaction model for these collisions leads to the selection rule  $\Delta m_l = 0$  or 1, where  $\Delta m_l$  is the difference between the  $|m_l|$  values of the initial and final collision state. Since we start from  $m_l = 0$  ns state, the final states must have  $|m_l| = 0$  or 1. We note that the calculated cross sections for the higher-multipole process is  $\sim 10^5$   $\text{\AA}^2$ .

To show that the results presented are representative we show in Fig. 8 collisional resonances between pairs of Na atoms initially excited to the  $22s$  state. The resonances obtained here are evidently qualitatively similar to those observed with  $20s$  state described earlier. The first four resonance peaks on the low-field side correspond to the transitions  $22s \rightarrow 21s \rightarrow 22p \rightarrow 21p$  (the second and third resonances are unresolved, as in Fig. 5). Sharp resonances

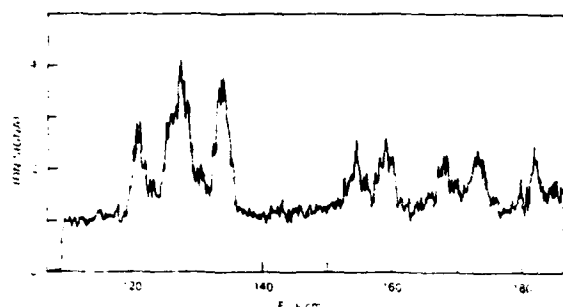


FIG. 8. Plot of ion current as the static electric field is increased, showing the collision resonances for the Na atoms initially excited to the 22s state. Amplitude of the SFI pulse used to selectively ionize the Na atoms 1  $\mu$ s after the laser pulses is set so that only atoms with  $n^* = 22$  ionize. The first three sharp peaks (at low field) correspond to the process  $22s + 22s \rightarrow 22p + (21p)$ , while the subsequent peaks are due to enhancement in the collision process  $22s + 22s \rightarrow (21p + n = 21, l = 20, 19) + 22p$  or  $22s + 22s \rightarrow 22p + (n = 20, l = 19)$ . Note the similarity to Fig. 5, which is essentially the same but starting at 20s.

seen at higher electric field correspond to a large transfer of population either to the 22p state which corresponds to the resonant-collision process  $22s + (22s) \rightarrow 22p + (n = 21, l)$  or to the  $n = 22, l$  state which corresponds to the process  $22s + 22s \rightarrow (21p) + (n = 22, l)$ . In the dipole-dipole collision model the  $m_l$  value of the final states can again be either 0 or 1.

#### IV. OBSERVATION OF Na( $nd$ ) + Na( $nd$ ) $\rightarrow$ Na[( $n-1$ ) $f$ ] + Na( $np$ ) RESONANT COLLISIONS

While all the previous observations of the resonant collisions were with Na atoms initially in excited  $ns$  Rydberg states, there are no fundamental limitations to the use of other Rydberg states. For instance, at relatively low fields (approximately 17 V/cm) the process  $(15d) + (15d) \rightarrow (15p + 16f)$  becomes resonant. This process is confirmed by our observation of a sharp transfer of population into the 16f state as shown in Fig. 9. The SFI pulse amplitude in Fig. 9 is set to detect states with  $n^* \sim 16$  or higher and therefore atoms in the laser-excited 15d state are not detected. Only atoms with final  $n^* \sim 16$  (for instance 16d or 16f) are detected via the ion multiplier. At zero electric field (see Fig. 9) a very small nonresonant black-body-radiation-induced signal is observed.<sup>12</sup> Large ion signals are observed when the electric field is set around 17 and 23 V/cm. From the Stark-shift calculations it is clear that at low fields the only resonance condition occurs for the process  $(15d) + (15d) \rightarrow (16f) + (15p)$ , i.e., the 15d state lies midway between 16f and 15p, respectively. The fine-structure splitting of the 15p state results in the two resonances observed at 17 and 23 V/cm, respectively. At this point it is worth mentioning that for Na observation of resonant collisions with  $ns$  initial states is much easier than it is for other initial states. This is because as the electric field is changed the Stark shift of the initially excited state necessitates the change in the fre-

quency of the blue laser (the Stark shift of the  $3p_{3/2}$  level is insignificant at fields of less than 1 kV/cm) to ensure that the transition frequency lies with the laser bandwidth (approximately  $0.3 \text{ cm}^{-1}$ ). For instance, the 20s state experiences very little Stark shift up to relatively high fields ( $0.3 \text{ cm}^{-1}$  at 0.4 kV/cm). The  $nd$  states, on the other hand, experience significant Stark shifts. However in the specific case we have just considered (15d), the Stark shift of the 15d state at 25 V/cm is much smaller than the laser linewidth. We note that calculations show that a similar resonance condition does not occur for the 16d state or higher- $n$  states and none is observed experimentally. Finally we note that the calculation [Eq. 1] shows that both  $m = 0, 1$  15d states contribute roughly equally to this collisional process.

#### V. DISCUSSION

Since extensive measurements of the  $(ns) + (n') \rightarrow np + [(n-1)p]$  resonant-collision cross sections have been reported previously, we can estimate the cross sections for these new resonances reported here by comparing the magnitude of the ion signals for the various  $nl$  final states. For instance, the cross section for the resonance (19,18,0;19,1,0) at  $E = 255 \text{ V/cm}$  in Fig. 5 resulting from the  $m_l = 0$  collision process  $20s + 20s \rightarrow 19p + (n = 19, l = 18)$  can be estimated by comparing the ion signal at 213 V/cm corresponding to the resonance (19,1,0;20,1,0). From the previous measurement of the cross section for the resonance (19,1,0;20,1,0) (approximately  $2 \times 10^{-16} \text{ Å}^2$ ) (Ref. 7) we estimate the cross section for the (19,18,0;19,1,0) resonance to be approximately  $10^{-16} \text{ Å}^2$ .

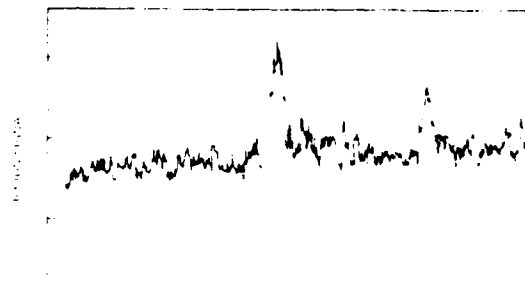


FIG. 9. Plot of the ion current representing the population in the 16f state (or a nearby Stark state) as a function of the static electric field. Atoms are initially excited to the 15d state. Amplitude of the SFI pulse is set to ionize states with  $n^* \sim 16$ . Sharp drop in the ion current near  $E = 0$  is due to the lasers being blocked from the atoms. Unstructured baseline is due to black-body-radiation induced transitions from the optically pumped 15d state into states with  $n^* \geq 16$ . Sharp increase in the ion current (and hence the population in the 16f state) at  $E = 17 \text{ V/cm}$  occurs when  $W_{16f} = W_{15d} = W_{15d} + W_{15p}$  and results in the resonant-collision process  $(15d) + (15d) \rightarrow (16f) + (15p)$ . The pair of resonances seen in this trace is due to the fine-structure splitting of the 15p state.



Since the theoretical calculations of the resonant collision have been described in detail elsewhere,<sup>7</sup> we shall only quote the important results here. The cross section for the resonant collision process  $|i\rangle + |i\rangle \rightarrow |f\rangle + |f\rangle$  between two atoms in an initial state  $|i\rangle$  and final states  $|f\rangle$  and  $|f'\rangle$  is given (in a.u.) by

$$\sigma = 4.6\mu_1\mu_2/v, \quad (3)$$

where  $\mu_1 = \langle f|\mu|i\rangle$ ,  $\mu_2 = \langle f'|\mu|i\rangle$ ,  $v = 0.34(8kT/\pi m)^{1/2}$  is the mean relative velocity between the two atoms,<sup>13</sup>  $m$  is the reduced mass,  $k$  is Boltzmann's constant, and  $T$  is the Na oven temperature. Equation (3) is obtained by performing the classical trajectory calculation for the collision process which results from the resonant dipole-dipole interaction between the two atoms. From our calculations of Stark wave functions<sup>10</sup> for the Na Rydberg states we obtain  $\mu_1 = \langle 19p|\mu|20s\rangle = 200$  a.u. and  $\mu_2 = \langle n=19, l=18|\mu|20s\rangle = 80$  a.u. for the (19,18,0;19,1,0) collision resonance observed at 255 V/cm in Fig. 5. For the (20,1,0;19,1,0) resonance,  $\mu_1 = \mu_2 = 200$  a.u. The calculated ratio between the cross sections for the (19,18,0;19,1,0) and (20,1,0;19,1,0) resonances is therefore approximately 0.4. From Fig. 5 (and other similar data not shown here) we see the observed ratio is approximately 0.4 (see also Table II). As stated earlier, the resonance at approximately 255 V/cm in Fig. 5 is actually composed of two superimposed resonances (19,18,0;19,1,0) and (19,18,0;19,1,1), respectively. In the preceding argument we have assumed that the cross sections for the two unresolved resonances are equal. Calculated cross sections of some of the high-field ( $m_l = 0$ ) resonances and their ratio compared to the lowest-field resonance, the (20,1,0;19,1,0) cross section, are listed in Table II. As shown by Table II the magnitude of the cross section depends directly on the product of the dipole matrix elements, not on the geometric size of the atoms which is roughly constant for all the cases listed in Table II. Conversion of the electric field scale to the frequency scale indicate that the widths of the newly observed resonances are approximately 2 GHz (see Fig. 5) which is comparable to the width of the previously observed lower-field resonances.

It is worth mentioning at this point that the observed  $n^*$  dependence of the  $s$ - $p$  resonant collision process follows the  $n^{*4}$  behavior predicted by the dipole-dipole interaction model calculation [Eq. (3)] quite well. The calculated cross sections are, however, only approximately 6.2 times as large as the absolute cross sections observed in Ref. 7. This discrepancy is most likely due to inherent uncertainty in the determination of experimental parameters like atomic number density or relative velocity; it is also possible that the cross section averaged over the relative velocity which has been ignored in the calculation leads to a different normalization for the cross section. In the present work, however, we are mostly interested in obtaining the relative cross sections.

Finally we have also observed resonant collisions between two Na atoms with  $l > 2$ . The Na atoms are initially excited to an  $nd$  state and subsequently excited to an  $n^*$  state by applying a microwave field in the presence of a small static field (approximately 20 V/cm). Resonant collisions between a pair of laser-microwave-excited atoms then result in one of the atoms being excited to a state with  $n^* \sim n + 1$ . Since the FI threshold of the final state following the microwave transition and the subsequent resonant collision is much lower than that for the initial laser-excited state, using the SFI technique, we can detect the final state with a high signal-to-background ratio. We have in fact observed microwave transition from the  $18d$  (and  $16d$ ) state using the resonant collisions. The  $18d - 18l$  ( $l \geq 2$ ) transitions occur as the microwave frequency is swept from 12.4 to 18.0 GHz in the presence of a 20-V/cm electric field. These microwave transitions are easily detected with the SFI amplitude set to detect states with  $n^* \approx 19$ .

From the above discussion and from Figs. 5 and 8 it is clear that the newly observed resonant-collision process  $(ns) + (ns) \rightarrow (np) + [(n-1)l]$  (or  $(ns) + (ns) \rightarrow [(n-1)p] + nl$ ) occurs quite generally and has a large cross section, approximately  $10^9$  A<sup>2</sup>, at resonance. As can be seen from Figs. 5 and 8 these resonances are easily observed. As shown here the large cross sections and narrow linewidths observed are largely due to the long-range dipole-dipole interaction between highly polarizable Rydberg atoms.

TABLE II. Calculated and observed cross section for resonances with both final states with  $m_l = 0$  and their ratio  $R$  with the lowest-field (20,1,0;19,1,0) resonance cross section. Numbers in parentheses represent the statistical uncertainty in our data.

Resonance	Calculated cross section ( $10^{-9}$ A <sup>2</sup> )	Ratio relative to calculated cross section for (20,1,0;19,1,0)	Ratio relative to observed cross section for (20,1,0;19,1,0)
20,1,0;19,1,0	3.2	1.0	1.0
19,18,0;19,1,0	1.3	0.4	0.4(0.08)
20,1,0;19,1,0	0.77	0.2	0.15(0.03)
19,17,0;19,1,0	1.1	0.3	0.2(0.04)

The large collision cross section and the long interaction time (approximately 1 ns) opens up the possibility of observing microwave-assisted collisions similar to the one observed recently for the process  $(ns) + (ns) + h\nu \rightarrow (np) + [(n-1)p]$ . It is quite feasible to observe resonant collisions between atoms in two dissimilar states and more generally between atoms of two different species. Resonant collisions involving higher-multipole

interactions between two atoms are also feasible. Such experiments are in progress.

#### ACKNOWLEDGMENT

This work was supported by the U.S. Navy Office of Naval Research under Contract No. N00014-79-C-0212.

\*Permanent address: Centre d'Etudes Nucleaires de Saclay, Service de Physique des Atomes et des Surfaces, du Centre National de la Recherche Scientifique, F-91191 Gif-sur-Yvette Cedex, France.

†Permanent address: Laboratoire Aime Cotton, Centre National de la Recherche Scientifique II, Bâtiment 505, F-91405 Orsay Cedex, France.

<sup>1</sup>N. F. Mott and H. S. W. Massey, *The Theory of Atomic Collision* (Clarendon, Oxford, 1950).

<sup>2</sup>P. W. Anderson, Phys. Rev. **76**, 647 (1949).

<sup>3</sup>T. Oka, in *Advances in Atomic and Molecular Physics*, edited by D. R. Bates and I. Esterman (Academic, New York, 1973), Vol. 9.

<sup>4</sup>T. F. Gallagher, G. A. Ruff, and K. A. Safinya, Phys. Rev. A **22**, 843 (1980).

<sup>5</sup>K. A. Smith, F. G. Kellert, R. D. Rundel, F. B. Dunning, and R. F. Stebbings, Phys. Rev. Lett. **40**, 1362 (1978).

<sup>6</sup>K. A. Safinya, J. F. Delpech, F. Gounand, W. Sandner, and T. F. Gallagher, Phys. Rev. Lett. **47**, 405 (1981).

<sup>7</sup>T. F. Gallagher, K. A. Safinya, F. Gounand, J. F. Delpech, W. Sandner, and R. Kachru, Phys. Rev. A **25**, 1905 (1982).

<sup>8</sup>R. Kachru, N. H. Tran, and T. F. Gallagher, Phys. Rev. Lett. **49**, 191 (1982).

<sup>9</sup>This numerical value of the dipole moment for Na is obtained by explicit calculation of the Coulomb wave function for the  $ns$  and  $np$  [or  $(n-1)p$ ] states using the procedure outlined in Ref. 10.

<sup>10</sup>M. L. Zimmerman, M. G. Littman, M. M. Kash, and D. Kleppner, Phys. Rev. A **20**, 2251 (1979).

<sup>11</sup>T. F. Gallagher, L. M. Humphrey, W. E. Cooke, R. M. Hill, and S. A. Edelstein, Phys. Rev. A **16**, 1098 (1977).

<sup>12</sup>T. F. Gallagher and W. E. Cooke, Phys. Rev. Lett. **42**, 835 (1979).

<sup>13</sup>W. E. Baylis, Can. J. Phys. **55**, 1924 (1977).

END  
FILMED

5-86

DTIC